Studies of superfluid stiffness in anisotropic superconductors and randomness in the coupling of superconducting planes

Thesis Submitted for the Degree of Doctor of Philosophy (Science) in Physics

of

Jadavpur University

by

Payel Das

Supervisor: Prof. Ajay Kumar Ghosh

Department of Physics

Jadavpur University

Kolkata – 700 032, India

যাদবপুর বিশ্ববিদ্যালয়
কলকাতা-৭০০০৩২, ভারত

* JADAVPUR UNIVERSITY
KOLKATA-700 032, INDIA

FACULTY OF SCIENCE: DEPARTMENT OF PHYSICS

Certificate from the Supervisor

This is to certify that the thesis entitled "**Studies of superfluid stiffness in anisotropic superconductors and randomness in the coupling of superconducting planes**" submitted by Miss **Payel Das** who got her name registered on **04.08.2016** for the award of Ph.D. (Science) degree of Jadavpur University, is absolutely based upon her own work under the supervision of **Prof. Ajay Kumar Ghosh** and that neither this thesis nor any part of it has been submitted for either any degree/diploma or any other academic award anywhere before.

Ajay Kumar Ghosh

(Prof. Ajay Kumar Ghosh)
02/08/2022
Signature of Supervisor
with Date and Official Seal

Professor Dr. Ajay Kumar Ghosh
Department of Physics
Jadavpur University
Kolkata-700032

*Established on and from 24th December, 1955 vide Notification No. 10986-Edn/IU-42/55 dated 6th December, 1955 under Jadavpur University Act, 1955 (West Bengal Act XXXIII of 1955) followed by Jadavpur University Act, 1981 (West Bengal Act XXIV of 1981)

ফোন: ০৩৩-২৪১৪-৬৬৬৬ Ext. ২৭৬১ Website: www.jaduniv.edu.in Phone: 033-2414-6666 Ext. 2761
মো: +৯১-৯৮৩০৮৪৮৯২০ M: +91-9830848920
Email: ajayk.ghosh@jadavpuruniversity.in

Acknowledgements

I would like to express my deep sense of thanks and sincere gratitude to my supervisor Professor Ajay Kumar Ghosh, Department of Physics, Jadavpur University, who made this work possible. I am very grateful to him for giving me the golden opportunity to study on the topic “Studies of superfluid stiffness in anisotropic superconductors and randomness in the coupling of superconducting planes” and for his continuous support and enthusiasm. His guidance and advice carried me through all the stages of writing my thesis. I sincerely admire his patience, motivating attitude and passion towards work.

I am also very thankful to all my group members Dr. S. Mollah, Dr. I. Mukherjee, Dr. B. Biswas, S. Roy, S. Haldar, T. Sk, P. Mandal, D. Rakshit, Ipsita Mukherjee, and R. K. Saha for their sincere cooperation and support during this journey of my research. I will always cherish all the fun moments that we have had together in the last few years.

I would like to acknowledge Department of Science & Technology, INSPIRE for awarding me the fellowship during the five years tenure (INSPIRE Registration No. – IF160305).

Finally, I would like to extend my gratitude and thanks to my family and friends for their constant moral support. I am forever thankful to my parents for giving me continuous mental strength, love and affection during this journey. Their selfless encouragement helps me to explore new directions in life and inspires me to follow my dreams.

List of Publications

Journals:

1. **P. Das**, Ajay Kumar Ghosh, Superfluid phase stiffness in electron doped superconducting Gd-123, Physica C 548 (2018) 27.
2. **Payel Das**, Ajay Kumar Ghosh, Scaling of current-voltage characteristics without and with finite superfluid phase stiffness below T_c, Physica C 593 (2022) 1354005.
3. **Payel Das**, Tasaul Sk, Ajay Kumar Ghosh, Dynamic and static exponents in FFH scaling using superfluid phase stiffness in co-doped superconducting systems, Journal of Superconductivity and Novel Magnetism 35 (2022) 3477.
4. **Payel Das**, Ajay Kumar Ghosh, An evidence of the second order BKT phase transition in three dimensional underdoped RE-123 superconductors (submitted).
5. S. Haldar, **P. Das**, Ajay Kumar Ghosh, Three dimensional phase diagram of superfluidity controlled voltage nonlinearity in superconductors, Physica C 563 (2019) 78.
6. D. Rakshit, T. Sk, **P. Das**, S. Haldar, Ajay Kumar Ghosh, Exponential reduction in critical current density in $Eu_{1-x}Ce_xBa_2Cu_3O_{7-\delta}$

superconductors near critical temperature, Physica C 588 (2021) 1353909.

7. **P. Das**, I. Mukherjee, Ajay Kumar Ghosh, Current-voltage characteristics of co-doped Eu-123system, accepted by ICCM-21, October 28, 2021, The Academy of Sciences, Chennai.

Conferences:

1. **P. Das**; Shaping the Future of Indian Power Sector Through Renewable Energy; Department of Power Engineering, Jadavpur University, Kolkata 700032, India; September 09-10, 2016.
2. **P. Das**; Recent Trend in Frontier Research in Physics; Department of Physics, Jadavpur University, Kolkata 700032, India; March 6, 2018.
3. **P. Das**, S. Haldar and Ajay Kumar Ghosh; International Conference on Complex and Functional Materials (ICCFM); S. N. Bose National Centre for Basic Sciences, Kolkata, India; December 13-16, 2018.
4. **P. Das**, S. Haldar, T. Sk and Ajay Kumar Ghosh; Third International Conference on Advanced Materials (ICAM-2019); International Unit on Macromolecular Science and Engineering (IUMSE), Mahatma Gandhi University, Priyadharshini Hills, P.O: Kottayam Kerala 686560, India; August 09-11, 2019.
5. **P. Das**, I. Mukherjee and Ajay Kumar Ghosh; International Conference

on Condensed Matter (ICCM-21); The Academy Of Sciences, Chennai, India; October 28-30, 2021 in online mode.

6. B. Biswas, I. Mukherjee, **P. Das**, T. Sk, L. Ghosh, S. Mollah, S. Haldar and Ajay Kumar Ghosh; Twists and Turns in Physics Research: Special Emphasis on Condensed Matter and Biophysics (TTPR-2017); Department of Physics, Jadavpur University, Kolkata 700032, India; February 21-22, 2017.
7. S. Haldar, **P. Das**, L. Ghosh and Ajay Kumar Ghosh; Condensed Matter Days- 2017; Department of Physics, Tezpur University, Tezpur 784028, Assam, India; August 29-31, 2017.
8. T. Sk, **P. Das**, S. Haldar and Ajay Kumar Ghosh; 3rd International Conference on Condensed Matter & Applied Physics (ICC 2019); Department of Physics, Government Engineering College, Bikaner, Rajasthan, India; Oct. 14-15, 2019.

Contents

Chapter 2: Experimental technique

Chapter 3: Superfluid phase stiffness in electron doped superconducting Gd-123

Chapter 4: Scaling of current-voltage characteristics without and with finite superfluid phase stiffness below T_c

Chapter 1

Introduction

1.1 Objective

Cuprate high temperature superconductors (HTS) with a wide variation of superconducting transition temperature are having a common feature of the origin of superconducting pairs in the two dimensional planes **[1-3]**. However, coupling between such planes makes several HTS a three dimensional system. Detection of the Berezinskii - Kosterlitz - Thouless (BKT) phase transition in any HTS is really challenging research. Recently development of the BKT transition involves numerous unresolved questions. Nonlinear variation of current-voltage (*IV*) characteristics in HTS has drawn significant attention in analysing transport data of the HTS by following the basic idea the BKT and other theories capable of microscopic understanding of the order - disorder phase transition. The present thesis focuses on how we can make an advancement in analysing and applying the BKT phase transition observed in cuprates and apply other theories of vortex phase such as the Fisher-Fisher-Huse (FFH) scaling theory to understand nonlinearity of *IV* below superconducting phase transition.

1.1.1 Berezinskii - Kosterlitz - Thouless (BKT) phase transition:

The concepts of the BKT phase transition is formulated in the context of 2D-XY model **[4-6]**. Berezinskii proposed a theoretical work based on the low temperature behaviour of a 2D superfluid **[4]**. A thermodynamic model of topological order related to the quasi-long range order in low temperature states of two dimensional (2D) systems was introduced by Kosterlitz and Thouless **[5]**. In 2D system the phase transition from quasi long range order to disordered phase is named as the BKT transition. Primarily it was believed that the BKT phase transition is restricted only in 2D systems. Later the idea of BKT transition has been very successfully extended and tailored in anisotropic quasi-2D superconducting systems **[7-10]**. The layered structure HTS exhibits quasi-2D as well as 3D character due to its weakly coupled conducting CuO_2 planes. The superconducting state is characterized by a complex order parameter having an amplitude and phase. The superconducting state is considered as phase ordering of cooper pairs. In HTS, phase fluctuations have a huge impact due to its quasi-2D structure and low density of cooper pairs. To study phase fluctuation effect the position dependent order parameter can be considered as $\Psi(r) = \Psi_0 e^{i\phi(r)}$, where Ψ_0 represents amplitude and $\phi(r)$ represents position dependent phase. The distributions of phase variable associated with the cooper pair is known to be responsible for the origination of the BKT phase transition. The layered

superconducting cuprate system exhibits the BKT phase transition even in presence of very high thermal fluctuations. The BKT transition is related to the point to point variation of the phase variable in space. In zero magnetic field condition vortex state is formed by the phase variable of a superconducting pair. Usually in type-II superconductors the vortices are formed due to the flux quantization. A different class of vortex system based in the BKT theory is associated in our present research. The vortices of different origin including the phase gradient needs intensive research to have an idea about the commonalities of phase transition in the context of several superconducting systems. The BKT phase transition is related to the vortex - antivortex unbinding at the temperature known as the BKT phase transition temperature, T_{BKT} **[5]**. The BKT phase transition can be described in the context of the dissociation of bound vortex-antivortex pairs into unbound vortices rather than vortex generation. Bound vortex-antivortex pairs have lower energies and lower entropy than free vortices. At T_{BKT} the unbinding of vortices are different from the concept of depinning of vortices in type-II superconductors. T_{BKT} can be tuned in different superconducting systems. Individual CuO_2 layers and their coupling play a very crucial role in the BKT phase transition in layered superconducting cuprates. The BKT phase transition is observed in both bulk polycrystalline samples and single crystal below the onset of superconducting transition temperature, T_c **[11]**. Our main objective is to understand how we can implement the ideas of the BKT

phase transition in zero field transport properties of several superconducting systems.

1.1.2 Sample Selection:

It is observed that few non-Cu-based superconductors exhibit comparatively low transition temperature in which the BKT phase transition may be investigated **[12, 13]**. Detection of the BKT phase transition in layered structure anisotropic bulk cuprate superconductors is an important step in our present study. The occurrence of the BKT phase transition can be investigated in rare earth (RE) based layered superconducting cuprate system. In HTS doping can be provided either by changing oxygen content from copper oxide chain or by chemical substitution. Superconductivity is discovered in electron doped cuprates and theoretically it is proposed that hole carriers may be essential for superconductivity in the oxide superconductors **[14]**. We have selected several undoped RE (Gd, Nd and Eu) based HTS samples, electron doped and hole doped REBCO samples. Substitution of Ce at the RE site enormously affects the carrier concentration of superconductors. The physical properties such as the transition temperature, the normal state properties and several parameters related to the superconducting phase transitions are affected by the substitution of Ce. We are interested to investigate the possible nature of the BKT phase transition and nature of variation

of the superfluid phase stiffness (SPS) in several chosen doped HTS samples. Generally changes in physical properties of the pure superconducting cuprate systems are being compared with the electron doped systems. To understand how change in carrier concentration affects SPS in HTS, we have chosen $Gd_{1-x}Ce_xBa_2Cu_3O_{6.9}$ superconductors with x = 0.0, 0.1, 0.2 and 0.3. The pure sample is labeled as S1 (GBCO) with x = 0.0 and Ce-doped samples are labeled as (GCBCO) S2, S3 and S4 with x = 0.1, 0.2 and 0.3 respectively. A hole doped sample $Nd_{0.7}Ca_{0.3}Ba_2Cu_3O_{7-\delta}$ labeled as S5 (NCBCO) is prepared to understand the resistive states in HTS around T_{BKT} following a suitable theory in the zero field condition. To check the impact of SPS on data collapsing followed by suitable theory in zero field condition a system $Eu_{1-x-y}Ca_xCe_yBa_2Cu_3O_{7-\delta}$ (ECCBCO) is chosen in which (i) the pure one is labeled as S6 (EBCO) with x = 0.0, y = 0.0; (ii) hole doped sample is labeled as S7 (ECBCO) with x = 0.3, y = 0.0; (iii) co-doped samples are labeled as (ECCBCO) S8, S9, S10 and S11 with x = 0.3, y = 0.05; x = 0.3, y = 0.1; x = 0.3, y = 0.15 and x = 0.3, y = 0.2 respectively. Following the idea of the BKT phase transition which is usually applicable for 2D superconducting systems whether the occurrence of second order BKT phase transition may be possible in a 3D cuprate superconducting system we have chosen several co-doped $Nd_{1-x-y}Ca_xCe_yBa_2Cu_3O_{7-\delta}$ (NCCBCO) superconductors. Co-doped samples are labeled as S12, S13 and S14 with x = 0.3, y = 0.1; x = 0.3, y = 0.15 and x = 0.3, y = 0.2 respectively.

1.1.3 Detection of the Berezinskii - Kosterlitz - Thouless (BKT) phase transition in vortices:

The BKT phase transition is a topological phase transition in which bound vortex excitation pairs unbind at a critical temperature T_{BKT} **[4, 5]**. The type of this phase transition is different from conventional Landau symmetry breaking phase transition **[15]**. There is no symmetry breaking order parameter on either side of this transition **[4, 5, 15]**. There exists a change in the behaviour of the two point correlation function. All thermodynamic quantities remain continuous at all derivative orders across the transition. For studying the BKT phase transition thin superconducting films became the main experimental realization. A lot of effort has been done to understand the nature of the BKT transition in various systems and it is expected to be universal in nature. The BKT phase transition plays a crucial role to determine different superconducting properties such as resistivity and superfluid density of a 2D superconductors as well as the HTS with weak interlayer coupling **[16]**.

Generally dealing with a vortex system in which the phase vectors are considered to form vortices within the BKT framework needs detection of the phase transition between different vortex states. In the zero field condition vortices form the vortex states by the positional variations of the phase angles of

superconducting pairs. At low temperature existing vortex states are bound pairs and unbinding happens at a higher temperature, T_{BKT}. Vortex states and phase transition can be detected by using several experimental techniques **[17, 18]**. The BKT transitions have been detected experimentally in several systems such as trapped two dimensional Bose gases, liquid helium films, superconducting Josephson junctions, 2D atomic hydrogen **[19-21]**.

The nonlinearity in current-voltage (*IV*) characteristics of anisotropic bulk superconducting systems in zero magnetic field can be explained within the BKT framework to understand the nature of the vortex states. The study of nonlinear behaviour in *IV* characteristics in zero field in several superconducting systems gives the idea to determine the existence of the BKT phase transition temperature, T_{BKT}. In different superconducting systems below T_c the BKT phase transition is associated with a power exponent η following the equation;

$$V = aI^{\eta} \qquad \ldots\ldots\ldots\ldots\ldots\ldots (1.1)$$

where a is constant **[4, 5]**. The exponent η explains the nonlinear behaviour of *IV* characteristics and η (T) undergoes an abrupt change at a particular temperature, T_{BKT} below T_c **[4, 5]**. There exists several techniques to obtain the power exponent η **[22, 23]**. Each *IV* curve at different T for different superconducting systems can be fitted by using the power law equation (1.1) and the BKT exponent η can be extracted for each case. Below T_{BKT} the *IV* characteristics are nonlinear in nature

for $\eta > 1.0$ and nonlinear to linear transformation in *IV* occurs at T_{BKT} above which the *IV* curves are linear as η becomes 1.0 in zero field.

The BKT phase transition in superconductors is usually detected from a discontinuous jump in the SPS, J_s (T) from a finite value below T_{BKT} to zero above it **[24]**. It can be observed via the direct measurements of penetration depth as a function of T, λ (T). In a superconducting system the BKT transition can also be detected from a nonlinear exponent of the *IV* characteristics below the superconducting critical temperature **[25]**.

1.1.4 Crystal Structure:

A typical structure of unit cell of $REBa_2Cu_3O_{7-\delta}$ (RE = Rare Earth) is shown in **Figure 1.1** containing two CuO_2 planes and a single CuO chain. Each CuO_2 plane consists of a square lattice of Cu and oxygen atoms. Excess oxygen content, δ, is sensitive in controlling the superconducting properties of RE-123 systems. Variation of δ from 1.0 to 0.0 may affect the structure of the RE-123 system from the tetragonal to orthorhombic symmetry **[26]**. The typical lattice parameters of an orthorhombic REBCO are a = 3.82 Å, b = 3.89 Å and c = 11.68 Å. The number of CuO_2 planes and CuO chains in a unit cell affects the superconducting properties of cuprates. CuO chains act as a charge reservoir and supplies charge

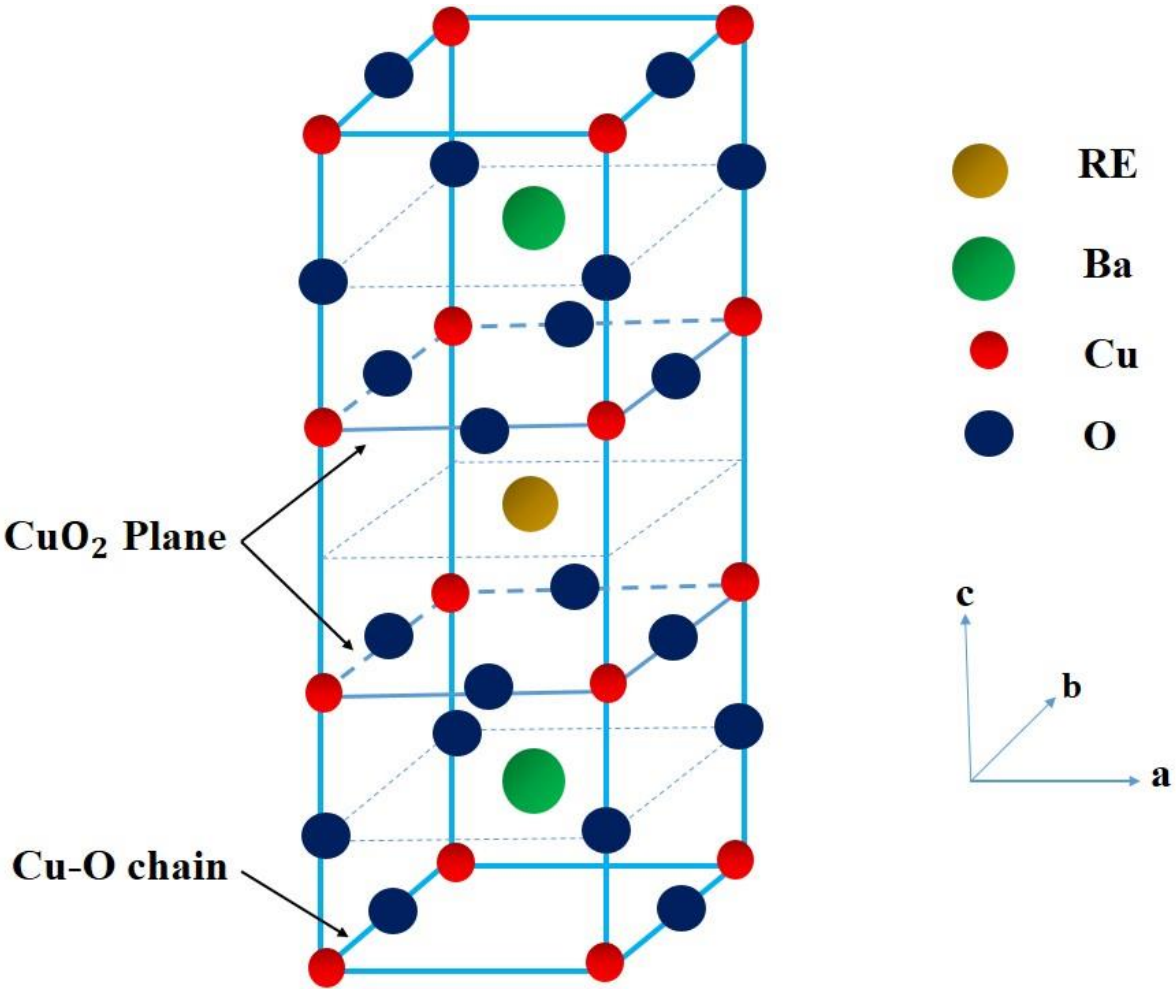

Figure 1.1 Unit cell structure of oxygen deficient $REBa_2Cu_3O_{7-\delta}$ (RE = Rare Earth).

carriers to the CuO_2 planes. In layered cuprates CuO_2 planes play a crucial role for the origin of superconductivity as the charge carriers in CuO_2 planes are responsible for the formation of Cooper pairs. Charge carrier density in CuO_2 planes influences the onset critical temperature T_c of superconducting cuprates. The superconducting current carried by pairs remain mostly in the CuO_2 planes.

However, tunnelling of pairs between two layers are also important. In RE-123 system the estimated distance between two CuO_2 planes is 3.2 Å. The estimated distance between CuO_2 plane and CuO chain is about 0.42 nm. The Cu atom in CuO chain is denoted as Cu (1) and in CuO_2 plane is denoted as Cu (2).

1.1.5 Superfluid Phase Stiffness (SPS):

The superfluid phase stiffness (SPS), J_s is an important physical quantity for superconductors. The concept of SPS is very much similar to the concept of 'spin rigidity' or 'spin stiffness' and it is a finite quantity for superconductor. Here, stiffness represents rigidity of phase of the superconducting order parameter. The superfluid density, n_s is known to be proportional to the SPS, J_s. The SPS of a superconducting system can be well understood with the help of *IV* characteristics below the transition temperature. The nonlinear to linear transformation of *IV* characteristics with temperature can be described by the extracted exponent η and hence the change of SPS. The stiffness of the superconducting order parameter gets affected by the phase fluctuation **[27, 28]**. In the HTS at $T < T_c$ the phase fluctuations play an important role for the reduction of n_s because the modified SPS of the condensate **[27]**.n_s is an inherent property of the HTS and it is also known to be proportional to the superconducting electron density at zero temperature. A universal property between the superconducting transition

temperature, T_c and n_s is proposed by Uemera relation **[29]**. n_s can be measured by a two-coil mutual inductance apparatus **[17, 30]**. To calculate n_s one can directly measure λ. From the muon-spin-relaxation measurements the magnetic field penetration depth λ can be determined **[18]**.

An enough strong thermal superconducting phase fluctuations can break the coherence of the superfluid **[27]**. The ability to carry supercurrent of the superconducting state is measured by the SPS **[27].** The SPS of a superconducting system is related to the phase coherence **[31]**. Quasiparticle excitations can be responsible for the reduction of the superfluid density at low temperatures **[32]**. In underdoped BSCCO superconductor linear scaling can also be achieved between T_c and superfluid density **[33]**. To understand the behaviour and nature of SPS it is necessary to know the features of *IV* characteristics below the critical temperature of superconductors **[23, 34]**. For the determination of J_s (T) the BKT exponent η (T) is extracted from the *IV* curve at each temperature. In addition, the existence of the BKT transition and the vortex phase unbinding can be explained by the variation of the SPS with T **[35]**.

The nonlinearity in *IV* curve and electron concentration in cuprates are related but it is unclear how it controls the SPS by order of magnitude. From nonlinearity in *IV* one can get an idea of J_s. It is very complex to study the dependence of SPS on doping content and temperature in the HTS which generally differs from the

standard results of the BCS approach [36]. In several superconducting systems doping dependent n_s has been studied [37]. Low valued n_s has also been observed in cuprates [38]. Suppression of the SPS have been studied in electron doped cuprates [39]. The nature of SPS with temperature has also been studied in composite systems [40].

Doping of Ce at the rare earth site affects its carrier concentration which influences the superfluid properties in superconducting state. To study the sensitiveness of the SPS in electron doped cuprate superconductor in zero field condition is one of the areas of research interest. Ambegaokar-Halperin-Nelson-Siggia (AHNS) model has been used to understand the variation of the SPS with T in different composite systems [40]. Within the BKT framework the dependence of the SPS of Ce doped cuprates can be studied by using the AHNS theory. According to AHNS the SPS, J_s (T) can be extracted by using the following equation,

$$J_s(T) = (\eta(T) - 1)T/\pi \quad \ldots\ldots\ldots\ldots\ldots\ldots (1.2)$$

in which η (T) is the exponent at T [34]. Nonlinearity in IV characteristics signifies a finite SPS below T_{BKT} in cuprates [41]. J_s and n_s are two closely related quantities. In two dimensional layered cuprate system n_s is expressed as the number of super-carriers per unit area of CuO_2 layers. Considering the fact that J_s and n_s are proportional to each other, n_s per m^2 can be estimated by using the formula

$$n_s = J_s\left(\frac{4K_B m^*}{\hbar^2}\right) \quad \text{..... (1.3)}$$

for different superconducting systems, where K_B is the Boltzman constant, m^* is the electron effective mass and $m^* = 2m_e, m_e$ is the electron mass, ħ is the reduced planck's constant **[36]**. In cuprates within each cell of thickness d = 11.68 Å there are two strongly coupled CuO_2 layers, here the unit cell size is considered along the c direction. n_s per m^3 can be obtained by using the conversion formula

$$n_s^{2D} = n_u d n_s^{3D} \quad \text{..... (1.4)}$$

where n_u represents the total number of unit cells in measured sample **[42]**. To calculate the total volume of the bulk type rectangular bar shaped sample which we use, we take the typical value of length (l) = 6.36 mm, width (w) = 2.27 mm and thickness (t) = 0.6 mm of bar shaped sample as a representative. By taking the typical lattice parameters of RE-123 cuprate system as a = 3.82 Å, b = 3.89 Å and c = 11.68 Å, volume of each unit cell, $V = 3.82 \times 3.89 \times 11.68$ Å^3 can be calculated. Thus the total number of unit cell, n_u present in our bar shaped used sample can be estimated around 4.99×10^{19}.

Attempts to scale *IV* characteristics above and below T_{BKT} can be made in superconducting systems by using a suitable scaling function. The possibility of the collapsing of the *IV* data of several cuprate systems has been analysed by using suitable scaling model. The impact of the SPS on data collapsing has been investigated within the BKT framework following the AHNS theory.

1.1.6 Fisher, Fisher and Huse (FFH) theory:

In the HTS in presence of strong magnetic fields and low temperatures the nature of the mixed state is an enrich area of research. Disorder plays a crucial role in the static and dynamic properties of the mixed state in type-II superconductors. The translational long-ranged order of the Abrikosov flux lattice is destroyed when disorder pins the vortex lines leading to a low voltage at small currents **[43-45]**. The destruction of the translational long-ranged order of the flux lattice due to disorder leads the possibility of existence of a sharp equilibrium phase boundary which separates the normal phase at high temperatures and fields from the low *T* flux creep phase **[44]**. In a bulk disordered system there exist a sharp equilibrium phase boundary below which a new thermodynamic phase exists, known as a vortex-glass (VG) phase **[46]**. The evidence of the freezing of a vortex-fluid (VF) phase into an ordered Abrikosov - flux lattice is given from the data of torsional-oscillator experiments **[47]**. In the dirty superconductors glass phases have been suggested in numerical simulations on Josephson-junction-array models and within a mean-field treatment of a granular superconductor **[48]**. From the work of Larkin and Ovchinnikov it is shown that the long-range crystalline order of the Abrikosov lattice is destroyed and it freezes into a truly ordered solid phase **[49]**. With the contradiction of the flux creep model, at low *T* in a bulk system it is argued that in the presence of an applied field the vortex

lines should freeze into a new VG phase which is supposed to be a true superconductor with $R_L = 0$ **[46, 50, 51]**. The idea of the detection of possible existence of VG transition temperature, T_g comes from dc voltage versus current (*IV*) data **[52]**. Fisher has proposed that these *IV* curves should collapse onto two scaling functions on either side of the transition **[53, 54]**. A common test of scaling has been proposed by Fisher, Fisher and Huse (FFH) by data collapsing of *IV* measurements relating the electric field *E* to an applied current density *J* **[53]**. At low temperature in the HTS Fisher has explained the possible existence of a new thermodynamic phase known as the vortex glass phase in presence of the magnetic field **[46]**. According to the FFH model, in presence of magnetic field a new transition temperature, T_g, the vortex glass transition temperature lies below T_c, the onset of superconducting transition temperature. T_g basically defines the transition from the VG state to the VF state. The FFH describes VG state as the conversion of the long range translational order of Abrikosov type vortex lattice into freezed amorphous type short range order vortex state at low *T* in presence of the magnetic field. The VG state undergoes a continuous phase transition while increasing *T* due to the high thermal fluctuations resulting the melting of a VG to form VF state. The VG state is more ordered state and VF state is supposed to be more disordered. In addition, around the phase transition the FFH describes the static critical exponent, *v* and the dynamic critical exponent, *z* which characterizes the size of the phase fluctuations and the lifetime of fluctuations respectively **[55]**.

The FFH theory can be applied in different class of vortex system based on the BKT theory in which vortices are generated from the distribution of the phase field of the individual pairs. The origin of these vortices are different from the vortices formed as a result of flux quantization observed in type-II superconductors. Within the BKT framework without applying an external magnetic field below T_c the *IV* curves can be analysed following FFH scaling theory. The approach of scaling is very successful to determine the nature of the phase transition and to analyse experimental data around the phase transition in different electron and hole doped superconducting systems **[56, 57]**. To understand the nature of observed resistive states in the zero field condition and the SPS as a function of T around T_{BKT} within the FFH framework an attempt of scaling on *IV* characteristics of bulk superconducting HTS has been made by choosing T_{BKT} as T_g. Both T_{BKT} and T_g are associated with the two different order disorder phase transitions. Above T_{BKT} vortex-antivortex unbinding happens and this state is considered as disordered state. Below T_{BKT} the paired vortices form an ordered state. According to FFH theory, below T_g the VG state is considered as ordered state and above T_g the VF state is considered as disordered state. Identification of T_g is not possible from the analysis of *IV* characteristics within BKT framework in zero field condition. From the analogy of order disorder transition T_{BKT} can be labelled as T_g. Therefore, it is reasonable to use T_{BKT} as an analogous transition of T_g in the zero field study within the BKT framework to follow the FFH scaling theory.

1.2 Outline of the thesis

There are several unresolved aspects of superfluidity in the vicinity of the BKT phase transition in HTS in zero field condition. We have mostly focused our research to understand the nature of the SPS around the phase transition within BKT framework in pure and doped RE-123 (RE = Rare Earth) systems. An exponent η related to BKT theory can be extracted and it is suitable for the explanation of nonlinear to linear transformation of *IV* curves. The nonlinearity in *IV* curves can be related to SPS by following AHNS theory which helps to understand several aspects of *IV* curves in zero field condition. Change in carrier concentration affects the SPS in RE-123 system. FFH theory has explained the broadening of resistive phase transition in presence of magnetic field **[53]**. Our present research work focuses to understand the nature of resistive states within the BKT framework following FFH scaling theory in HTS in zero field condition. The behaviour of the SPS around T_{BKT} has been determined following FFH formulation in HTS.

Our detail research works have been presented in several chapters. In **Chapter 2**, we have explained in detail the solid state synthesis technique, sample characterization technique and the four probe technique by showing several schematic diagrams. In **Chapter 3**, we have studied the effects of the change in

SPS with the carrier concentration in S1 and S4. In **Chapter 4**, we have studied the applicability of the FFH scaling to the *IV* characteristics to understand the resistive states within the BKT framework in S5 without presence of externally applied magnetic field. In **Chapter 5**, we have determined the static and dynamic critical exponent related to FFH scaling model in S6, S7, S8, S9, S10 and S11 respectively. The variation of critical exponents with temperature has been studied within the BKT framework and the impact of the SPS on collapsing of transport data has also been checked in each case. In **Chapter 6**, we have investigated the broadening of the BKT phase transition in different 3D superconducting systems S12, S13 and S14 respectively. The future direction of our present research work has also been clarified.

1.3 References

[1] J. G. Bednorz, K. A. Muller, Z. Phys. B 64 (1986) 189.

[2] A. Schilling, M. Cantoni, J. D. Guo, H. R. Ott, Nature 363 (1993) 56.

[3] J. Orenstein, A. J. Millis, Science 288 (2000) 468.

[4] V. L. Berezinskii, Zh. Eksp.Teor. Fiz. 61 (1971) 1144.

[5] J. M. Kosterlitz, D. J. Thouless, J. Phys. C 6 (1973) 1181.

[6] I. Maccari, L. Benfatto, C. Castellani, Phys. Rev. B 96 (2017) 060508 (R).

[7] Y. Matsuda, S. Komiyama, Phys. Rev. B 48 (1993) 10 498.

[8] S. Martin, A. T. Fiory, R. M. Fleming, G. P. Espinosa, A. S. Cooper, Phys. Rev. Lett. 62 (1989) 677.

[9] D. H. Kim, A. M. Goldman, J. H. Kang, R. T. Kampwirth, Phys. Rev. B 40 (1989) 8834.

[10] H. H. Wen, P. Ziemann, H. A. Radovan, S. L. Yan, Europhys. Lett. 42 (1998) 319.

[11] M. A. Dubson, S. T. Herbert, J. J. Calabrese, D. C. Harris, B. R. Patton, J. C. Garland, Phys. Rev. Lett. 60 (1988) 1061.

[12] J. Nagamatsu, N. Nakagawa, T. Muranaka, Y. Zenitani, J. Akimitsu, Nature 410 (2001) 63.

[13] Y. Kamihara, T. Watanabe, M. Hirano, H. Hosono, J. Am. Chem. Society 130 (2008) 3296.

[14] F. Marsiglio, J. E. Hirsch, Phys. Rev. B 41 (1990) 6435.

[15] Ze Hu et al., Nat. Commun. 11 (5631) (2020).

[16] P. A. Lee, N. Nagaosa, X. G. Wen, Rev. Mod. Phys. 78 (2006) 17.

[17] S. J. Turneaure, T. R. Lemberger, J. M. Graybeal, Phys. Rev. B 63 (2001) 174505.

[18] C. Bernhard, J. L. Tallon, Th. Blasius, A. Golnik, Ch. Niedermayer, Phys. Rev. Lett. 86 (2001) 1614.

[19] D. J. Bishop, J. D. Reppy, Phys. Rev. Lett. 40 (1978) 1727.

[20] D. J. Resnick, J. C. Garland, J. T. Boyd, S. Shoemaker, R. S. Newrock, Phys. Rev. Lett. 47 (1981) 1542.

[21] A. I. Safonov, S. A. Vasilyev, I. S. Yasnikov, I. I. Lukashevich, S. Jaakkola, Phys. Rev. Lett. 81 (1998) 4545.

[22] V. Ambegaokar, B. I. Halperin, D. R. Nelson, E. D. Siggia, Phys. Rev. B 21 (1980) 1806.

[23] P. Minnhagen, O. Westman, A. Jonsson, P. Olsson, Phys. Rev. Lett. 74 (1995) 3672.

[24] D. R. Nelson, J. M. Kosterlitz, Phys. Rev. Lett. 39 (1977) 1201.

[25] B. I. Halperin, D. R. Nelson, J. Low. Temp. Phys. 36 (1979) 599.

[26] P. Benzi, E. Bottizo, N. Rizzi, J. Cryst. Growth 269 (2004) 625.

[27] V. J. Emery, S. A. Kivelson, Nature (London) 374 (1995) 434.

[28] J. Orenstein, A. J. Millis, Science 288 (2000) 468.

[29] Y. J. Uemura et al., Phys. Rev. Lett. 62 (1989) 2317.

[30] S. J. Turneaure, T. R. Lemberger, J. M. Graybeal, Phys. Rev. Lett. 84 (2000) 987.

[31] O. Simard, C. D. Hebert, A. Foley, D. Senechal, A. M. S. Tremblay, Phys. Rev. B 100 (2019) 094506.

[32] J. Mesot et al., Phys. Rev. Lett. 83 (1999) 840.

[33] J. Yong, M. J. Hinton, A. McCray, M. Randeria, M. Naamneh, A. Kanigel, T. R. Lemberger, Phys. Rev. B 85 (2012) 180507R.

[34] V. Ambegaokar, B.I. Halperin, D.R. Nelson, E.D. Siggia, Phys. Rev. Lett. 40 (1978) 783.

[35] G. Venditti, J. Biscaras, S. Hurand, N. Bergeal, J. Lesueur, A. Dogra, R. C. Budhani, Mintu Mondal, John Jesudasan, Pratap Raychaudhuri, S. Caprara, L. Benfatto, Phys. Rev. B 100 (2019) 064506.

[36] I. Bozovic, X. He, J. Wu, A.T. Bollinger, Nature 536 (2016) 309.

[37] S. Steers, T. R. Lemberger, J. Draskovic, Phys. Rev. B 94 (2016) 094525.

[38] M. V. Feigel'man, L. B. Ioffe, Phys. Rev. B 92 (2015) 100509.

[39] T. Sk, A. K. Ghosh, AIP Advances 10 (2020) 065117.

[40] T. Sk, A. K. Ghosh, J. Low Temp. Phys. 198 (2020) 224.

[41] P. Das, A. K. Ghosh, Physica C 548 (2018) 27.

[42] L. Benfatto, C. Castellani, T. Giamarchi, Phys. Rev. B 77 (2008) 100506 (R).

[43] P. W. Anderson, Y. B. Kim, Rev. Mod. Phys. 36 (1964) 39.

[44] A. I. Larkin, Zh. Eksp. Teor. Fiz. 58 (1970) 1466.

[45] A. I. Larkin, Yu. N. Ovchinnikov, J. Low Temp. Phys. 34 (1979) 409.

[46] M. P. A. Fisher, Phys. Rev. Lett. 62 (1989) 1415.

[47] P. L. Gammel, L. F. Schneemeyer, J. V. Waszczak, D. J. Bishop, Phys. Rev. Lett. 61 (1988) 1666.

[48] S. John, T. Lubensky, Phys. Rev. B 34 (1986) 4815.

[49] A. I. Larkin, Yu. N. Ovchinnikov, J. Low Temp. Phys. 34 (1979) 409.

[50] C. Ebner, D. Stroud, Phys. Rev. B 31 (1985) 165.

[51] S. John, T. Lubensky, Phys. Rev. B 34 (1986) 4815.

[52] M. E. Fisher, Rev. Mod. Phys. 70 (1998) 653.

[53] D. S. Fisher, M. P. A. Fisher, D. A. Huse, Phys. Rev. B 43 (1991) 130.

[54] D. A. Huse, D. S. Fisher, M. P. A. Fisher, Nature 358 (1992) 553.

[55] D. R. Strachen, M. C. Sullivan, C. J. Lobb, Proc. SPIE 4811 (2002) 65.

[56] R. H. Koch, V. Foglietti, W. J. Gallagher, G. Koren, A. Gupta, M. P. A. Fisher, Phys. Rev. Lett. 63 (1989) 1511.

[57] M. C. Sullivan, R. A. Isaacs, M. F. Salvaggio, J. Sousa, C. G. Stathis, J. B. Olson, Phys. Rev. B 81 (2010) 134502.

Chapter 2

Experimental technique

Several anisotropic bulk type high T_c cuprate superconductors have been prepared and characterized in order to study the superfluid phase stiffness (SPS) within the Berezinskii-Kosterlitz-Thouless (BKT) framework in zero field condition. Sample synthesis has been performed by conventional solid state synthesis method **[1-4]**. All prepared samples have been characterized by using X-ray diffraction (XRD) method and Scanning electron microscope (SEM). Four probe method has been used to measure resistivity, ρ of the sample as a function of temperature (T) by using a closed cycle cryogenerator. Current-voltage (IV) measurements have been carried out for the current range of 100 nA to 5 mA by using the four probe technique at several temperatures. In this chapter we discuss about the experimental techniques that we have used. The outline of our experimental research work is discussed here in detail.

2.1 Solid State Synthesis Method:

Our target is to prepare polycrystalline bulk superconducting quality sample. We have prepared all the samples by using conventional solid state synthesis technique **[5-7]**. In this process firstly typical mixtures of stoichiometrically weighted pure oxides are used to make pellets. Samples are sintered several steps under required sintering conditions followed by several intermediate grindings. Annealing has been performed of the prepared samples in oxygen atmosphere under suitable condition.

The prepared sample series are

(i) $Gd_{1-x}Ce_xBa_2Cu_3O_{6.9}$ (GCBCO) with x = 0.0, 0.1, 0.2 and 0.3 (S1, S2, S3, S4),

(ii) $Nd_{0.7}Ca_{0.3}Ba_2Cu_3O_{7-\delta}$ (δ = 0.1)(NCBCO) (S5),

(iii) $Eu_{1-x-y}Ca_xCe_yBa_2Cu_3O_{7-\delta}$ (δ = 0.1) (ECCBCO) with x = 0.0, y = 0.0 (S6); x = 0.3, y = 0.0 (S7); x = 0.3, y = 0.05 (S8); x = 0.3, y = 0.1 (S9); x = 0.3, y = 0.15 (S10); x = 0.3, y = 0.2 (S11) and

(iv) $Nd_{1-x-y}Ca_xCe_yBa_2Cu_3O_{7-\delta}$ (δ = 0.1) (NCCBCO) with x = 0.3, y = 0.1 (S12); x = 0.3, y = 0.15 (S13) and x = 0.3, y = 0.2 (S14).

The charge carrier density per CuO_2 plane, x' can be estimated for S1-S14 in the underdoped regime from T_c measurements by using the formula

$$1 - \frac{T_c}{T_{c,max}} = 82.6\,(x' - 0.16)^2 \qquad \ldots\ldots\ldots\ldots\ldots\ldots (2.1)$$

with $T_{c,max}$ = 92K, generally found for cuprates **[8]**. The charge carrier density can be measured by performing the Hall effect measurements **[9, 10]**. Instead of performing hall measurement, we have estimated the charge carrier density, *n* of respective samples by using the formula

$$n = \frac{2x'}{V} \qquad \ldots\ldots\ldots\ldots\ldots\ldots (2.2)$$

where x' is the charge carrier density per CuO_2 plane and *V* is the volume of the cuprate unit cell containing the CuO_2 planes **[9, 10]**. By taking the typical lattice parameters of RE-123 cuprate system as a = 3.82 Å, b = 3.89 Å and c = 11.68Å, $V = 3.82 \times 3.89 \times 11.68$ $Å^3$ can be calculated.

To synthesize (i) GCBCO we have used highly pure powders of Gd_2O_3, $BaCO_3$, CuO and CeO_2 with proper stoichiometry. Our target is to substitute Ce with different concentrations at the Gd site to get electron doped Gd-123 series. To synthesize (ii) NCBCO we have used stoichiometric amount of highly pure powders of Nd_2O_3, $BaCO_3$, $CaCO_3$ and CuO. To synthesize Eu-based co-doped HTS we have prepared (iii) ECCBCO by using highly pure powders of Eu_2O_3, $BaCO_3$, $CaCO_3$, CeO_2 and CuO in proper stoichiometry. To synthesize Nd-based

co-doped HTS we have prepared (iv) NCCBCO by using highly pure powders of Nd_2O_3, $BaCO_3$, $CaCO_3$, CeO_2 and CuO in proper stoichiometry.

Firstly the stoichiometrically weighted required sample powders are mixed properly. We have used agate mortar and pestle to grind the powder mixture for more than three hours to get better homogeneity. The mixture is then transformed into small pellets of diameter nearly 8.0 mm and thickness nearly around 0.6 mm by using a dice and a high pressure hydraulic press. Calcination of these sample pellets has been performed around the temperature 850°C for 24 hours in a high temperature tube furnace. The carbonates are decomposed into oxides and release the produced CO_2 during calcination. After calcination the sample pellets are again ground and mixed by the mortar and pestle and the mixture is again transformed into pellets. The sample pellets are then sintered around the temperature 930°C for 24 hours. RE-123 (RE = Rare Earth) phase has formed during sintering. To get the final prepared sample sintering has been performed for several times of these sample pellets with intermediate grinding. The oxygen stoichiometry in RE-123 unit cell can be controlled during annealing. Annealing has been performed in the tube furnace in oxygen atmosphere maintaining the temperature around 450°C for 24 hours. During calcination, sintering and annealing the samples are cooled down by normal cooling process.

2.2 Scanning Electron Microscope (SEM)

The schematic diagram of Scanning Electron Microscope (SEM) is shown in **Figure 2.1**. SEM is used to get information about sample surface topology, morphology and compositions **[11-13]**. A focused beam of high energy electrons is used in SEM to generate signal at the surface of solid specimen. The signals are derived from electron-sample interactions which reveal the informations about the sample including external morphology, chemical composition and grain orientations of the sample. SEM consists of an electron source, an anode, condenser lens, scanning coil, objective lens, sample holder and detectors. SEM works in the accelerating voltage range in between 1.0 kV to 30.0 kV. In SEM the accelerated electrons carry kinetic energy which is dissipated as a variety of signals produced by electron-sample interactions when the incident electrons are decelerated in the sample. These signals consist of secondary electrons, backscattered electrons, diffracted backscattered electrons, photons, visible light and heat. Secondary electrons and backscattered electrons are responsible for imaging of the samples. Secondary electrons are mostly effective to illustrate contrasts in composition in multiphase samples. Inelastic collisions occur in between the incident electrons and the electrons in discreate orbitals of atoms in the sample to produce generation of X-ray. X-rays of a fixed wavelength is produced as the excited electrons return to lower energy states. Thus

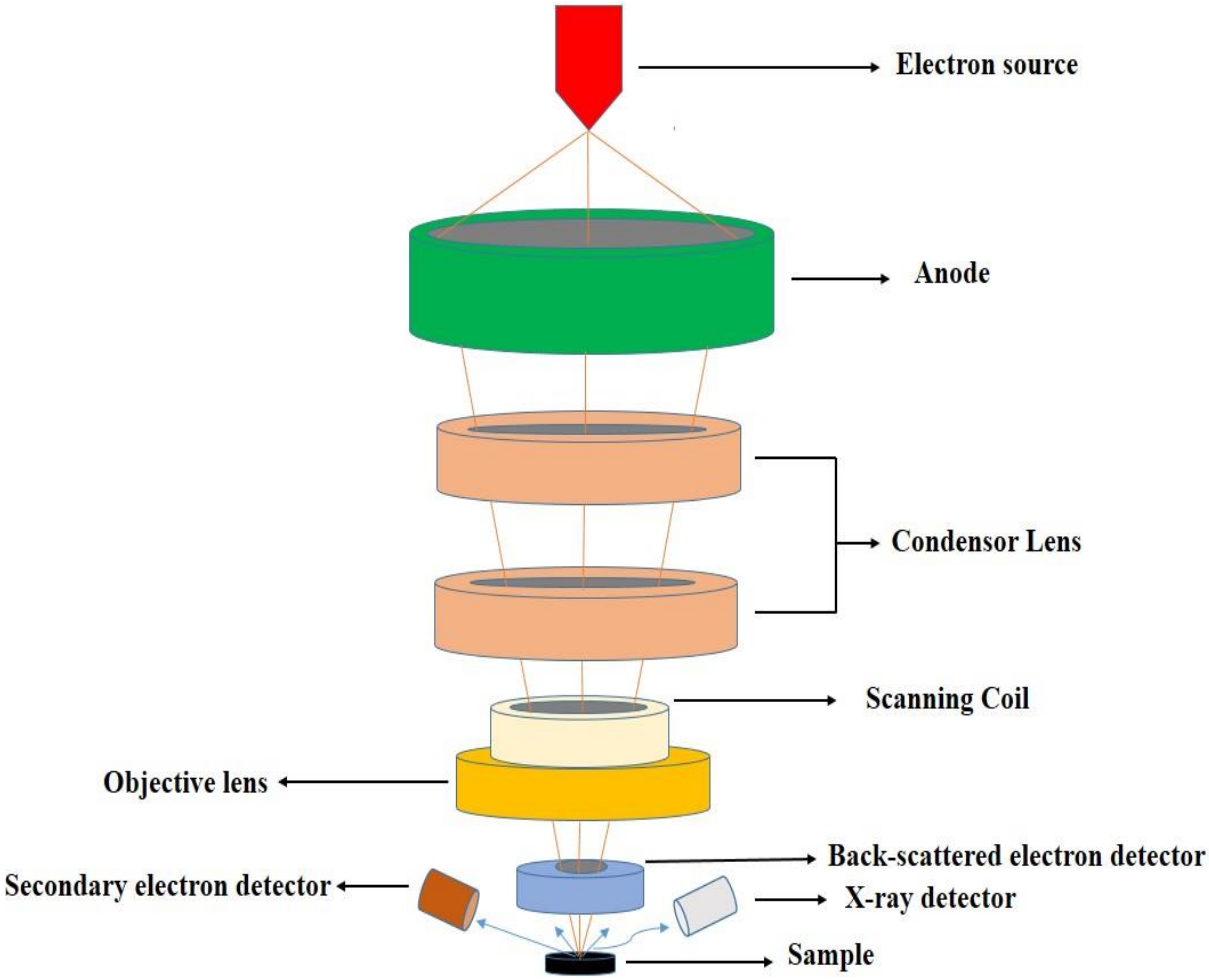

Figure 2.1 Schematic diagram of Scanning Electron Microscope (SEM).

characteristic X-rays are produced for each element. SEM analysis is a non-destructive process. As X-rays generated by electron interactions do not lead to any kind of volume loss of the sample, it is possible to analyse same sample repeatedly. We have used field emission scanning electron microscope (FESEM) to study the surface morphology of our samples. The main difference in between the scanning electron microscope (SEM) and field emission scanning electron

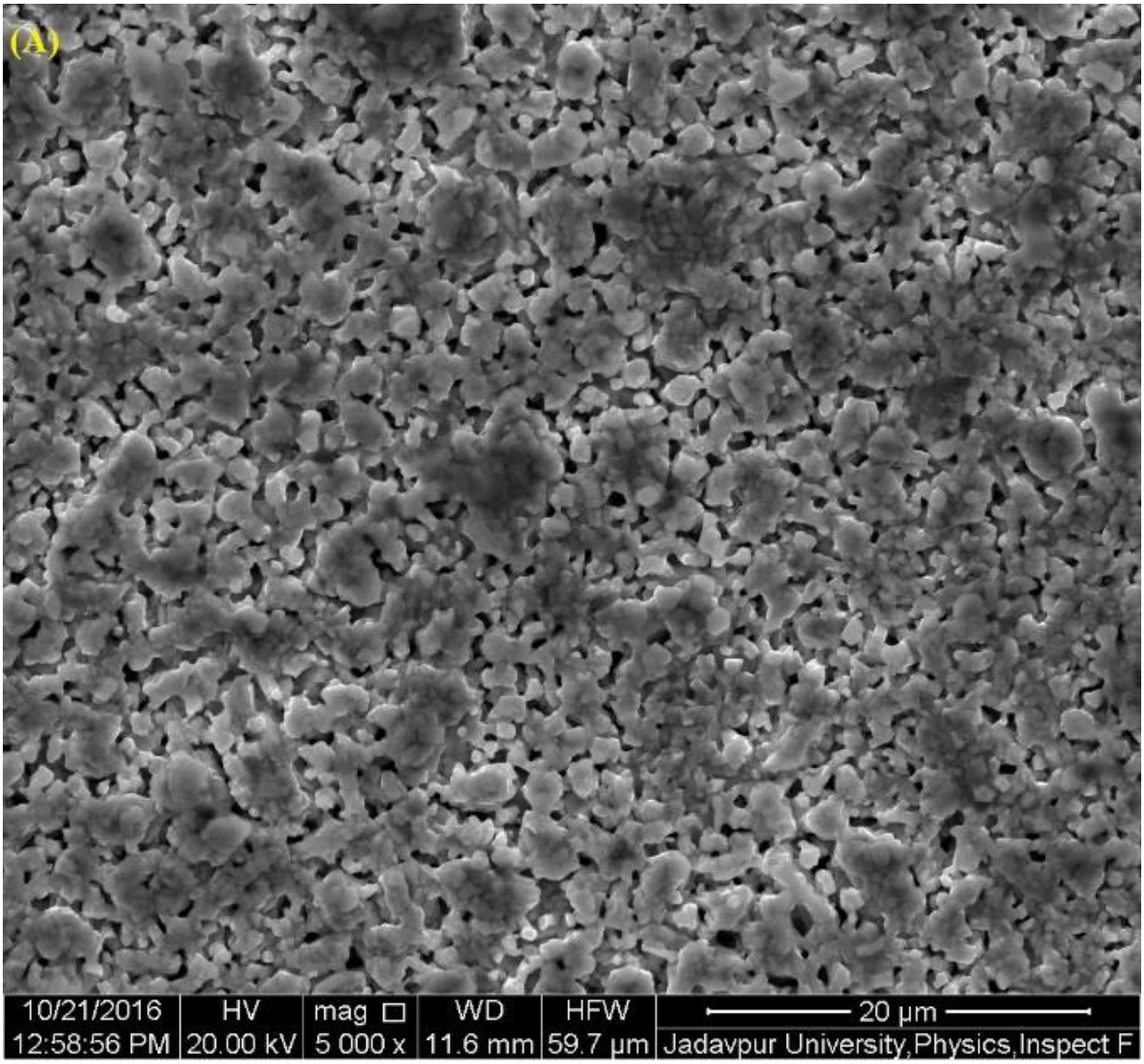

Figure 2.2 (A) Representative Scanning electron micrograph of $GdBa_2Cu_3O_{6.9}$ (S1).

microscope (FESEM) is the type of the emitter used. In FESEM the emission happens by placing the filament in a huge electrical potential gradient. A wire of tungsten having very sharp tip is used as a field emission source. The small tip radius is nearly 100 nm and the significance of the sharp tip is that an electric

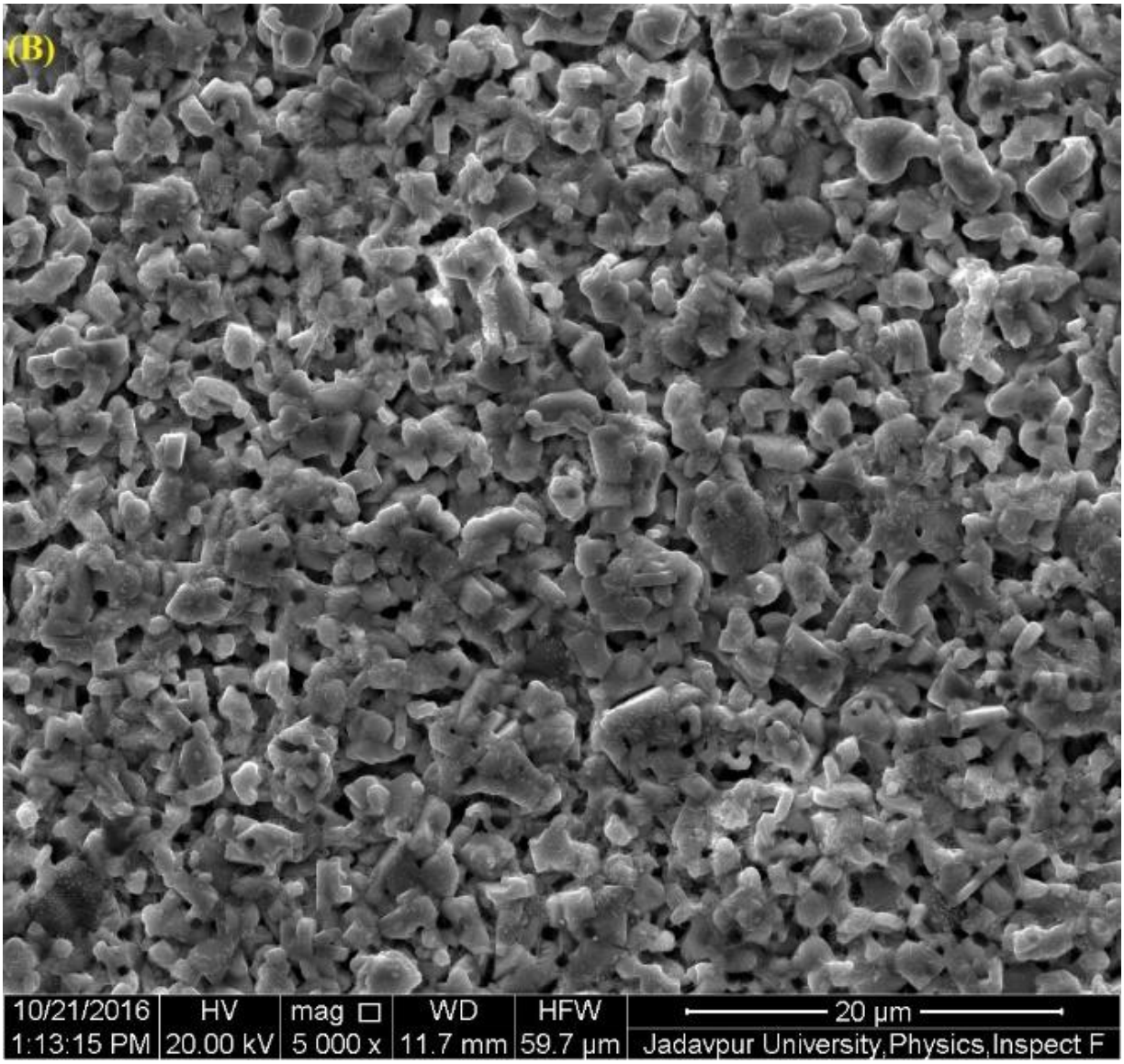

Figure 2.2 (B) Representative Scanning electron micrograph of $Gd_{0.9}Ce_{0.1}Ba_2Cu_3O_{6.9}$ (S2).

field can be concentrated to an extreme level, it becomes so large that the material work function is lowered and electrons can leave the cathode field emitter. The apparatus requires extremely high vacuum in the column of the microscope. The

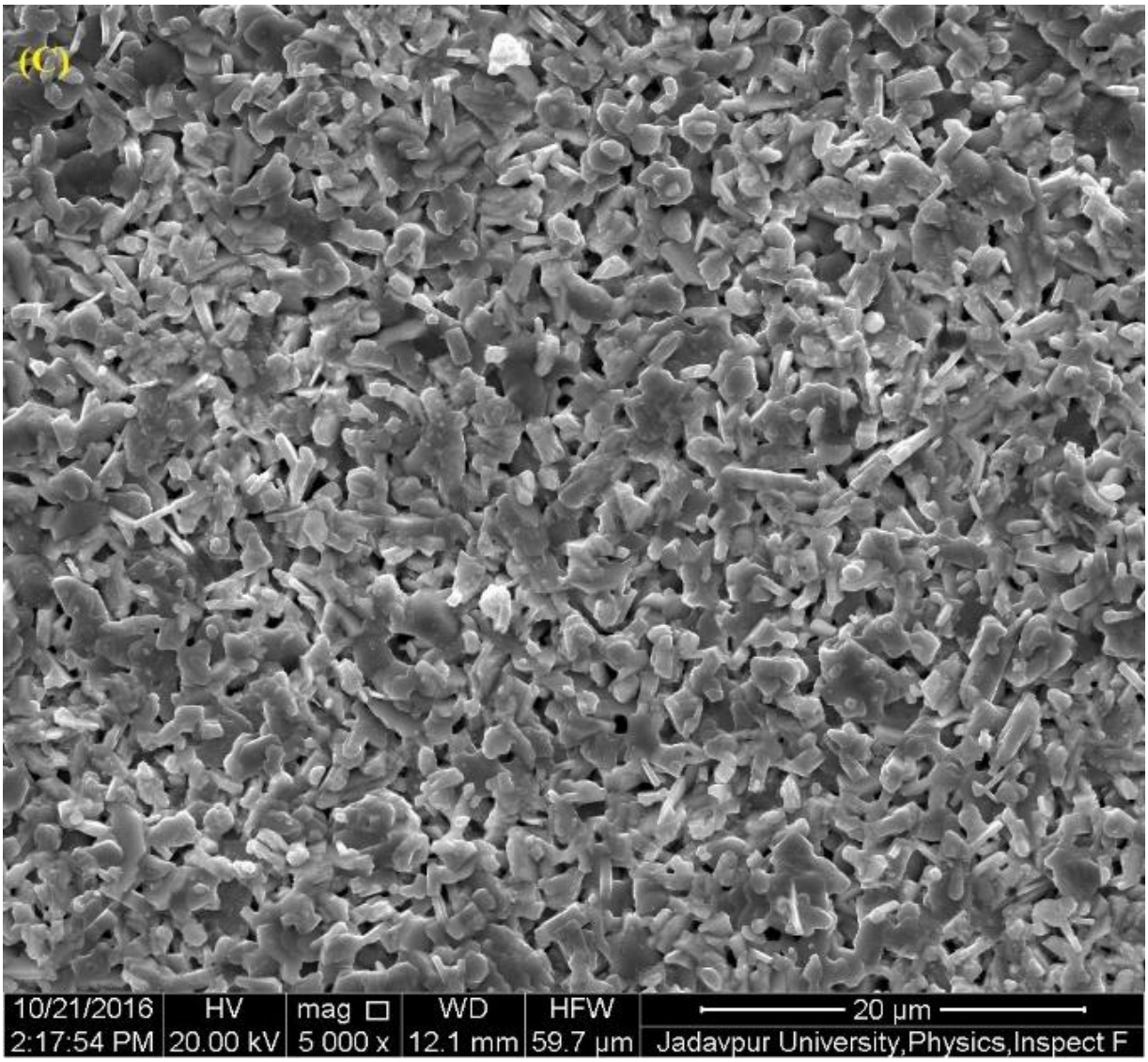

Figure 2.2 (C) Representative Scanning electron micrograph of $Gd_{0.8}Ce_{0.2}Ba_2Cu_3O_{6.9}$ (S3).

anode helps to accelerate the electron stream towards the sample. The diameter of electron beam produced by the source must be smaller than the feature on the specimen surface. Therefore, it is necessary to condense the electron beam. The

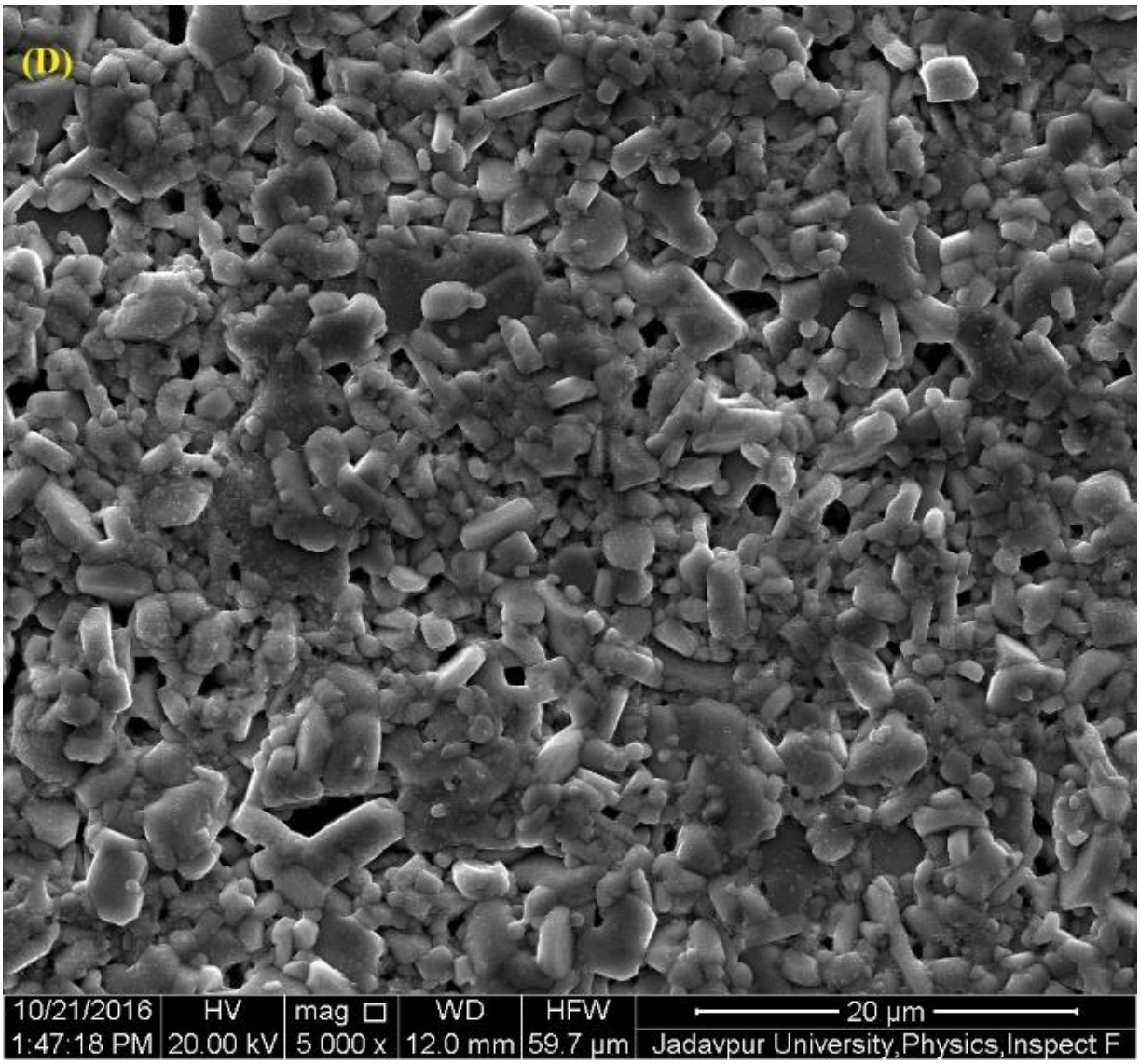

Figure 2.2 (D) Representative Scanning electron micrograph of $Gd_{0.7}Ce_{0.3}Ba_2Cu_3O_{6.9}$ (S4).

size of the electron beam is defined by the condenser lens. The diameter of the electron beam is determined by the current in the condenser. A low current results in a small diameter, a higher current results a larger beam. The scanning coils

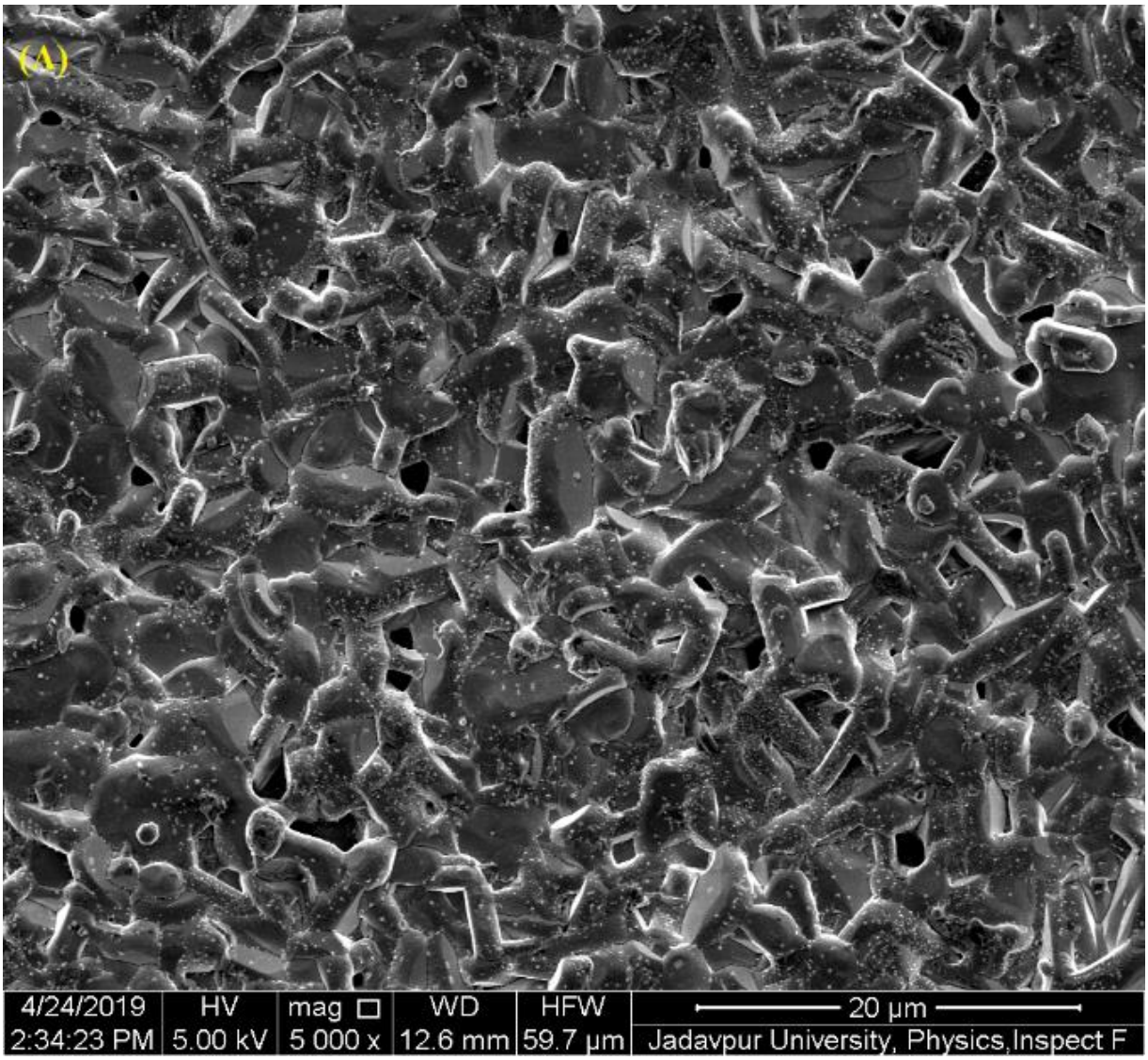

Figure 2.3 (A) Representative Scanning electron micrograph of $Nd_{0.7}Ca_{0.3}Ba_2Cu_3O_{7-\delta}$ (S5).

help to deflect the electron beam over the object in the *X* and *Y* axes. Above the objective lens the position of the electron beam is controlled by the scanning coils. The image formation on the monitor occurs in synchrony with this scan movement. On the object the smaller the scanned region, the larger the selecting

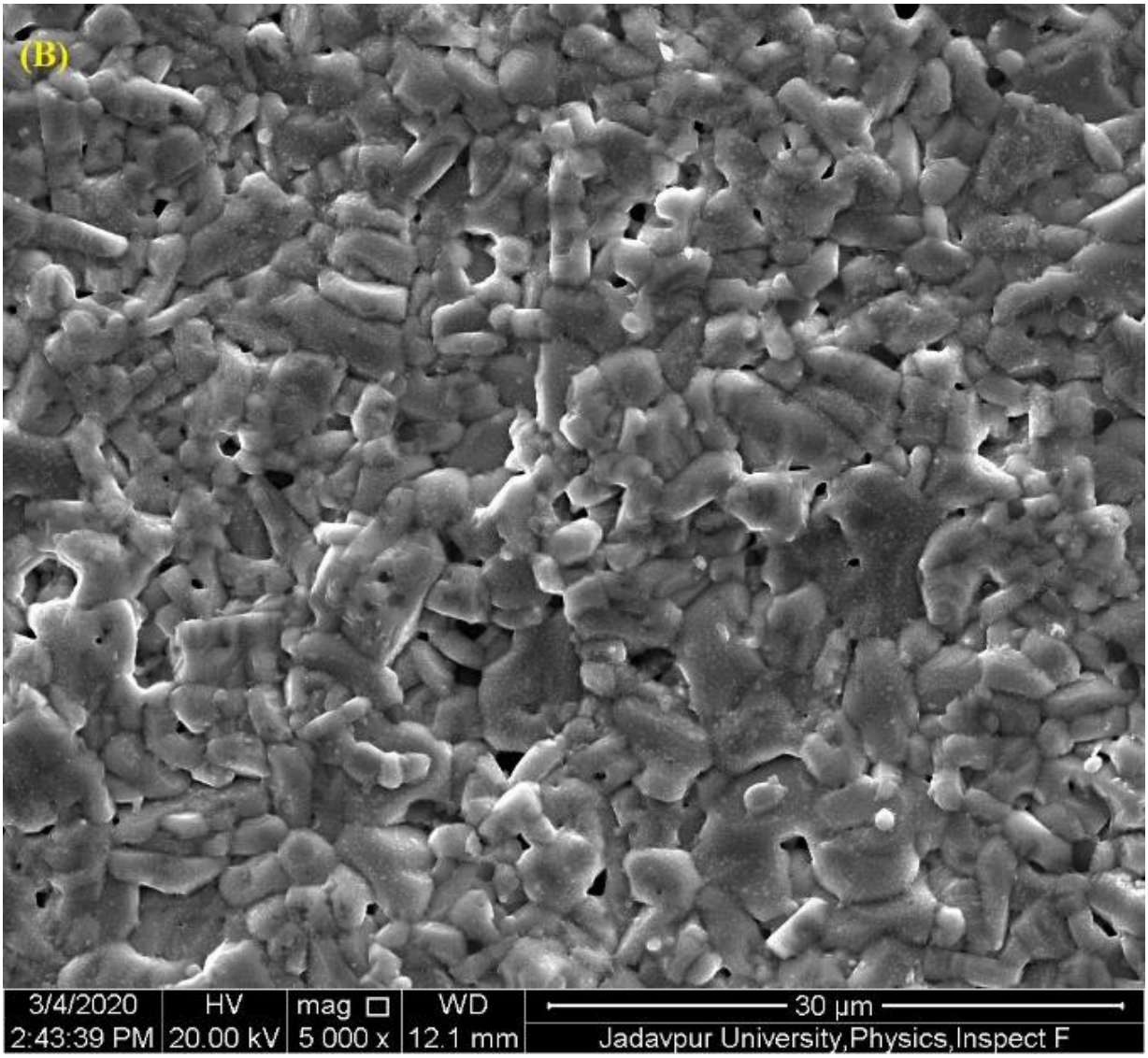

Figure 2.3 (B) Representative Scanning electron micrograph of $EuBa_2Cu_3O_{7-\delta}$ (S6).

magnification becomes at a constant window size. Data are collected by selecting an area of the surface of the sample and a two dimensional image is generated displaying the spatial variations in these properties. The objective lens is used to

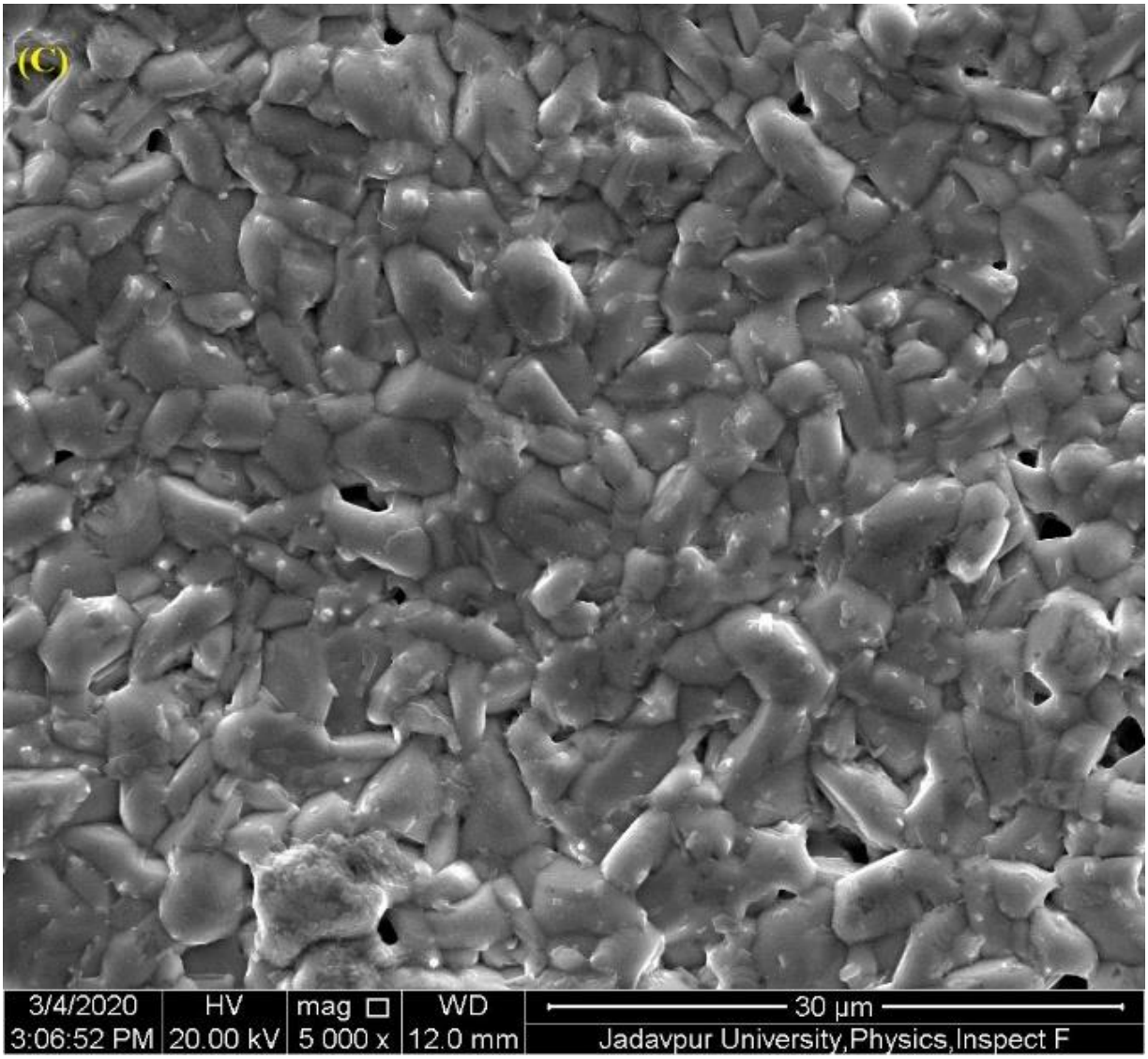

Figure 2.3 (C) Representative scanning electron micrograph of $Eu_{0.65}Ca_{0.3}Ce_{0.05}Ba_2Cu_3O_{7-\delta}$ (S8).

focus the electron beam on the object. The objective lens needs to apply a greater force to deflect the electron beam at a short working distance. The shortest working distance produces the smallest beam diameter and better resolution. The scanning electron microscope detects two different types of electrons which are

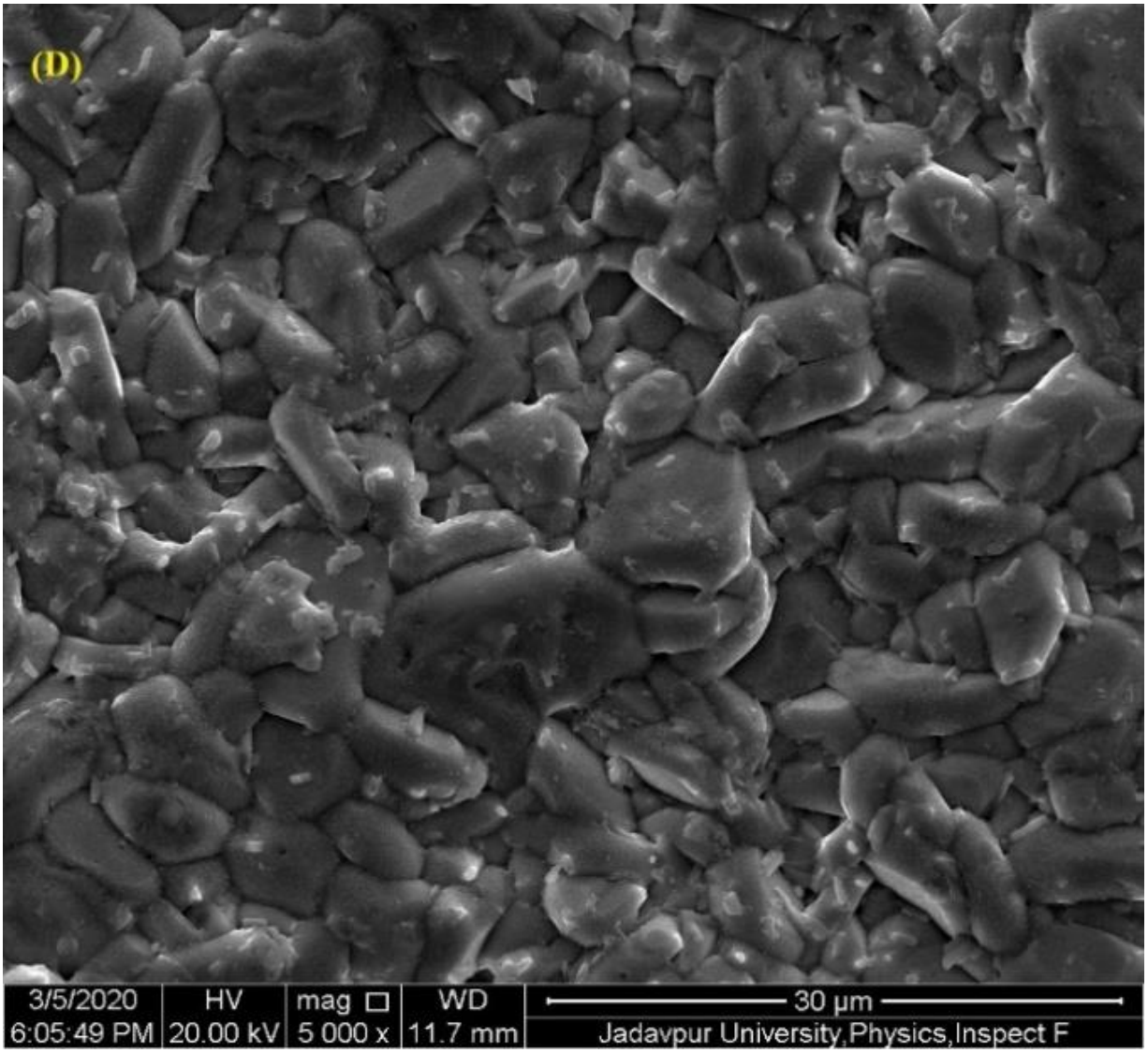

Figure 2.3 (D) Representative scanning electron micrograph of $Eu_{0.6}Ca_{0.3}Ce_{0.1}Ba_2Cu_3O_{7-\delta}$ (S9).

backscattered electrons and secondary electrons. Both type of electrons carry different informations about the sample. The backscattered electrons originate from the deeper region of the sample and the secondary electrons originate from the surface part of the sample. The backscattered electrons are the result of elastic

collisions between the incident electrons and the atoms of the sample. Secondary electrons originate due to the inelastic interactions between the electron beam and the atoms of the sample. In the backscattered electron imaging higher signal is produced when electrons are scattered by larger atoms of the sample. The number of backscattered electrons received by the detector is proportional to the atomic number of the scatterer. From backscattered electron imaging one can get informations about crystallography, sample topography etc. The amount of energy carried by backscattered electrons and secondary electrons are different. Secondary electrons have lower energy than backscattered electrons and secondary electron imaging provides information about the sample surface. Backscattered electrons are actually the incident electrons emitted from the field emission gun and it excite an atomic electron in the sample by losing own energy. After gaining energy these excited electrons from the atoms of the sample reach to the surface undergoing collisions and finally escape from the surface. These escaped electrons are called secondary electrons which carry the informations about the topography of the sample surface. Detectors are used for detecting secondary electrons and backscattered electrons separately. Elastically scattered electrons are detected by the backscattered electron detector. In SEM the Everhart-Thornley detector is used as both type of electron detector. Typical energy range of high energetic backscattered electrons is in between 50 eV and 5000 eV. Low energetic secondary electrons have energy value typically 50 eV or less. In SEM one can magnify the selected portion of the sample maximum

around 50,000 times. SEM is the instrument by which one can analyze particle size as it has high resolution around 2 nm ~ 20 nm.

We have shown typical scanning electron micrographs of pure GBCO as S1, electron doped GCBCO with Ce (x = 0.1, 0.2 and 0.3) as S2, S3 and S4 in **Figure 2.2 (A), (B)**, **(C)** and **(D)** respectively. **Figure 2.3 (A)**, **(B)**, **(C)** and **(D)** shows the representative scanning electron micrographs of hole doped NCBCO with Ca (x = 0.3) as S5, pure EBCO as S6 and co-doped ECCBCO with Ca (x = 0.3) and Ce (y = 0.05, 0.1) as S8 and S9 respectively. In each case grains are randomly distributed and the grain shapes, sizes and orientations are anisotropic. The microstructures of respective samples are found to be well – separated granular nature with a distribution of the size of grains. The average grain size for different bulk type pure and doped superconducting systems from the few of mentioned samples can be estimated by using ImageJ as a representative. The estimated values of grain size of Ce doped GBCO samples are 2.35 ± 0.73 μm for Ce (x = 0.0), 2.58 ± 0.75 μm for Ce (x = 0.1) and 2.59 ± 0.89 μm for Ce (x = 0.3). It can be concluded that for bulk type polycrystalline cuprates grain size remains unaffected by electron doping. In GBCO (S1), electron doped GCBCO (S2, S3 and S4) and hole doped NCBCO (S5), compactness of the grains are poor and pores are introduced in the intergranular regions. The compactness of grains is better in co-doped ECCBCO (S8 and S9). Grains are smaller in size in GBCO

and electron doped GCBCO than in hole doped NCBCO, pure EBCO and co-doped ECCBCO. Comparatively broader grains are observed in co-doped ECCBCO (S8 and S9).

2.3 X-ray diffraction (XRD)

To study the crystal structures, unit cell dimensions, sample purity, phases of crystalline materials X-ray diffraction is commonly used technique **[14-19]**. **Figure 2.4** shows the schematic diagram of Bragg's diffraction of a crystalline sample where d_{hkl} denotes the interplaner separation between the crystal planes having miller indices (h k l), λ is the wavelength of the monochromatic radiation, θ is the angle between the incident ray and the scatter plane. The total path difference between the rays reflected back from the two adjacent planes is $2d_{hkl}\sin\theta$.

It is based on the constructive interference of monochromatic X-rays and the crystalline sample. The condition for constructive interference is the path difference must be the integral multiple of λ i.e.

$$2d_{hkl}\sin\theta = n\lambda \qquad \text{..... (2.3)}$$

where n is integral number and order of diffraction. X-rays are generated by a cathode ray tube, these X-rays are then filtered to produce monochromatic

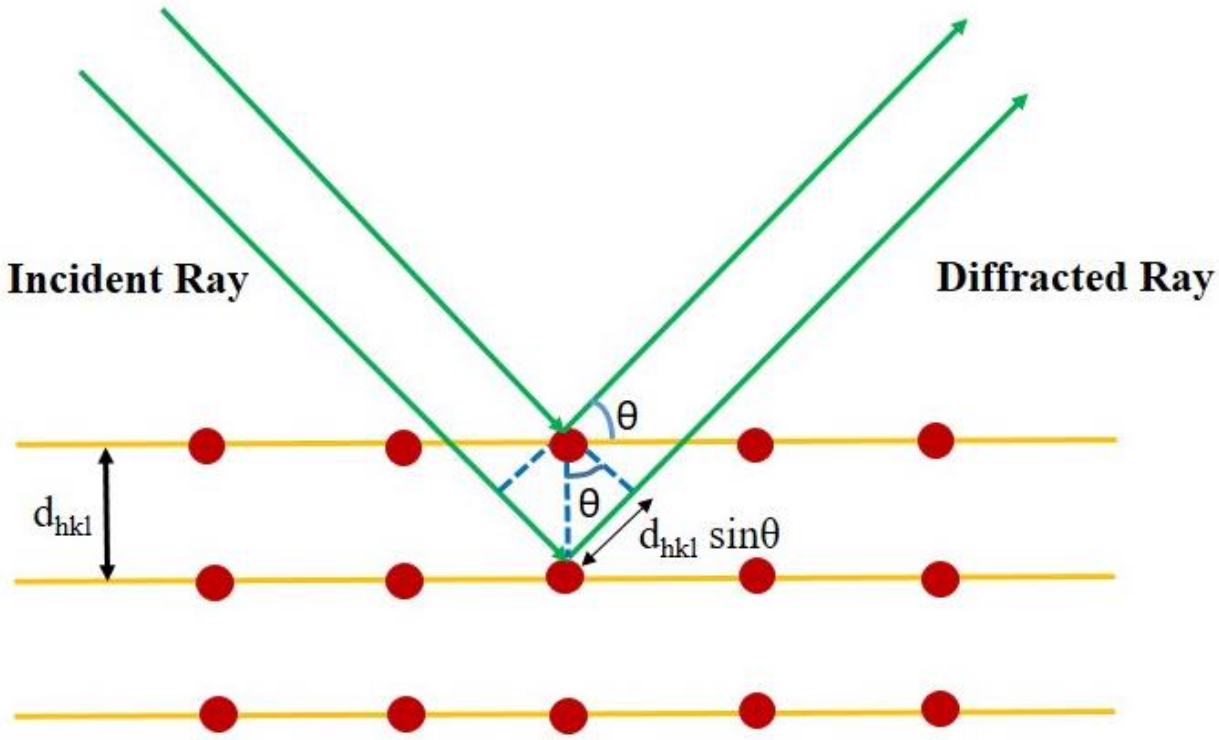

Figure 2.4 Schematic diagram of Bragg's diffraction of crystalline sample.

radiation, collimated to concentrate, and directed toward the sample. The interaction between the incident rays and the crystalline material produces constructive interference when conditions satisfy Bragg's law i.e. equation (2.3). For diffraction, the wavelength of X-ray, λ should be of the order of interplaner spacing of the crystalline material.

Figure 2.5 shows the schematic diagram of an X-ray diffractometer. X-ray diffractometer consists of three basic elements which are an X-ray tube, a sample holder and an X-ray detector. X-rays are generated in a cathode ray tube in which

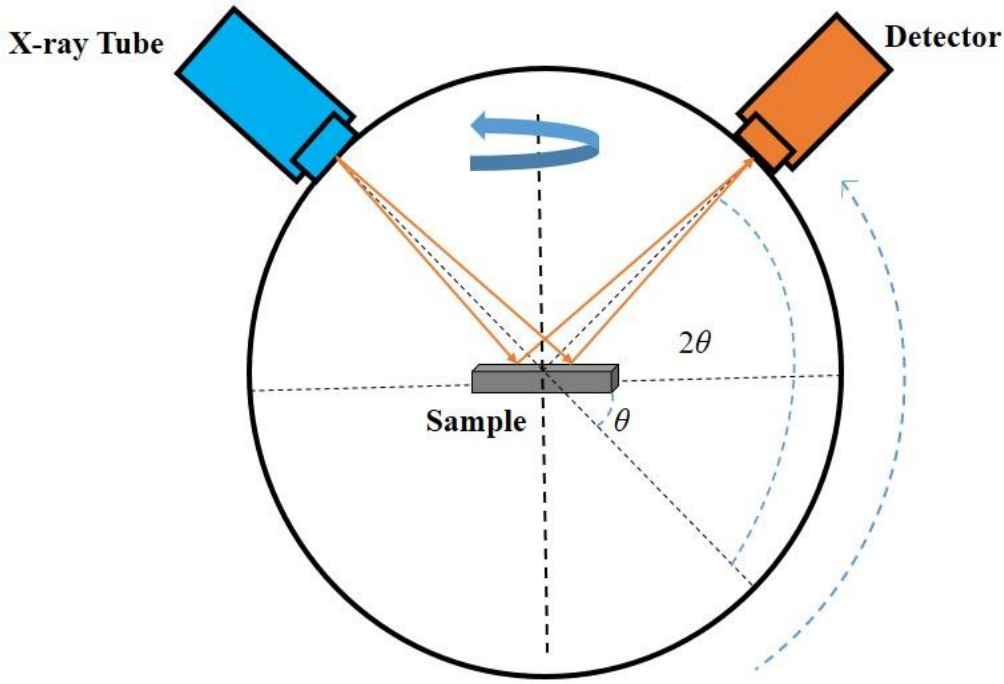

Figure 2.5 Schematic diagram of an X-ray diffractometer.

the filament is heated to produce the electrons, these electrons are accelerated toward the target by applying a voltage and are bombarded the target material. These electrons have sufficient energy to dislodge the inner shell electrons of the target material to produce characteristic X-rays. These characteristic X-ray spectra consist of several components, the most common being K_α and K_β. K_α consists of K_{α_1} and K_{α_2} in which K_{α_1} has a slightly short wavelength and twice the intensity as K_{α_2}. The wavelength of K_{α_1} and K_{α_2} are sufficiently closed so that an average of the two is used. As monochromatic X-rays are required for diffraction,

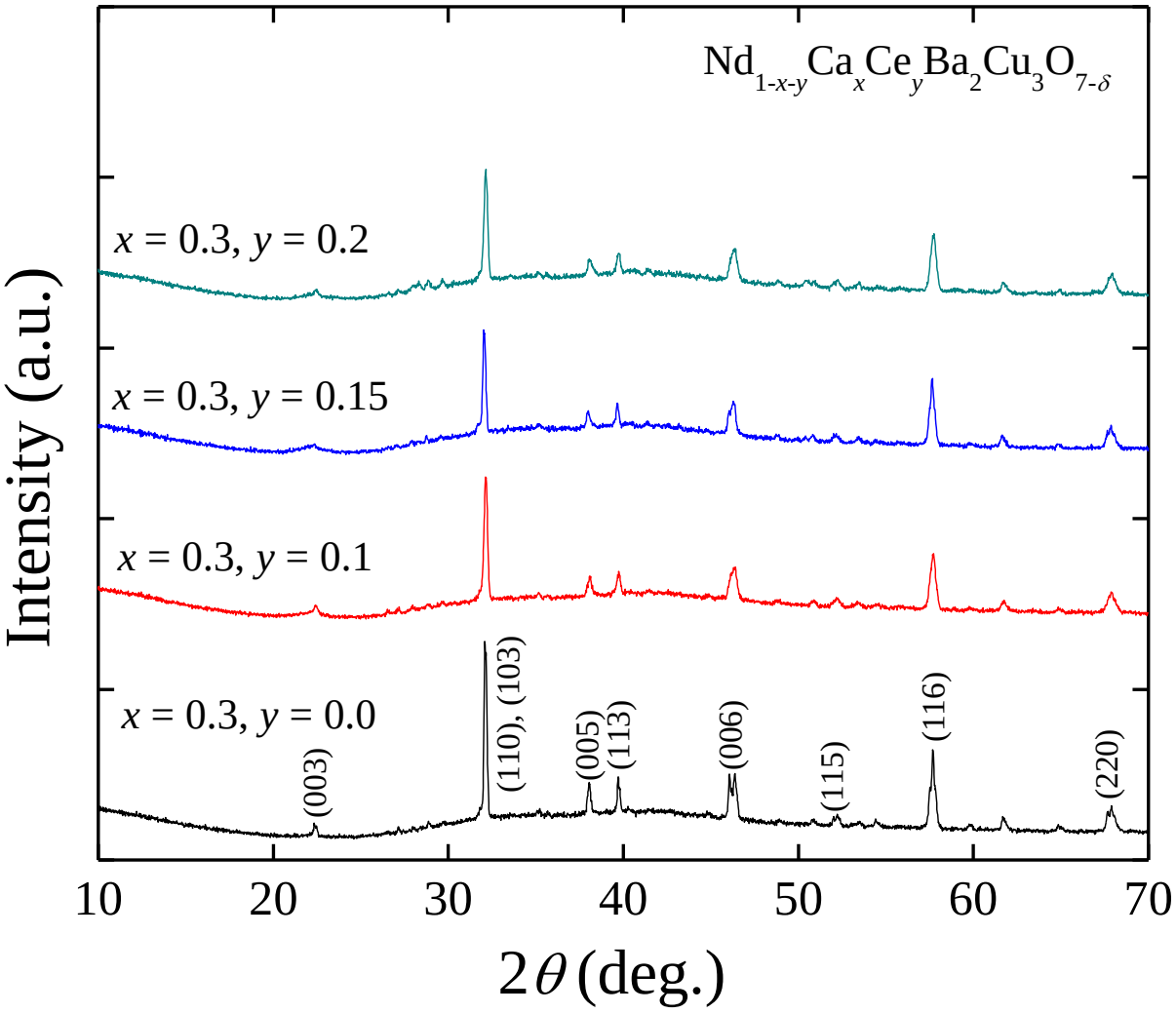

Figure 2.6 Representative X-ray diffraction patterns of $Nd_{1-x-y}Ca_xCe_yBa_2Cu_3O_{7-\delta}$ with $x = 0.3$, $y = 0.0$ (S5); $x = 0.3$, $y = 0.1$ (S12); $x = 0.3$, $y = 0.15$ (S13) and $x = 0.3$, $y = 0.2$ (S14).

the characteristic X-rays are filtered to produce monochromatic X-rays and are

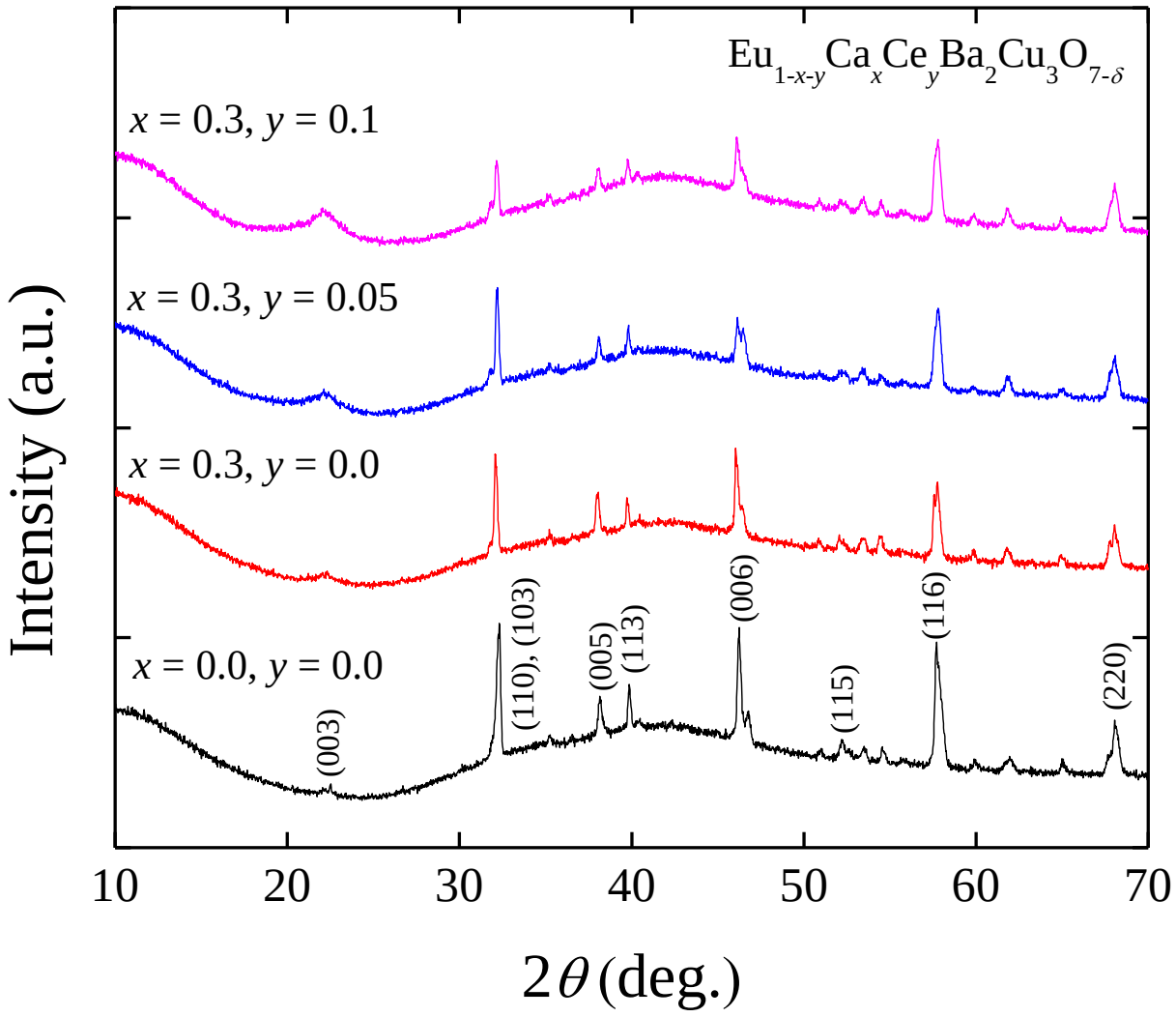

Figure 2.7 Representative X-ray diffraction patterns of $Eu_{1-x-y}Ca_xCe_yBa_2Cu_3O_{7-\delta}$ with $x = 0.0$, $y = 0.0$ (S6); $x = 0.3$, $y = 0.0$ (S7); $x = 0.3$, $y = 0.05$ (S8) and $x = 0.3$, $y = 0.1$(S9).

collimated and directed onto the sample at an angle θ. As the sample holder and detector are rotated, the intensity of the diffracted X-rays is recorded. Detector

basically rotates in a circle while the sample holder is rotated both in horizontal and vertical plane making several orientations of the crystalline planes of the sample with respect to the incident beam. When the geometry of the monochromatic incident X-ray beam impinging the sample satisfies the Bragg's condition, constructive interference occurs and a peak in the intensity occurs. The diffracted X-ray signals are recorded by the detector and are converted into count rate which is then output to a device such as a computer monitor. The geometry of the X-ray diffractometer is such that the sample rotates in the path of the collimated X-ray beam at an angle θ while the X-ray detector rotates at an angle 2θ. The instrument used to maintain the angle and rotate the sample is termed as a goniometer. Copper is the most common target material used in X-ray diffractometer. In our experimental set up (Bruker D8 Advanced X ray diffractometer), we have used Cu-K_α radiation of wavelength 1.54 Å and the angle 2θ is varied in the range from 10° to 70°.

In **Figure 2.6**, we have shown X-ray diffraction patterns of (i) hole doped Nd-123 with Ca (x = 0.3) (S5)**,** (ii) co-doped Nd-123 with Ca (x = 0.3) and Ce (y = 0.1, 0.15 and 0.2) (S12, S13 and S14) respectively. **Figure 2.7** shows the representative X-ray diffraction patterns of (i) Eu-123 (pure) (S6), (ii) hole doped Eu-123 with Ca (x = 0.3) (S7) and (iii) co-doped Eu-123 with Ca (x = 0.3) and Ce (y = 0.05, 0.1) (S8 and S9) respectively. Major peaks are labeled that

corresponds to RE-123 structure in all cases. The estimated lattice constants a = 3.93Å, b = 3.78Å and c = 11.78Å of Eu-123 system are comparable to the RE-123 system. No structural change has occurred due to doping at the rare earth site.

2.4 Four probe method

Four probe is a popular method to characterize a high T_c superconducting sample by performing a four point resistivity measurement as a function of temperature, ρ (T) to find out where the superconducting transition occurs **[20-22]**. Current-voltage (IV) characteristics of the samples are also measured by using four probe method **[20-22]**. The main advantage of using four probe method in transport measurements is to minimize the contribution of lead resistances and contact resistances.

The representative four probe contact on a sample piece is shown in **Figure 2.8.** For transport measurement we have used four probe technique with the help of a closed cycle cryogenerator (JANIS, USA). The sample is placed on a vertical oxide free copper made holder attached to the cryostat. As the sample needs to be electrically insulated from the sample holder, we have used apiezon n grease to place the sample piece on the sample holder. Apiezon n grease is electrically

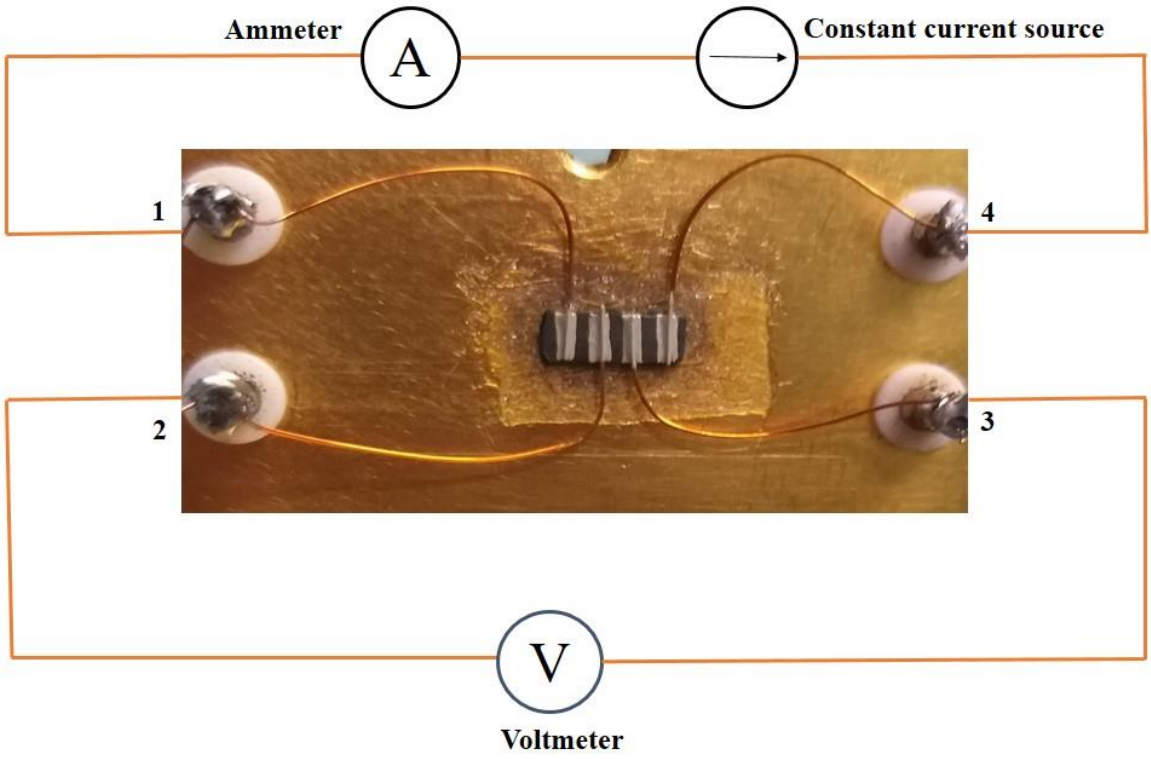

Figure 2.8 Representative four probe contact of a sample piece (RE-123) mounted on a sample holder of cryogenerator.

insulated but thermally conductive. To make four electrical connections on the sample we have used copper wire of diameter 0.24 mm. The current is passed through the two outer connections 1 and 4 (**Figure 2.8**) by a constant current source at a fixed temperature and voltage drop is measured across the two inner points of contact 2 and 3 (**Figure 2.8**) with the help of a nanovoltmeter. To make the contact we have applied silver paste on each copper wire attached on the sample surface. The voltage drop between 2 and 3 on the sample surface is measured by varying the temperature of the sample. After measuring the voltage

drop (V) across the junction 2 and 3 corresponding to the applied current (I) at particular temperature, we can get the sample resistance from $R = V/I$. We can calculate sample resistivity, ρ at a particular temperature by using the relation

$$R = \rho l_{vv}/A \qquad \text{..... (2.4)}$$

where l_{vv} is the separation between two voltage leads on the sample surface and A is the area of cross section of the used rectangular bar shaped sample piece. The area of cross section of the rectangular bar shaped sample, A = sample width (w) × sample thickness (t). Sample length (l), width (w) and thickness (t) are measured in each case by using digital vernier caliper which is a very conventional method. For each sample (S1 – S14) l_{vv} is calculated with high accuracy from the sample image file by pixel count method. For resistivity measurement we have used 1 mA fixed current at each temperature and the samples are cooled down with the help of a closed cycle cryogenerator from room temperature down to 10.0K. From the resistivity versus temperature ρ (T) plot one can obtain the value of $T_{c,onset}$ and $T_{c,R=0}$ of measured superconducting sample. During IV measurement by using the same technique we have used a current range of 100nA to 5mA at each temperature.

2.5 References

[1] T. Luty, C. J. Eckhardt, J. Am. Chem. Society 117 (1995) 2441.

[2] H. Schmalzried, Solid-State Reactions**,** Angew. Chem. Int. Ed. 2 (1963) 251.

[3] L. I. Dao-hua, H. E. Shao-fen, C. Jie, J. Cheng-yan, Y. Cheng, Mater. Sci. Eng. 242 (2017) 012023.

[4] A. Stein, S. W. Keller, T. E. Mallouk, Science 259 (1993) 1558.

[5] A. S. Sefat, Current Opinion in Solid State and Materials Science 17 (2013) 59.

[6] J. T. Vaughey, J. P. Thiel, E. F. Hasty, D. A. Groenke, Charlotte L. Stern, K. R. Poeppelmeier, B. Dabrowski, D. G. Hinks, A. W. Mitchell, Chem. Mater. 3 (1991) 936.

[7] M. Mazaheri, S. Ghasemi, A. Heidarpour, J Supercond. Nov. Magn. 28(9) (2015) 2637.

[8] J. L. Tallon, C. Bernhard, H. Shaked, R. L. Hitterman, J. D. Jorgensen, Phys. Rev. B 51 (1995) 12911.

[9] Y. Ando, A. N. Lavrov, S. Komiya, K. Segawa, X. F. Sun, Phys. Rev. Lett. 87 (2001) 017001-1.

[10] A. Stangl, A. Palau, G. Deutscher, X. Obradors, T. Puig, Sci. Rep. 11 (2021) 8176.

[11] K. C. A. Smith, C. W. Oatley, Br. J. Appl. Phys. 6 (1955) 391.

[12] A. V. Crewe, M. Isaacson, D. Johnson, Review of Scientific Instruments 40 (1969) 241.

[13] H Seiler, Journal of Applied Physics 54 (1983) R1.

[14] W. L. Bragg, Nature 90 (1912) 410.

[15] W. L. Bragg, The Structure of Some Crystals as Indicated by their Diffraction of X-rays, Proc. R. Soc. Lond. 89 (1913) 248.

[16] W. H. Bragg, W.L. Bragg, The Reflection of X-rays by Crystals, Proc. R. Soc. Lond. A. 88 (1913) 428.

[17] W. L. Bragg, The analysis of crystals by the X-ray spectrometer, Proc. R. Soc. Lond. 89 (1914) 468.

[18] I. V. Zakharchenko, M. Muhammed and K. V. Rao, Materials Science Forum 166 (1994) 91.

[19] A. Guinier, X-ray Crystallographic Technology, London, Hilger and Watts LTD. (1952) 271.

[20] D. W. F. James, R. G. Jones, J. Sci. Instrum. 42 (1965) 283.

[21] P. Das, A. K. Ghosh, Physica C 548 (2018) 27.

[22] Y. Z. Long, J. L. Duvail, M. M. Li, C. Gu, Z. Liu, S. P. Ringer, Nanoscale Res. Lett. 5 (2010) 237.

Chapter 3

Superfluid phase stiffness in electron doped superconducting Gd-123

3.1 Introduction

Current-voltage (*IV*) characteristics below the superconducting transition temperature are very important to understand several features in superfluid. Superfluid phase stiffness (SPS) is related to the nonlinearity in *IV* characteristics. The nonlinear feature has been explained by using the equation (1.1). The exponent, η has been derived in different ways **[1, 2]**. Variation of η with the temperature characterises the linear to nonlinear variation in phase transition. Sensitiveness of the superfluid density, n_s with temperature is related through the phase stiffness. SPS in several superconducting system has been studied both theoretically and experimentally to understand the nature of superfluid. Doping dependence of n_s has been studied in several superconducting systems **[3]**. Suppression of n_s on approaching the superconductor-insulator transition has been observed experimentally in underdoped $Y_{0.7}Ca_{0.3}Ba_2Cu_3O_{7-\delta}$ (Y-123). In underdoped $Bi_2Sr_2CaCu_2O_{8+x}$ (Bi-2212) n_s has been studied by using finest

control in doping level [4]. The disappearance of the superconductivity in the underdoped Bi-2212 has been attributed to the strong two dimensional quantum fluctuations in the superfluid.

In cuprate superconductor the SPS varies below the phase transition temperature depending on the superfluid areal density [5-7]. It is very unclear how the change in the carrier concentration affects the SPS and hence n_s in a superconducting system. The aspect of the change in the SPS with the carrier concentration has been studied in $Gd_{1-x}Ce_xBa_2Cu_3O_{6.9}$. We have used *IV* characteristics of the electron doped samples to extract η. An equation has been suggested by which we can understand the variation of η with T. Extracted exponents η have been used to obtain the SPS by using two different equations derived by Ambegaokar et al. [1] and Minnhagen et al. [2]. Change in the SPS as a result of the change in the carrier concentration has been discussed.

3.2 Experimental

Synthesis of $Gd_{1-x}Ce_xBa_2Cu_3O_{6.9}$ has been done by using standard solid state reaction method. We have used different concentrations x = 0.0, 0.1, 0.2 and 0.3 of Ce to get electron doped superconducting samples. Characterizations are done using X-ray diffraction (XRD) method. We have measured resistivity as a

function of temperature by using the standard four probe method and with the help of a cryogenerator (Janis, USA) **[8, 9]**. *IV* measurements have been carried out at constant temperatures around the phase transitions in the range of minimum and maximum current of 100 nA to 5.0 mA respectively. In addition, we have changed the maximum current for *IV* measurements depending on the sample resistivity at lower temperature **[10]**.

3.3 Results and discussions

We have plotted XRD patterns of $Gd_{1-x}Ce_xBa_2Cu_3O_{6.9}$ in **Figure 3.1**. Major peaks have been labeled which corresponds to Gd-123 structure in all cases. Samples are found to be in single phase. With the increase in Ce concentration we observed that ab-planes remain unaffected which is revealed in angular position of (110) lines. Typical *c* lattice constant remains almost unaffected which reveals that the separation between copper oxide planes is independent of the electron doping.

In **Figure 3.2**, we have plotted the variations of resistivity as function of temperature. $Gd_{1-x}Ce_xBa_2Cu_3O_{6.9}$ samples with x = 0.0, 0.1 and 0.3 are found to be superconducting in nature. The critical temperatures are 55.0 K, 45.9 K and 51.0 K corresponding to samples with x = 0.0, 0.1 and 0.3 respectively. In the normal state of all three samples the upturn in resistivity with T is observed. The

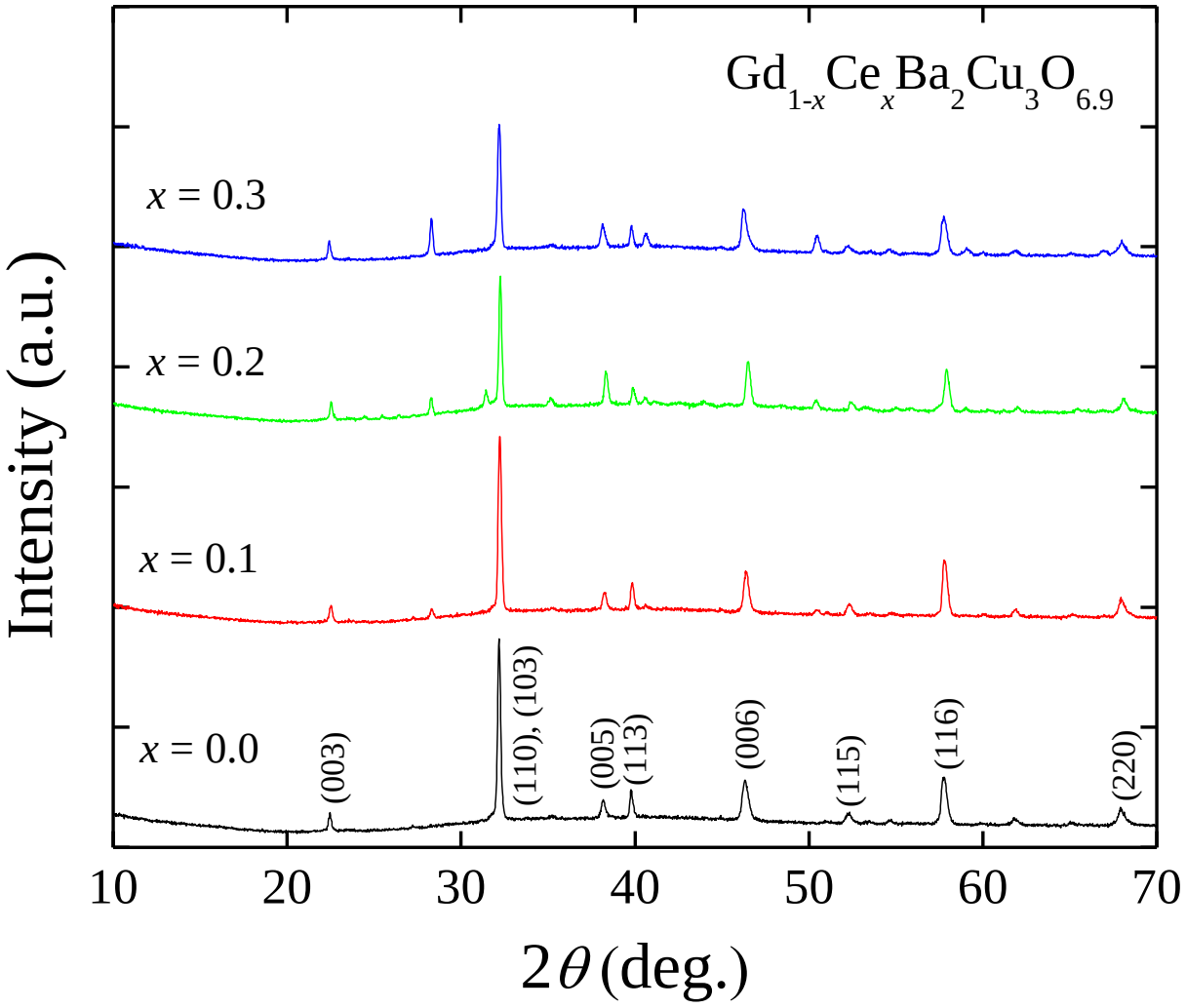

Figure 3.1 X-ray diffraction patterns of $Gd_{1-x}Ce_xBa_2Cu_3O_{6.9}$.

curvature of the upturn is sensitive to the electron doping through the substitution of Ce in the rare earth sites. In **Figure 3.3**, we have plotted the resistivity as a function of temperature of sample with x = 0.2. Interestingly, the sample shows no superconducting transition down to 10.0 K. The resistivity of the sample is also very high in comparison to the other three samples over the entire range of

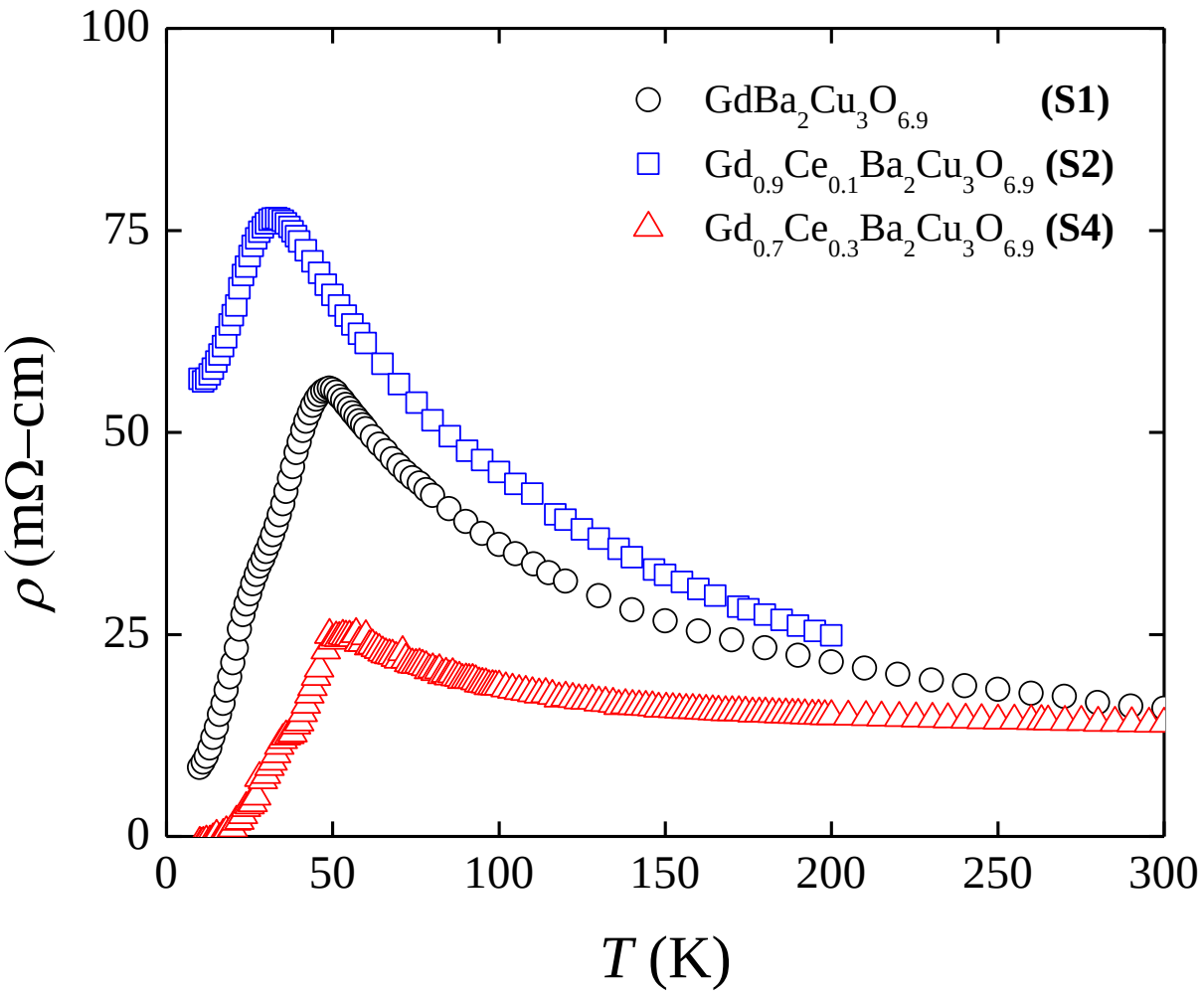

Figure 3.2 Resistivity as a function of temperature in $GdBa_2Cu_3O_{6.9}$ (S1), $Gd_{0.9}Ce_{0.1}Ba_2Cu_3O_{6.9}$ (S2) and $Gd_{0.7}Ce_{0.3}Ba_2Cu_3O_{6.9}$ (S4).

temperature starting at T = 300.0 K. It will not be unjustified to mention that at some critical concentration of electron concentration, samples may be even insulating in nature. In the inset of **Figure 3.3**, we have plotted the critical

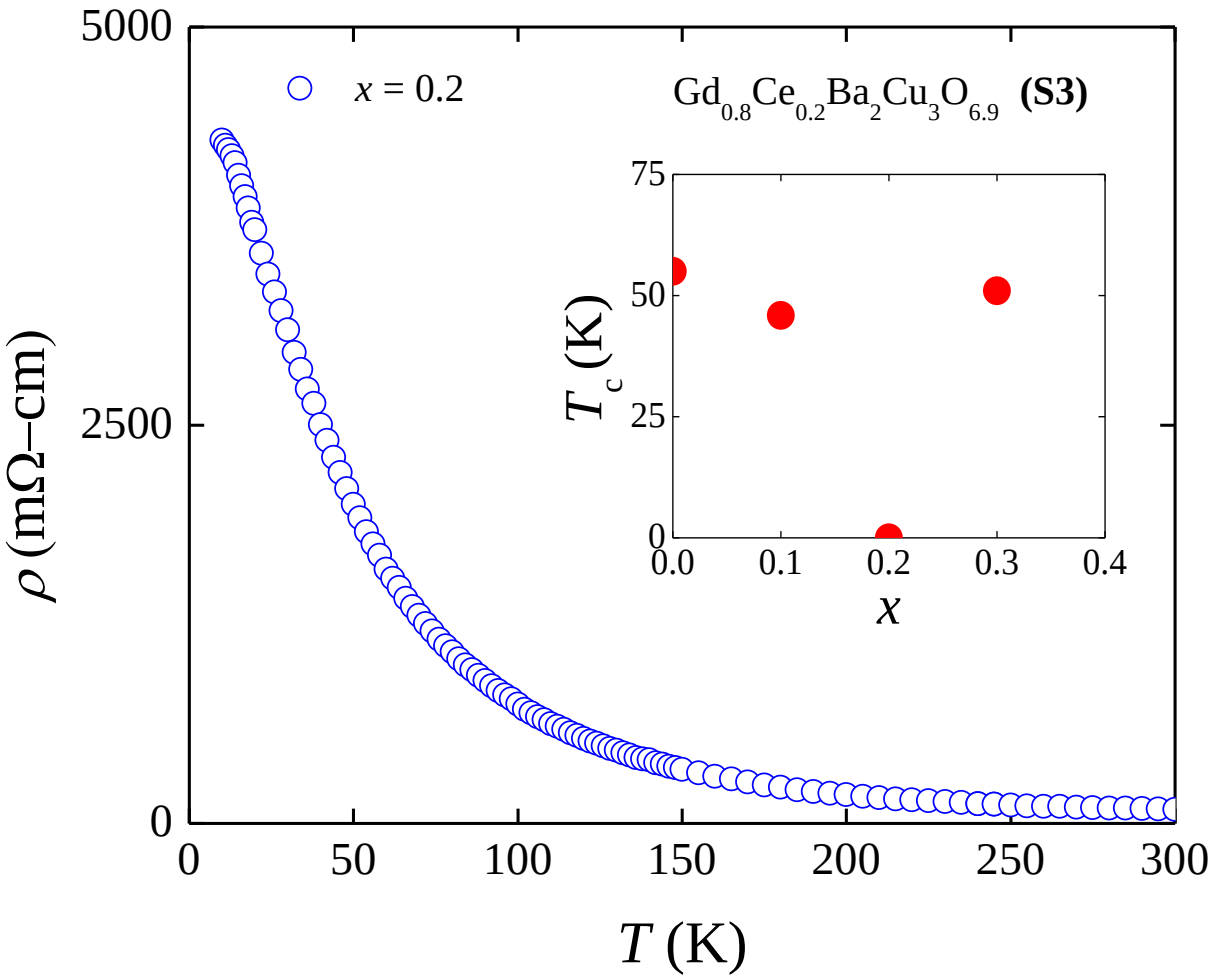

Figure 3.3 Resistivity as a function of temperature in $Gd_{0.8}Ce_{0.2}Ba_2Cu_3O_{6.9}$ (S3). Inset shows the variation of critical temperature with *x*, the concentration of Ce.

temperature versus the concentration of Ce. It reveals that in the intermediate concentration around $x \sim 0.2$, antiferromagnetic insulating phase may occur. It can be treated as a quantum critical point in the series formed by the electron doping. There may be two dome-shaped regions in the present series of

$Gd_{1-x}Ce_xBa_2Cu_3O_{6.9}$. In $CeCu_2Si_2$, the substitution of Ni in Cu site exhibits that upto certain concentration of Ni superconductivity is suppressed and above a certain Ni concentration ~ 0.12, superconductivity is observed because of the recovery of Fermi liquid state **[11, 12]**.

In **Figure 3.4**, we have plotted voltage drop, *V* as a function of current, *I* at constant temperature *T*. A range of temperature starting at 10.0 K has been selected for *IV* features in $GdBa_2Cu_3O_{6.9}$. We have observed a nonlinear variation in *IV* in a wide range of temperature. In the inset of **Figure 3.4**, we have plotted an *IV* curve measured at *T* = 16.0 K. In **Figure 3.5**, we have shown *IV* curves $Gd_{0.7}Ce_{0.3}Ba_2Cu_3O_{6.9}$ in a range of temperature of 12.0 K through 40.0 K. Nonlinear variation has been observed over a wide range of temperature. As a representative of the nonlinear variation we have shown an *IV* curve corresponding to *T* = 20.0 K in the inset of **Figure 3.5**. Concentration of electron can be very effective to alter the crossover temperature at which the linear to nonlinear transformation in *IV* curves occur. The variations in *IV* curves induced by the electron doping in rare earth site have been used to understand the nature of the superfluid state in these samples.

Following the idea of Berezinskii - Kosterlitz - Thouless (BKT) transition the nonlinearity in *IV* curves can be understood by using the equation (1.1) **[13, 14]**.

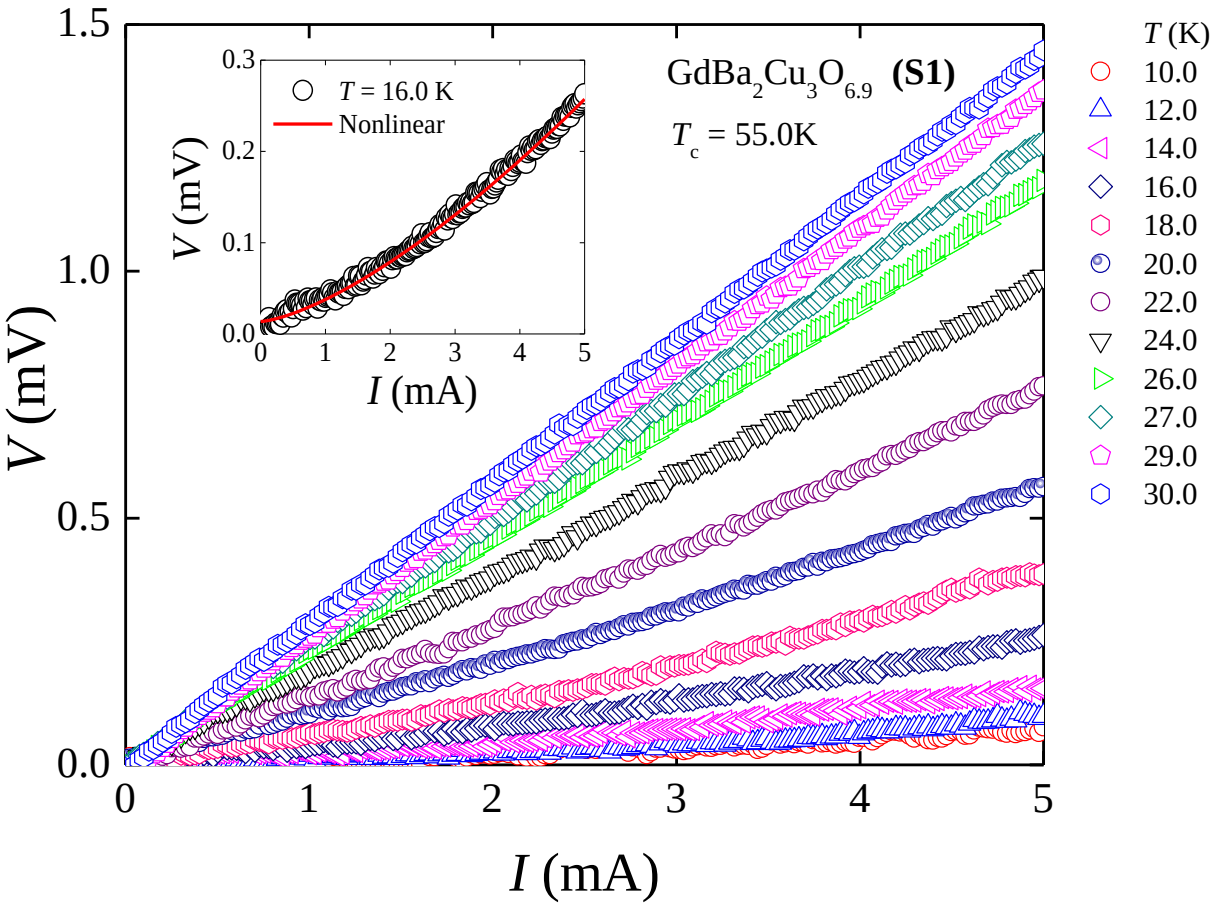

Figure 3.4 Current-voltage (*IV*) variations of $GdBa_2Cu_3O_{6.9}$ (S1) at several temperatures below the critical temperature.

We have extracted η at several temperatures in a range of temperature around the phase transition. In **Figures 3.6** and **3.7**, we have plotted the variation of η with T corresponding to $GdBa_2Cu_3O_{6.9}$ and $Gd_{0.7}Ce_{0.3}Ba_2Cu_3O_{6.9}$ respectively. In both cases, η (T) follows an exponential relation which can be expressed as follows,

$$\eta(T) = \eta_0 + \eta_a \exp(-T/T_0) \quad \text{..... (3.1)}$$

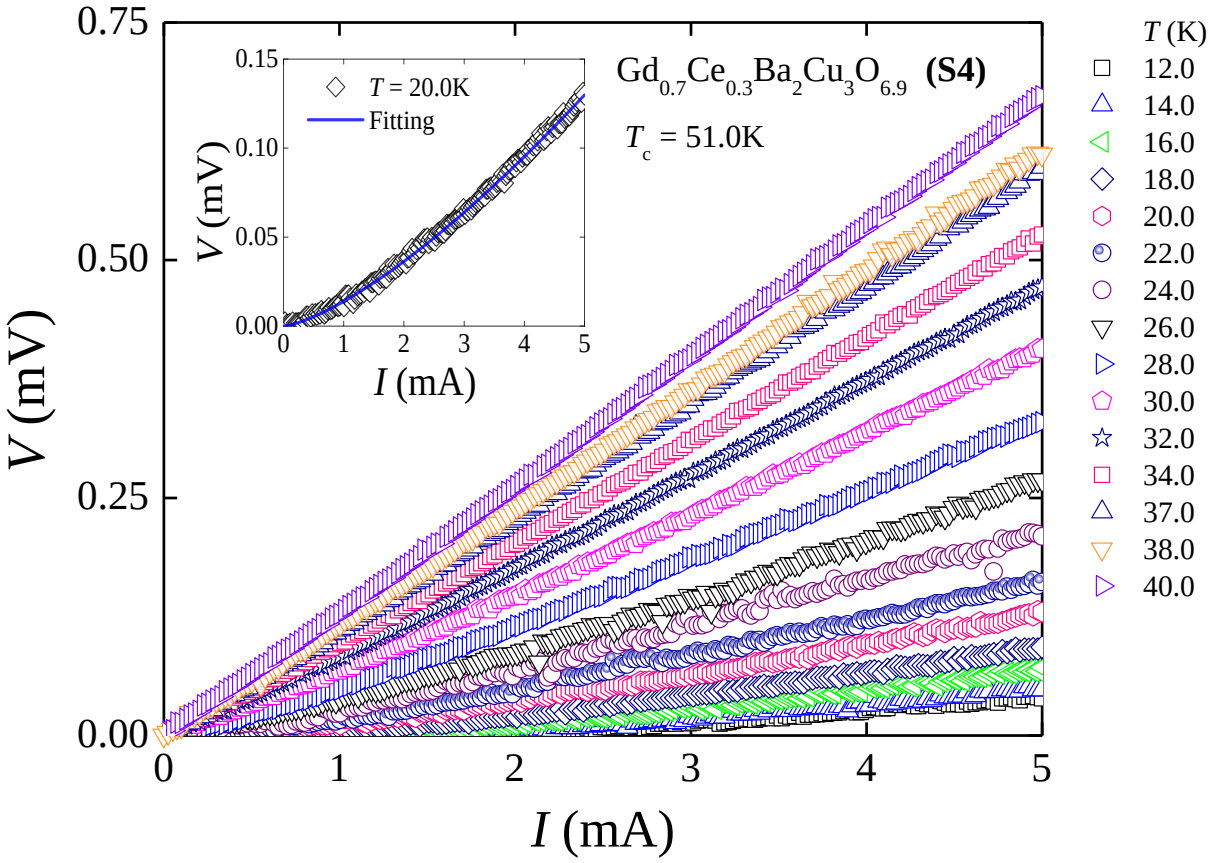

Figure 3.5 Current-voltage (*IV*) variations of $Gd_{0.7}Ce_{0.3}Ba_2Cu_3O_{6.9}$ (S4) at several temperatures below the critical temperature.

here η_0 and η_a are exponents and a coefficient respectively. A characteristic temperature T_0 is found to be responsible for the temperature variation of η. For $GdBa_2Cu_3O_{6.9}$, we obtain $\eta_0 = 0.998$, $\eta_a = 17.25$, $T_0 = 4.19$ K and for $Gd_{0.7}Ce_{0.3}Ba_2Cu_3O_{6.9}$ $\eta_0 = 1.005$, $\eta_a = 3.85$ and $T_0 = 8.61$ K. Therefore, the characteristic temperature is drastically increased in the electron doped sample.

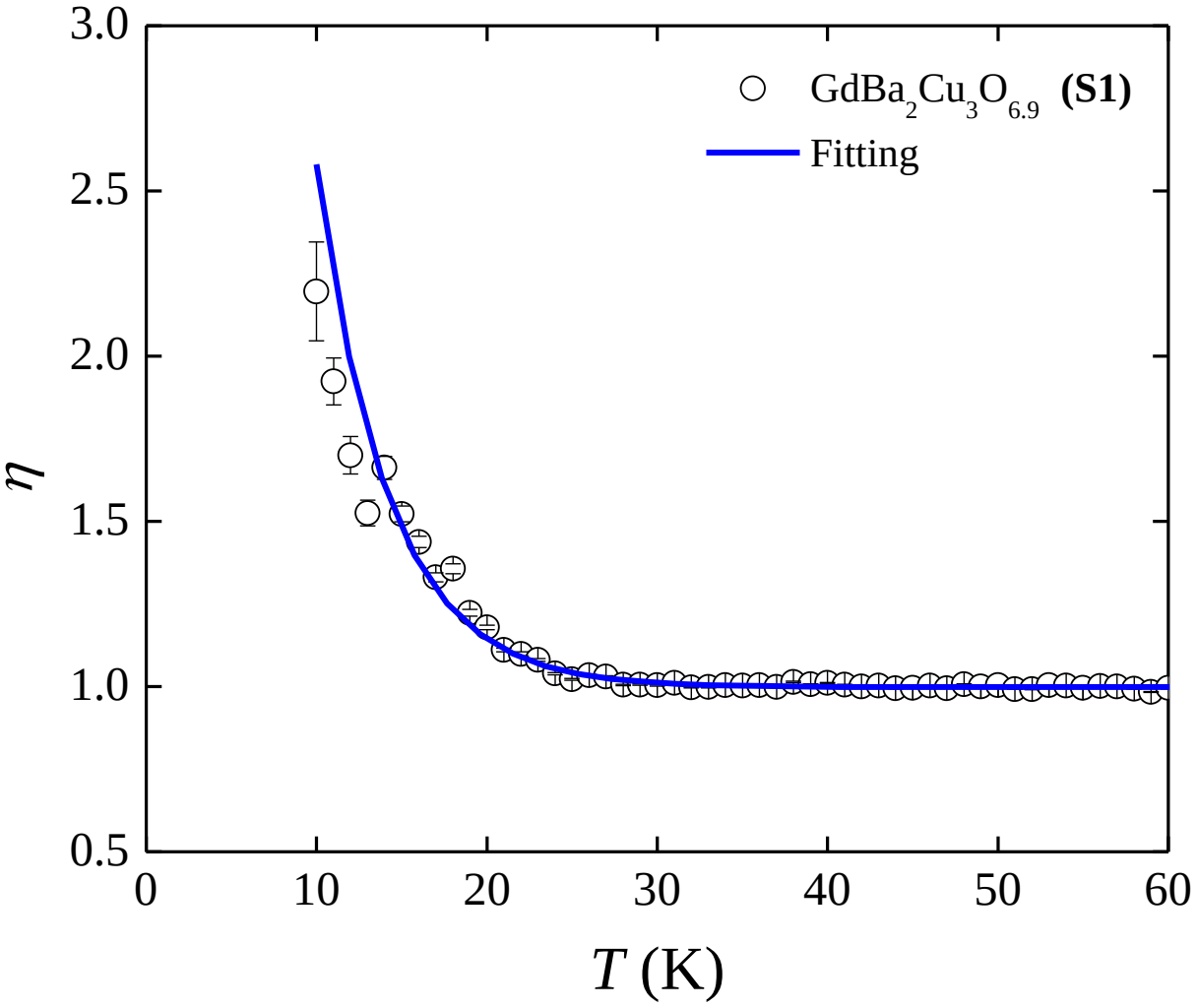

Figure 3.6 Variation of exponent η with the temperature in $GdBa_2Cu_3O_{6.9}$ (S1). Solid line is the fitting in the form of an exponential function as given in the text.

The sensitivity of the variation of the exponent with T is therefore an indicator of the existence of a carrier density sensitive characteristic temperature.

The SPS, $J_s(T)$ can be extracted by using conventionally accepted theory

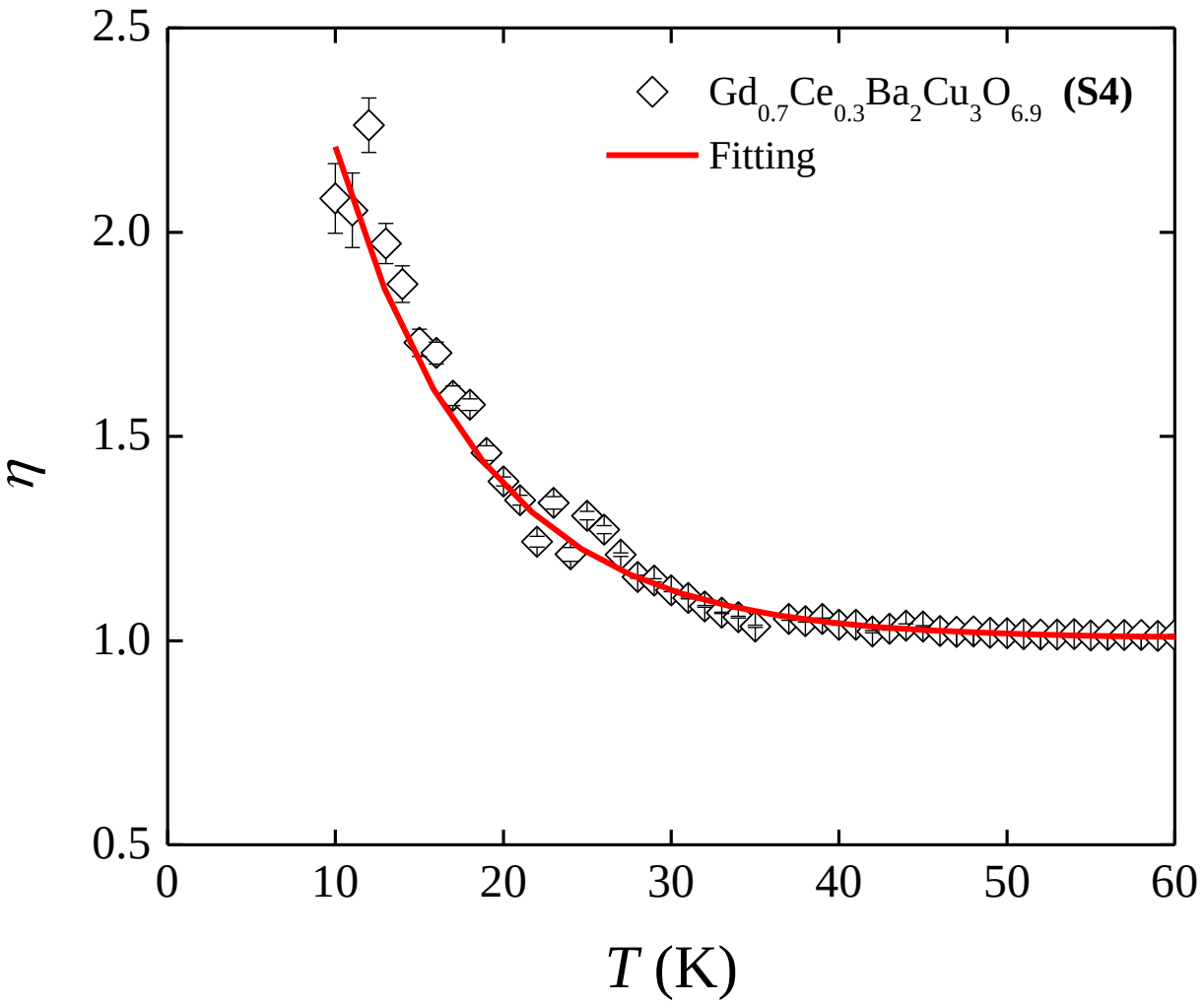

Figure 3.7 Variation of exponent η with the temperature in $Gd_{0.7}Ce_{0.3}Ba_2Cu_3O_{6.9}$ (S4). Solid line is the exponential fitting.

developed by Ambegaokar, Halperin, Nelson and Siggia (AHNS) [1]. There exists another theory in the literature developed by Minnhagen, Westman, Jonsson and Olsson (MWJO) which suggests an alternative formula from which

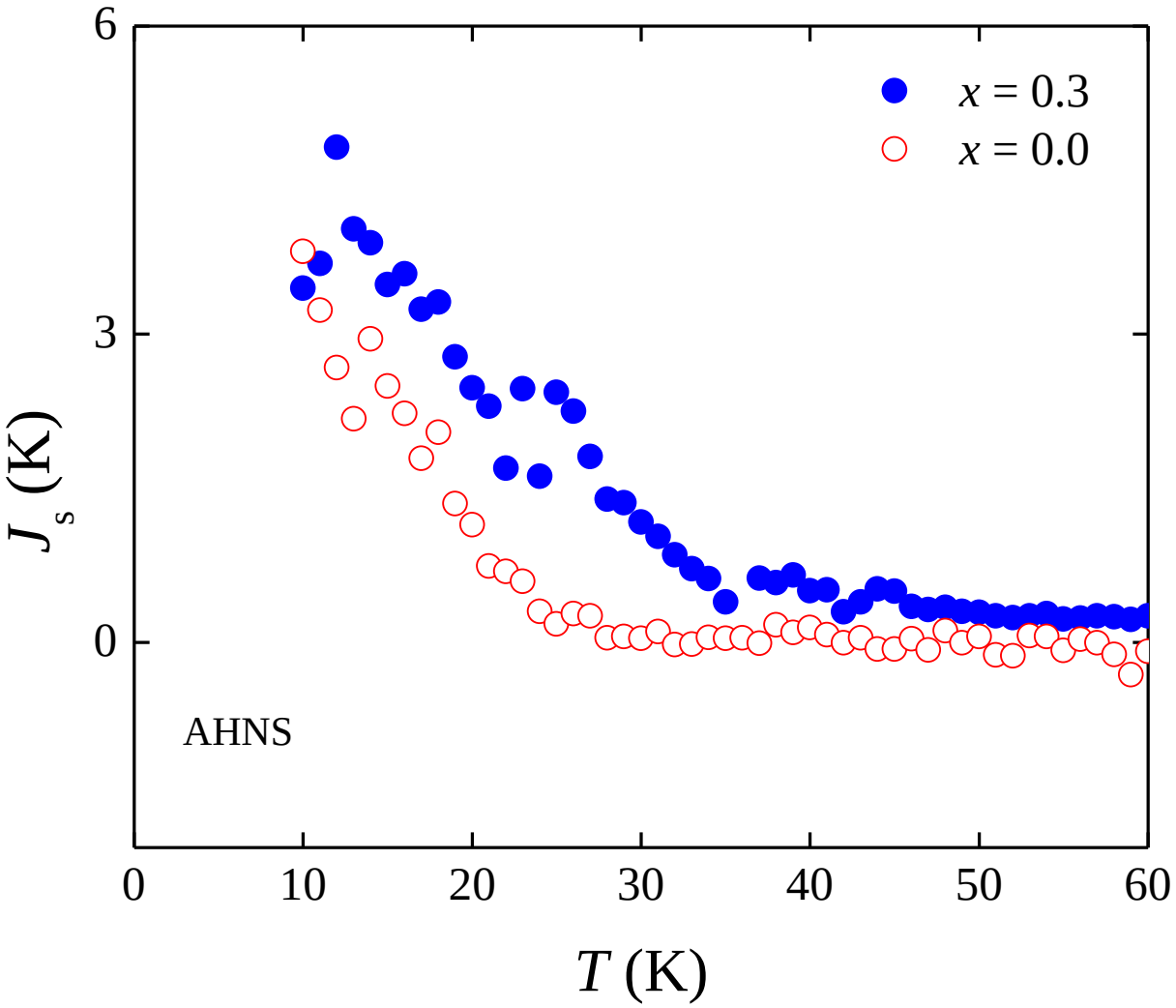

Figure 3.8 Variation of superfluid stiffness J_s extracted by using the theory of Ambegaokar, Halperin, Nelson and Siggia (AHNS) with the temperature in $GdBa_2Cu_3O_{6.9}$ (S1) and $Gd_{0.7}Ce_{0.3}Ba_2Cu_3O_{6.9}$ (S4).

$J_s(T)$ can be extracted **[2, 15, 16, 17]**. We have extracted SPS by using equations within the framework of (i) AHNS and (ii) MWJO. According to AHNS the SPS

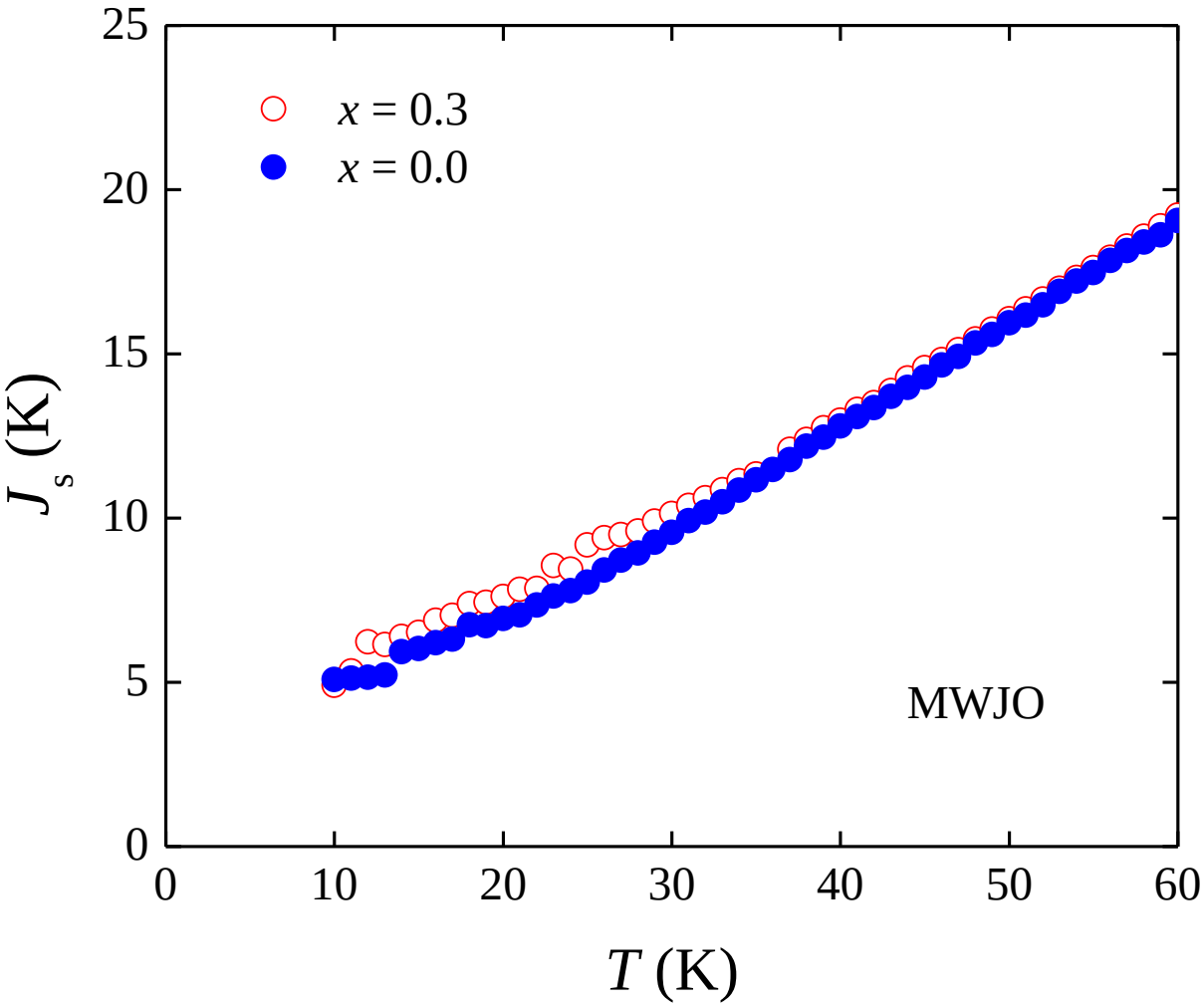

Figure 3.9 Variation of superfluid stiffness J_s extracted by using the theory of Minnhagen, Westman, Johnsson and Olsson (MWJO) with the temperature in $GdBa_2Cu_3O_{6.9}$ (S1) and $Gd_{0.7}Ce_{0.3}Ba_2Cu_3O_{6.9}$ (S4).

can be extracted by using the equation (1.2). In **Figure 3.8**, we have plotted the variation of the J_s (T) of both superconducting samples S1 and S4. A nonlinear

variation with temperature indicates that superfluidity is sensitive to the electron doping level and it may be related to the change in the energy gap. **Figure 3.9** is completely followed by the contradictory theory developed by MWJO **[2, 15, 16, 17]**. Following the equation developed by MWJO, the SPS is extracted as follows,

$$J_s(T) = (\eta(T) + 1)T/2\pi \qquad \text{..... (3.2)}$$

and we have shown the variation of SPS in **Figure 3.9** for S1 and S4. It shows that $J_s(T)$ decreases with decreasing T which is unexpected. Clearly the lower temperature range exhibits the sensitiveness of stiffness to the electron doping level.

We have estimated the charge carrier density, n for S1 and S4 by using equations (2.1) and (2.2) **[18-20]**. The estimated values of n per m^3 for S1 and S4 are 1.04×10^{27} and 9.97×10^{26} respectively. n_s can be estimated by using equations (1.2), (1.3) and (1.4) at experimentally lowest possible measured temperature for S1 and S4 **[21, 22]**. The estimated values of n_s per m^3 for S1 and S4 are 5.86×10^5 and 7.44×10^5 respectively. n_s can not exceed the total charge carrier density, n for a particular cuprate superconductor and this criteria is well maintained here.

Dependence of $\eta(T)$ is sensitive to the doping level x in $La_{2-x}Sr_xCuO_4$ **[23]**. It is observed that η varies nonlinearly with T for different concentrations of holes.

Therefore, n_s is also affected by the concentration of hole doping. Following a theoretical formulation by Lee and Wen, n_s in underdoped cuprates is found to be proportional to the doping concentration and temperature **[24]**. n_s can be expressed as $n_s(T) = \frac{x}{a^2} - m\alpha T$ in which a and x are related to the hopping integral and doping concentration respectively. α is inversely dependent on the gap which is assumed to be independent of doping level. Therefore, n_s varies linearly with temperature **[24]**. Any deviation from the linear variation is therefore attributed to the variation of the energy gap with the temperature and its evolution with the doping level.

Below the BKT transition in 3D anisotropic superconductors the variation of n_s and η are said to be nonlinear with temperature **[25]**. Several other superconducting samples also exhibit nonlinear variation of η with temperature even though n_s scales linearly with the critical temperature **[26–28]**. n_s is found to be nonlinearly dependent on the disorder level induced by several ways **[29]**. In Ca doped YBCO thin film the superfluidity is found to be sensitive to the hole doping level. A nonlinear variation of the superfluidity with temperature has been also observed **[30]**. In Bi-2212 superconductor BKT transition has been reported in which η varies with T nonlinearly **[31]**. A comparison of the variation of η with T in YBCO and BSCCO superconductors also reveals that a sharp transition may not be visible around the BKT transition and a nonlinear variation is visible **[32]**.

Change in the both type of carriers therefore affects the variation of the exponent in cuprates which can be even exponential in nature. It may be related to a characteristic temperature which has an important role in the determination of n_s around the BKT transition.

3.4 Summary

Nonlinear variation in *IV* characteristics has been observed below the superconducting transition in $Gd_{1-x}Ce_xBa_2Cu_3O_{6.9}$ with x = 0.0 and 0.3. The variation of power exponent with temperature exhibits nonlinear behaviour. An exponential variation is found to be consistent with the temperature variation of η in $Gd_{1-x}Ce_xBa_2Cu_3O_{6.9}$ with x = 0.0 and 0.3. A characteristic temperature has been suggested which may be relevant to the nonlinear variation of η. SPS has been extracted by using the exponents following two theories. Clearly SPS is found to be sensitive to the electron density.

3.5 References

[1] V. Ambegaokar, B. Halperin, D. Nelson, E. Siggia, Phys. Rev. Lett. 40 (1978) 783, Phys. Rev. B 21 (1980) 1806.

[2] P. Minnhagen, O. Westman, A. Jonsson, P. Olsson, Phys. Rev. Lett. 74 (1995) 3672.

[3] S. Steers, T.R. Lemberger, J. Draskovic, Phys. Rev. B 94 (2016) 094525.

[4] J. Yong, M.J. Hinton, A. McCray, M. Randeria, M. Naamneh, A. Kanigel, T.R. Lemberger, Phys. Rev. B 85 (2012) 180507.

[5] P.A. Lee, N.A. Nagaosa, X.G. Wen, Rev. Mod. Phys. 78 (2006) 17.

[6] L. Benfatto, C. Castellani, T. Giamarchi, Phys. Rev. Lett. 98 (2007) 117008.

[7] B.R. Boyce, J. Skinta, T. Lemberger, Physica C 341 (2000) 561.

[8] A. Roy, A.K. Ghosh, Physica B 432 (2014) 100.

[9] S. Mollah, B. Biswas, S. Haldar, A.K. Ghosh, Physica C 539 (2017) 40.

[10] B. Biswas, S. Haldar, I. Mukherjee, A.K. Ghosh, Physica B 506 (2017) 173.

[11] Y. Ikeda, S. Araki, T.C. Kobayashi, Y. Shimizu, T. Yanagisawa, H. Amitsuka, J. Phys. Soc. Jpn. 81 (2012) 083701.

[12] H. Yamaoka , Y. Ikeda , I. Jarrige, N. Tsujii , Y. Zekko, Y. Yamamoto, J. Mizuki, J.-F. Lin, N. Hiraoka, H. Ishii, K.-D. Tsuei, T.C. Kobayashi, F. Honda, Y. Onuki, Phys. Rev. Lett. 113 (2014) 086403.

[13] J.M. Kosterlitz and D.J. Thouless, J. Physics C 6 (1973) 1181.

[14] V.L. Berezinskii, Zh. Eksp, Teor. Fiz 61 (1971) 1144.

[15] Q. H. Chen, L. H. Tang, P. Tong, Phys. Rev. Lett. 87 (2001) 067001-1.

[16] L. H. Tang, Q. H. Chen, Phys. Rev. B 67 (2003) 024508-1.

[17] A. Andersson, J. Lidmar, Phys. Rev. B 87 (2013) 224506.

[18] J. L. Tallon, C. Bernhard, H. Shaked, R. L. Hitterman, J. D. Jorgensen, Phys. Rev. B 51 (1995) 12911.

[19] Y. Ando, A. N. Lavrov, S. Komiya, K. Segawa, X. F. Sun, Phys. Rev. Lett. 87 (2001) 017001-1.

[20] A. Stangl, A. Palau, G. Deutscher, X. Obradors, T. Puig, Sci. Rep. 11 (2021) 8176.

[21] I. Bozovic, X. He, J. Wu, A. T. Bollinger, Nature 536 (2016) 309.

[22] L. Benfatto, C. Castellani, T. Giamarchi, Phys. Rev. B 77 (2008) 100506 (R).

[23] P.G. Baity, X. Shi, Z. Shi, L. Benfatto, D. Popovic, Phys. Rev. B 93 (2016) 024519.

[24] P.A. Lee, X. Wen, Phys. Rev. Lett 78 (1997) 4111.

[25] B. Chattopadhyay, S.R. Shenoy, Phys. Rev. Lett. 72 (1994) 400.

[26] A. Hosseini, D. M. Broun, D. E. Sheehy, T. P. Davis, M. Franz, W. N. Hardy, R. Liang, D. A. Bonn, Phys. Rev. Lett. 93 (2004) 107003.

[27] C.C. Homes, Phys. Rev. B 80 (2009) 180509.

[28] Y. Imry, M. Strongin, C.C. Homes, Phys. Rev. Lett. 109 (2012) 067003.

[29] N.R. Lee-Hone, J.S. Dodge, D.M. Braun, Phys. Rev. B 96 (2017) 024501.

[30] I. Hetel, T.R. Lemberger, M. Randeria, Nature 3 (2007) 400.

[31] S.N. Artemenko, I.G. Gorlova, Y.I. Latysev, Phys. Lett. A 138 (1989) 428.

[32] C. Paracchini, L. Romano, L. Francesio, Physica C 175 (1995) 324.

Chapter 4

Scaling of current-voltage characteristics without and with finite superfluid phase stiffness below T_c

4.1 Introduction

Berezinskii - Kosterlitz - Thouless (BKT) transition in different systems is characterized by the abrupt change of an exponent, η in nonlinear current-voltage (IV) characteristics below the critical temperature in superconductors **[1, 2]**. An abrupt change in η (T) occurs at a temperature T_{BKT}. The resistive contributions of the BKT vortex states above T_{BKT} are linear whereas nonlinear IV curves are observed below T_{BKT} **[3]**. Following a theoretical formulation by Ambegaokar - Halperin - Nelson - Siggia (AHNS), the superfluid phase stiffness (SPS) can be calculated by using the exponent **[4, 5]**. The variation of the superfluid density, n_s with temperature in a superconductor is closely related to the critical temperature and resistive states **[6–9]**. T_{BKT} is lower than the superconducting transition, T_c. Generally the SPS is found to be zero within the range between T_c and T_{BKT}. However, below T_{BKT} the SPS varies with temperature in a very complex way **[10, 11]**.

In the presence of the magnetic field the broadening of the resistive phase transition has been explained by the Fisher, Fisher and Huse (FFH) theory **[12]**. Within the formulations of FFH, the formation of the vortex glass (VG) state and it's transition to the vortex fluid (VF) state can be explained **[13]**. The phase transition from VG to VF state is known to occur at a characteristic temperature, T_g. At $T > T_g$, the resistive states are collapsed by using a scaling equation **[12]**. The scaling relation has been very successful to explain experimental data near phase transition in hole and electron doped superconductors of different forms **[14, 15]**. Within the framework of the FFH formulations, the existence of the VG state can be detected by using the nonlinear *IV* curves around T_g. Extraction of the critical exponent related to the divergence of the coherence length is also possible using the nonlinear *IV* curves **[14]**. *IV* measurements at the zero magnetic field reveals the second order phase transition in different electron doped cuprates using the scaling analysis of the exponents **[15]**.

An important question is whether the resistive states observed around T_{BKT} at zero magnetic field can be understood within the framework of FFH formulation. To our knowledge no such attempt has been made. Even though the change in SPS is not abrupt around the BKT phase transition in cuprate superconductors, the ohmic state becomes stable above T_{BKT}. A finite phase stiffness and non-zero resistivity coexist at $T < T_{BKT}$. A finite phase stiffness corresponds to the nonlinear *IV* characteristics whereas the linear *IV* is observed with zero phase

stiffness. In this paper *IV* characteristics of $Nd_{0.7}Ca_{0.3}Ba_2Cu_3O_{7-\delta}$ (NCBCO) below the T_c = 75.8 K have been used. Within the framework of the AHNS theory the exponent η related to the BKT phase transition has been extracted. The T_{BKT} is found to be 54.0 K which has been used to extract the static exponent *v* required in FFH scaling equation. The nonlinear variation of SPS with *T* has also been observed below 54.0 K. We have studied the applicability of the scaling relation of FFH to understand the resistive states for $T < T_{BKT}$ and $T > T_{BKT}$ observed in the BKT transition.

4.2 Experimental

We have measured the resistivity of a highly pure $Nd_{0.7}Ca_{0.3}Ba_2Cu_3O_{7-\delta}$ as a function of temperature by using the standard four probe method. The picture of the bar shaped sample used for the present study has been shown in the inset of the **Figure 4.1**. The separation between two voltage leads is 0.97 mm. Below the critical temperature of 75.8 K, we have measured *IV* curves at several constant *T* **[16, 17]**. The lowest temperature for *IV* measurement has been selected down to 10.0 K. All the transport measurements of the bar shaped sample are carried out with the help of a closed cycle cryogenerator (Janis, USA). A typical value of current 1.0 mA is used for the measurement of resistivity with *T*. For the measurements of *IV* we have used current in the range of 100 nA through 5.0 mA.

4.3 Results and discussions

In **Figure 4.1** we have shown the resistivity as a function of T in the NCBCO superconductor. Broadening of resistivity as a function of T at zero applied magnetic field is observed as is revealed by $d\rho/dT$ as a function of T. The variation of $d\rho/dT$ with T has been shown in the inset of **Figure 4.1**. The onset critical temperature, T_c, has been obtained to be 75.8 K. It is determined as a temperature at which $d\rho/dT$ starts to increase in lowering T from the normal state. The width of the phase transition is found to be broad enough in comparison to that observed in conventional low - T_c type-II superconductors.

We have shown the IV curves of NCBCO below T_c in **Figure 4.2**. Nonlinearity in IV curves has been observed over a wide range of temperatures. The nonlinearity can be explained within the framework of the BKT transition **[1, 8, 18]**. The BKT transition in superconductor is actually related to the phase variation from point to point in space. In other words it solely depends on the phase associated with each Cooper pair. In cuprate superconductor the BKT transition has origin in the individual CuO_2 layers. Therefore, any bulk form of

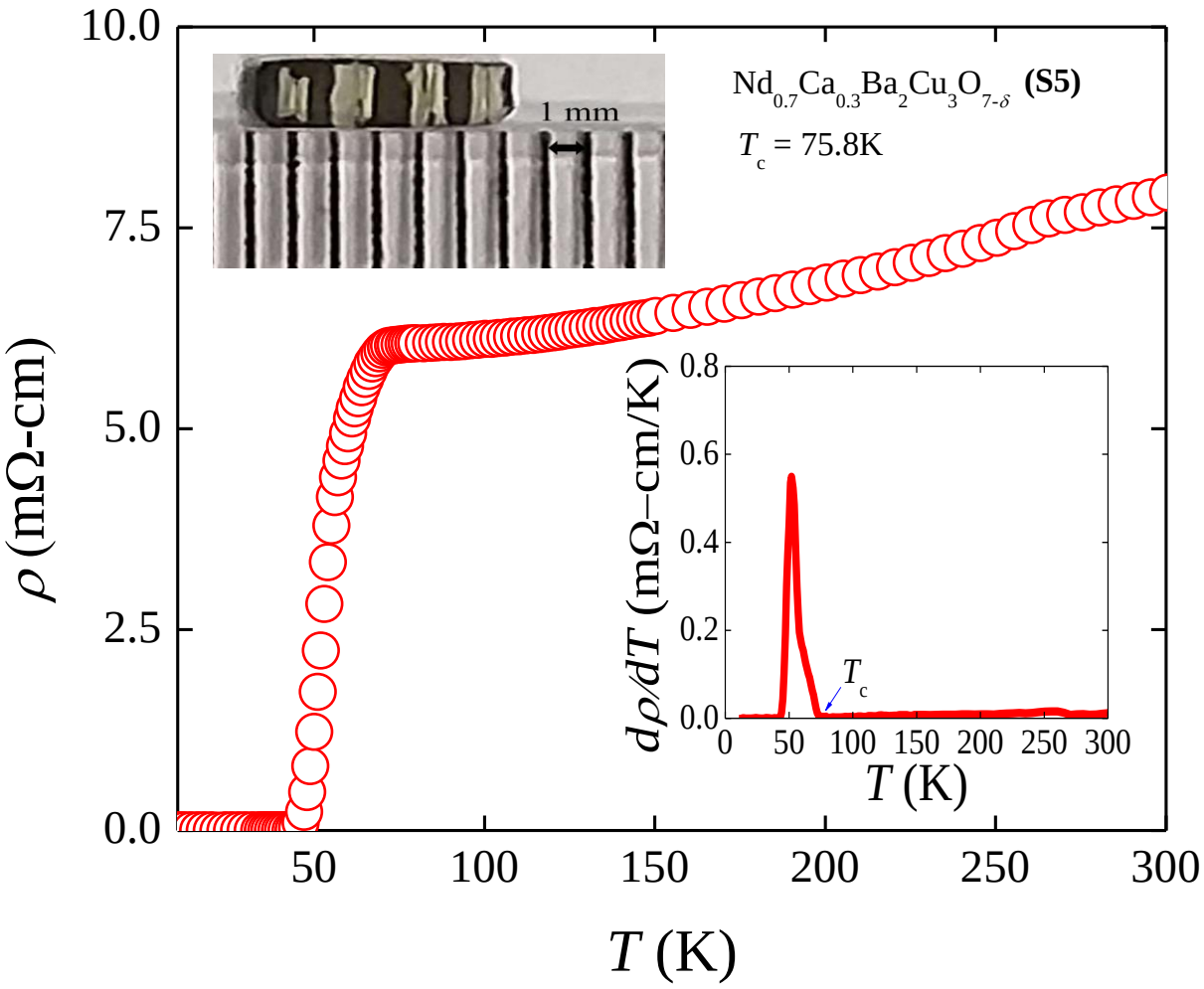

Figure 4.1 Resistivity of NCBCO (S5) as a function of temperature. A picture of the bar shaped sample with leads is shown in the upper left inset. The lower right inset shows the variation of dρ/dT as a function of T.

superconducting samples will exhibit BKT transition. The BKT transition can be observed even in bulk samples because the phase variation is identical as is observed in single crystals. Polycrystalline NCBCO samples are also suitable to

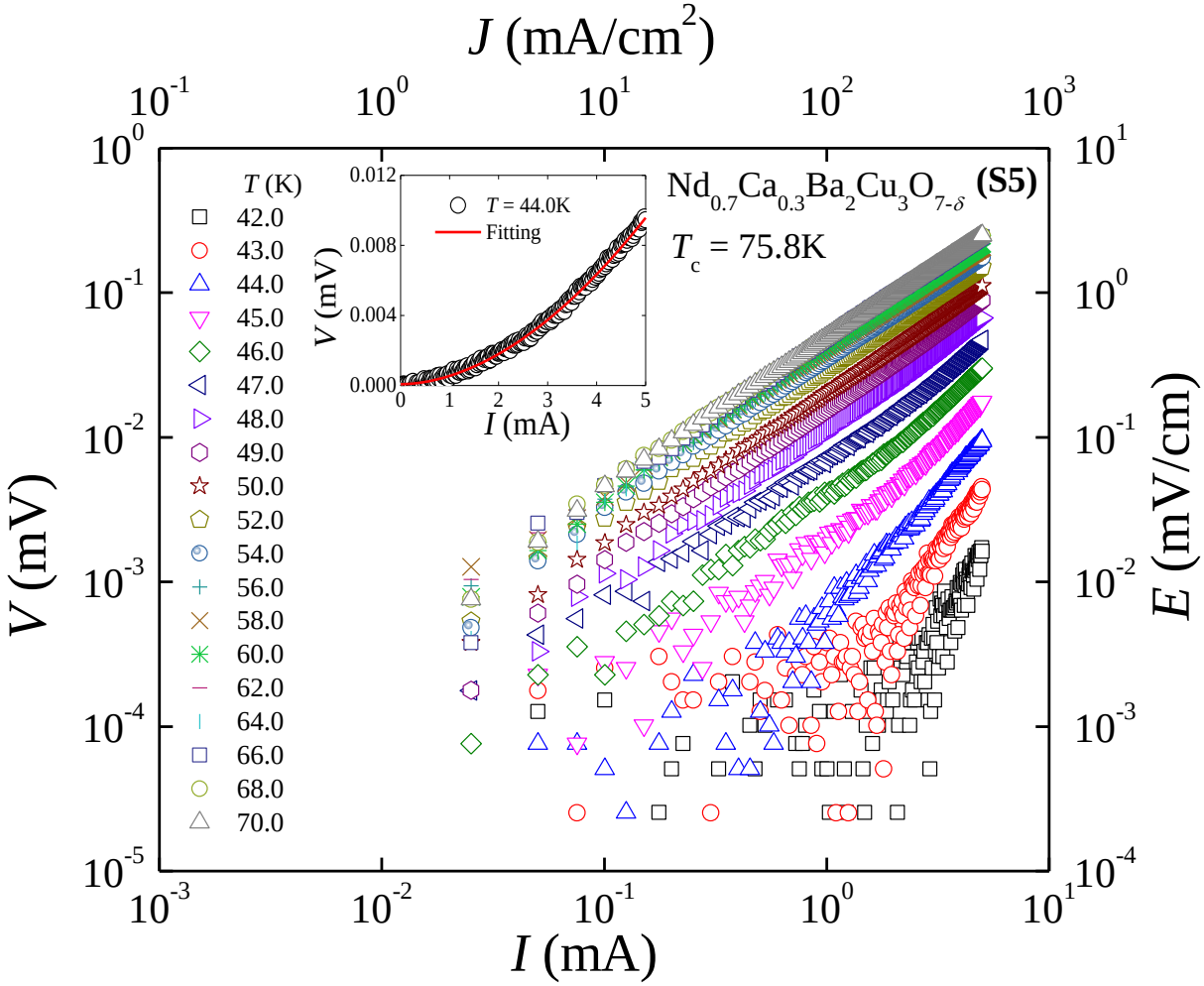

Figure 4.2 Current-voltage curves in log - log scale at several T below T_c in NCBCO (S5). Corresponding E as a function of J has also been shown. In the inset a typical variation of IV at T = 44.0K is shown in linear scale. A fitting by using $V = aI^{\eta}$ has been shown which is used to determine η.

exhibit the BKT effect. Several effects such as the energy gap, the BKT transition and T_c are very intrinsic in nature which are related to the momentum space and similar in both the single crystal and bulk samples. In two neighbouring grains

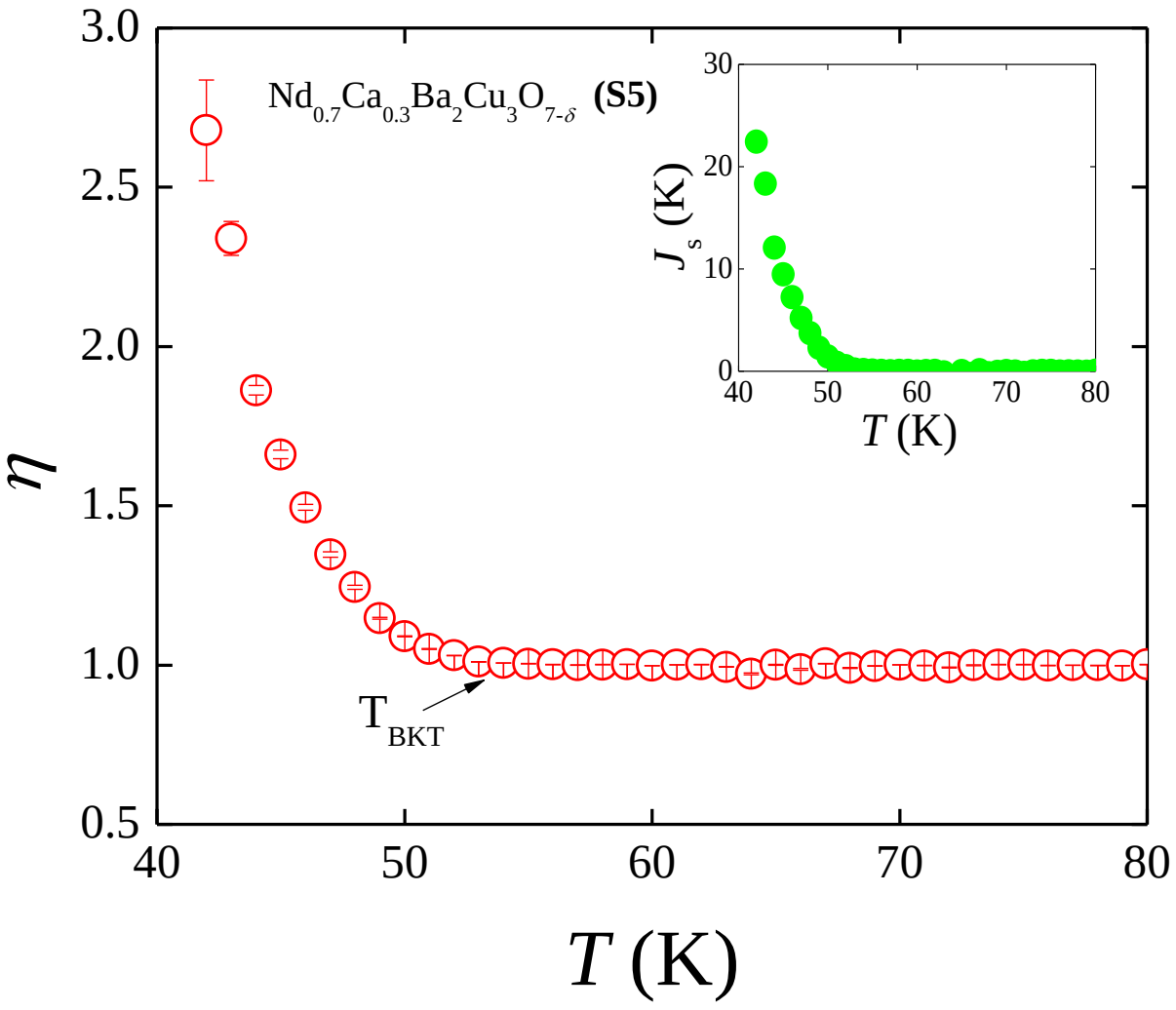

Figure 4.3 Variation of the exponent η with T in NCBCO (S5). At $T \geq 54.0$K, the exponent is 1.0 and T_{BKT} has been shown by an arrow. In the inset we have shown the variation of the SPS, J_s as a function of T following AHNS theory.

separated by a grain boundary in the real space the phases are different and therefore should not suppress the BKT transition. The transition width can be

tuned even in a single crystal of cuprate superconductors. Also, the polycrystalline sample in BKT transition has been tuned **[18–21]**. Moreover, the procedure we have researched is independent of the bulk or single crystal. In addition, there is no theory on how grain boundary affects the BKT transition. The nonlinear voltage drop is expressed following the equation (1.1) **[4, 5]**. In the inset of **Figure 4.2**, we have shown a typical *IV* curve at T = 44.0 K and the fitting curve. The exponent η has been extracted by using the power law fitting at different temperatures. In **Figure 4.3** we have shown variation of η (T) over a wide temperature range starting from 42.0 K. At $T = T_{BKT} \simeq 54.0$ K, η becomes 1.0 and *IV* curves are linear for T > 54.0 K. Using the AHNS theory, J_s and η are related by the equation (1.2) **[4, 5]**. We have extracted J_s as a function of T as shown in the inset of **Figure 4.3**. The estimated values of charge carrier density n per m^3 and superfluid density, n_s per m^3 at experimentally lowest possible measured temperature for S5 are around 1.31×10^{27} and 3.46×10^{6} respectively **[22-26]**. Nonlinear variation of J_s in several other cuprates has been observed by other techniques **[27, 28]**. At T_c = 75.8K > T > $T_{BKT} \geq$ 54.0K, J_s is zero in NCBCO because the linear nature of *IV* corresponds to η = 1.0. However, for $T < T_{BKT}$, the SPS increases nonlinearly with T **[29, 30]**. The finite value of J_s is related to the nonlinear variation of *IV*. Nevertheless, in the presence of nonzero SPS the nonlinear *IV* corresponds to vortex pairs in the BKT theory. The unbinding of such vortex pairs results in linear *IV* above $T_{BKT} \simeq 54.0$ K. T_c and T_{BKT} are not the same temperatures in HTS. The present understanding is that

these two temperatures (T_c and T_{BKT}) have different origins. There are two important regions (i) $T > T_{BKT}$ and (ii) $T < T_{BKT}$ where vortex phases are different according to the BKT theory. Below $T < T_{BKT}$, vortices are in the bound pair state whereas at $T > T_{BKT}$ pairs are broken (unbinding).

Next we have used the FFH scaling relation for collapsing the *IV* curves in two separate ranges of (i) 75.8 K > T > 54.0 K and (ii) 42.0 K < T < 54.0 K. The scaling relation for any continuous phase transition is expressed by using a scaling function. The functional dependence of the electric field on the electric current density at any temperature will be the same according to the scaling functions. The restriction on temperature is there with respect to a characteristic temperature. A very popular and much used scaling function in VG to VF phase transition is generally considered with respect to a transition temperature, T_g. On the basis of theory of FFH a scaling relation is written as follows **[12, 13]**.

$$\frac{\rho(J,T)}{\rho_L(0,T)} - 1 = G_+\left[\frac{J}{T}\left|1 - \frac{T}{T_g}\right|^{-(D-1)\nu}\right] \qquad \ldots\ldots\ldots\ldots\ldots\ldots (4.1)$$

Here ρ (J, T) is the resistivity depending on the current density and T. ρ_L ($J\rightarrow 0$, T) is the linear resistivity for the current density $J\rightarrow 0$ at T **[31]**. Here, G_+ is known as the scaling function. In the scaling function the characteristic temperature is T_g at which the transition of VG state to VF state is found in the FFH theory. For this continuous phase transition D is the dimensionality and ν is the static critical exponent. We have used the concept of scaling as given in equation (4.1) to

understand whether resistive states above and below the BKT transition temperature, $T_{BKT} \simeq 54.0$ K can be collapsed. For using the scaling relation we have taken the resistivity at a current of 100 nA as $\rho_L(T)$ **[31]**. In principle, we need a lower current as much as possible to obtain $\rho_L(T)$. We have used the lowest current as 100 nA chosen an experimental possible lowest current. For the higher noise level for few T we used an extrapolated value. The phase transition we are dealing with occurs at $T_{BKT} \simeq 54.0$ K for NCBCO. We have related the dynamical exponent, z of the FFH theory with the exponent, η which determines T_{BKT} and also used in the AHNS theory. In FFH the determination of the dynamical critical exponent z for $D = 3$ is done by using,

$$V \propto I^{(z+1)/2} \qquad \text{..... (4.2)}$$

Comparing equation (4.2) with the equation (1.1) as discussed in the AHNS theory we have,

$$z = 2\eta\text{-}1. \qquad \text{..... (4.3)}$$

It is important to mention that as a result of the moderate anisotropy (~6 and 7), NCBCO is basically a quasi-2D system. If we look at η values, we never observed $\eta = 3.0$. It indicates that the BKT transition is not exactly observed down to 10.0 K. However, we see that the possible BKT transition is broader in nature. It is therefore possible that the changed dimensionality (from $D = 2$) may impact the width of the BKT transition.

The scaling function depends on the choice of T_g known as the glass transition temperature according to the FFH theory. The determination of T_g by using *IV* is not unique in nature **[31, 32]**. We propose that T_{BKT} at zero field can be taken as T_g because T_{BKT} is also related with the unbinding of ordered pair vortex states according to the BKT theory **[1]**. BKT and FFH are comparable in such a way that both exhibits order-disorder transition. We know that the extraction of ν is possible by using an equation **[31]**,

$$\rho_L \propto \left(\left|1 - \frac{T}{T_g}\right|\right)^{-\nu(D-2-z)} \qquad \ldots\ldots\ldots\ldots\ldots\ldots (4.4)$$

In the inset of **Figure 4.4**, we have plotted $log\ (\rho_L)$ as a function of $log\left(\left|1 - \frac{T}{T_g}\right|\right)$ for T = 54.0 K and the static exponent, ν at 54.0 K has been extracted using the slope of the linear fitting to it. The variation of ν with T_g has been shown in **Figure 4.4** together with the variation of z with T. Even though the variation of z (T) is continuous an abrupt jump near 54.0 K has been observed in ν (T_g). The jump in ν reflects a transition from a BKT vortex paired state with finite superfluid density to an unbinding vortex state with the absence of the superfluid density. In Figure 4.4 the horizontal axis is supposed to correspond to both T and T_g. At first ν is obtained separately at each T by considering the fact that T_g is not unique. After getting a jump near $T = T_{BKT} \simeq 54.0$ K in ν (T_g), we propose T_{BKT} as T_g for S5. Moreover, at higher T, ν remains slowly varying with T_g in comparison to that in the lower range of $T < 54.0$ K. ν has a range of $1.0 \leq \nu \leq 2.0$ in VG **[33–35]**. Generally, $z > \nu$ in VG in superconductors. We have observed

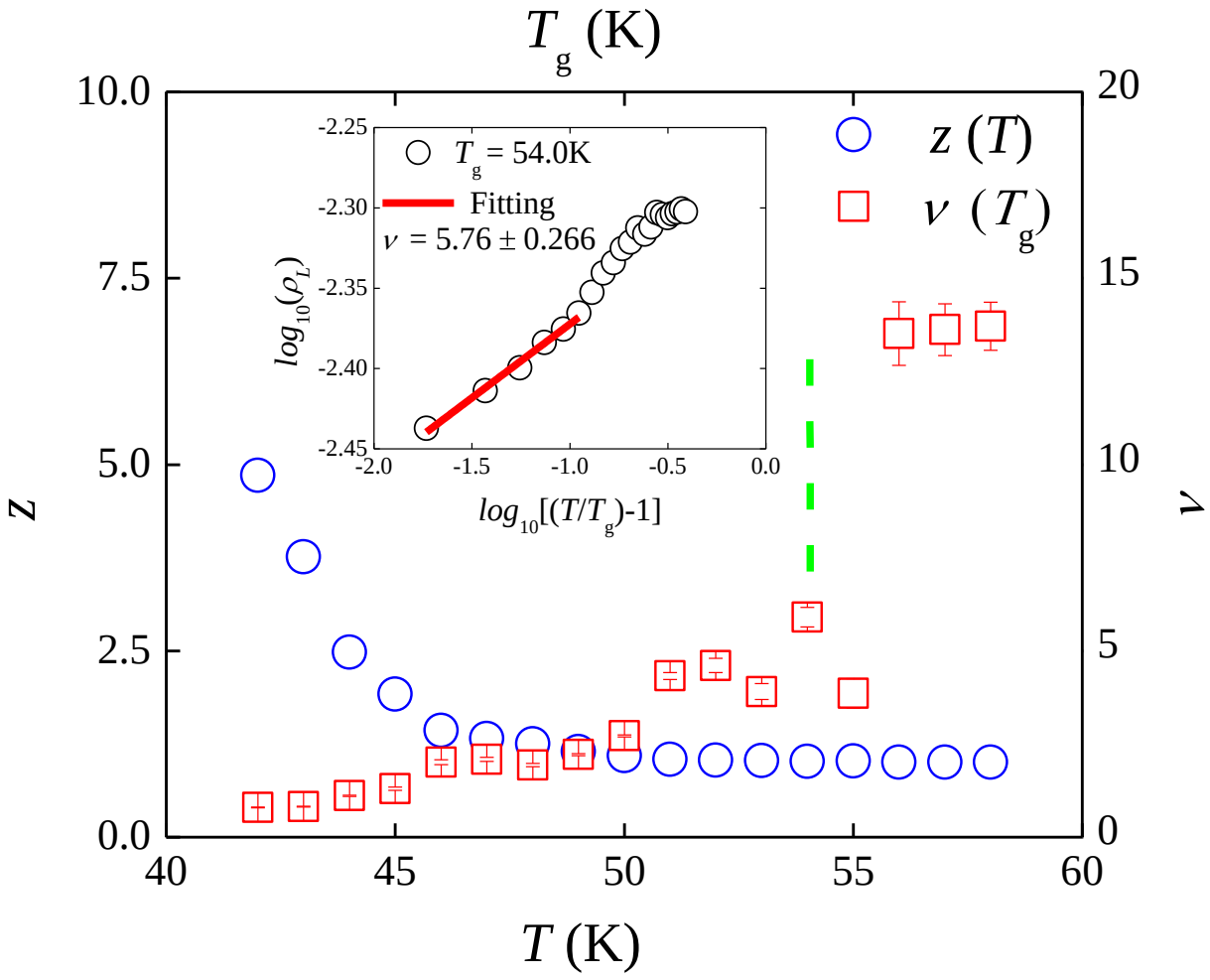

Figure 4.4 Variations of (i) the static critical exponent v as a function of T_g and (ii) variation of dynamic exponent, z (T). Around 54.0K, an abrupt variation of v is marked by a dashed line. Inset shows a typical plot of log (ρ_L) versus log [(T/T_g)-1] for $T_g = T_{BKT} \simeq 54.0$K.

that $v > z$ in above 54.0 K. It indicates that the vortex unbinding state in the BKT scenario is in analogy with the VG state found in FFH formulations. It is important to add a different class of vortex system based on BKT theory **[1, 2]** is

being discussed. Actually, we have done *IV* measurements below T_c without any external magnetic field. Therefore, we are mostly dealing with vortices arising out of the phase fields of the individual pairs. Following the BKT theory we associate a phase vector equivalent to spin. These vortices we discuss are not formed as a result of the usual flux quantization observed in type-II superconductors. The impact of the pinning centers on the associated vortex system which has a different origin in the phase gradient is not known theoretically. At the BKT temperature unbinding of (BKT) vortices takes place which is entirely different in comparison to the usual depinning of the type- II vortices. It will be interesting to mention that *v* of NCBCO is comparable with the static exponent results of other superconductors **[36]**. The variation of *v* is known to be dependent on the broadening of the transition region in YBCO **[36]**. We have extracted *v* = 5.76 at 54.0 K for NCBCO which has been used as one of the parameters required for the FFH scaling relation.

In **Figure 4.5(A)**, we have plotted $\rho(J,T)/\rho_L(0,T)-1$ as a function of $(J/T)\left(\left|1-T/T_g\right|\right)^{-(D-1)\nu}$ using $T_g = T_{BKT} \simeq 54.0$ K and corresponding $v = 5.76$. The motivation behind the choice is that at 54.0 K we have observed the onset of the BKT phase transition. Above 54.0 K *IV* curves are linear and the SPS becomes zero. In **Figure 4.5(A)**, we have included *IV* in the range of 55.0 K through 70.0 K to check how the scaling works in the range of *T* having zero SPS. As revealed

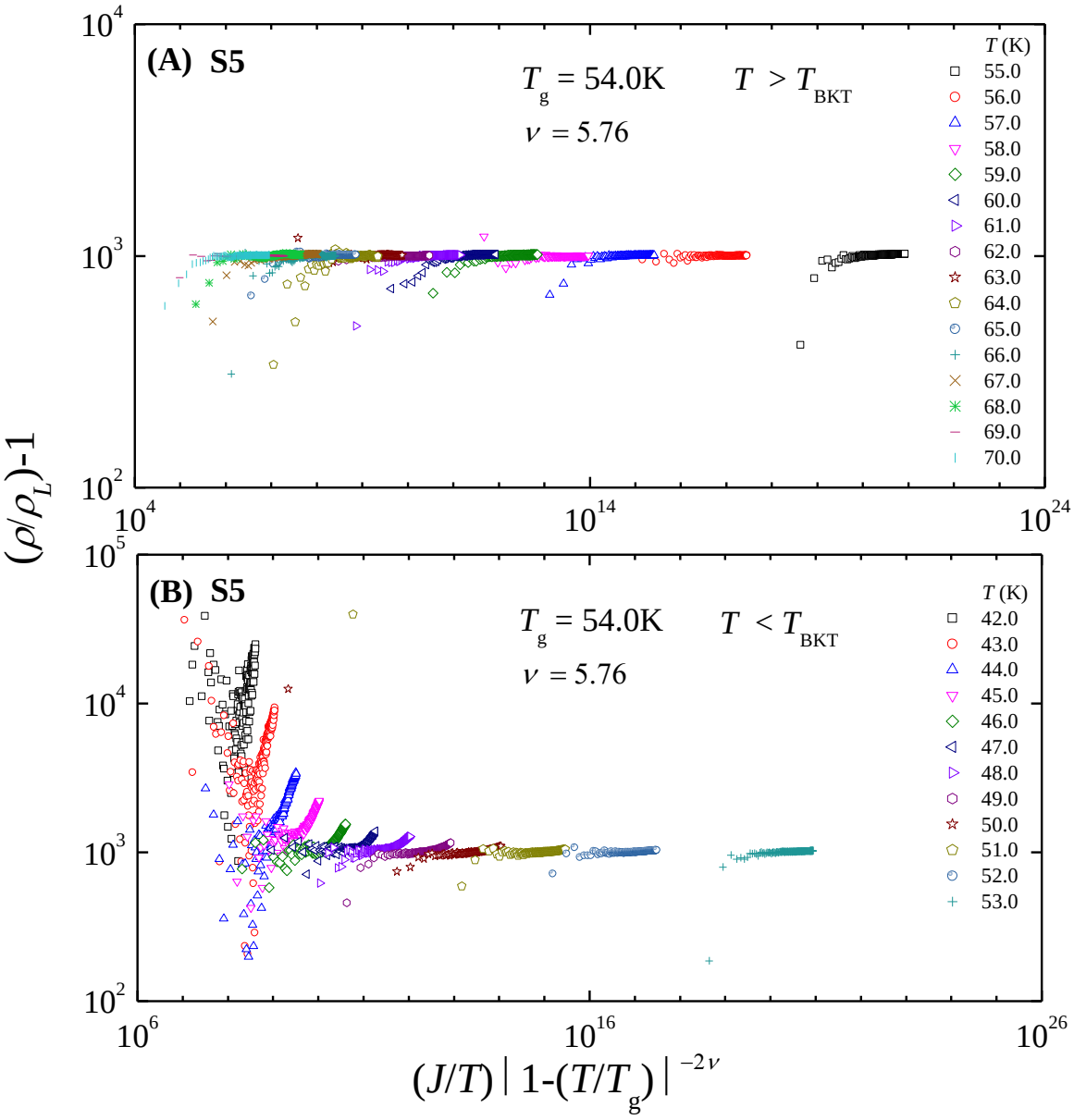

Figure 4.5 Variation of $\rho(J,T)/\rho_L(0,T)-1$ as a function of (J/T) $(|1-T/T_g|)^{-(D-1)\nu}$ with $T_g = T_{BKT} = 54.0$K in *log-log* scale for two temperature ranges - (A) $T > T_{BKT}$ and (B) $T < T_{BKT}$.

by **Figure 4.5(A)**, we observe that the scaling equation is efficient enough over a wide range of current density and T to collapse most of the data almost in a

collinear pattern. All $\rho(J,T)/\rho_L(0,T)-1$ are converging in nature at a very narrow range of the order of 10^3 for T > 54.0 K. In YBCO, the FFH scaling relation has been successfully used to collapse the $\rho(J,T)/\rho_L(0,T)-1$ for a set of *IV* data by assuming different T_g for lower current density. However, a deviation is reported for the higher current density **[31]**. The scaling equation exhibits collapsing over a different range of the scaling function **[37]**. A universal scaling method over a wide range of current density and T can be observed with limitations in the vortex dissipation state in NCBCO as well which is generally valid for VG state **[38]**. In **Figure 4.5(B)**, we have plotted $\rho(J,T)/\rho_L(0,T)-1$ as a function of $(J/T)(|1-T/T_g|)^{-(D-1)\nu}$ using ν = 5.76 but using a different range of 42.0 K < T < 54.0 K. In this range of T, the SPS (J_s) is finite and increases as the temperature is lowered. It is clear that FFH scaling does not help to collapse data with lowering T in NCBCO with the increasing J_s. Therefore, the FFH scaling relation can be used to identify the vortex unbinding state above T_{BKT} observed in BKT phase transition.

4.4 Summary

Nonlinear *IV* curves below 75.8 K are used to extract the SPS within the framework of BKT phase transition and AHNS theory in zero magnetic field. The variation of η with T reveals that the continuous BKT transition has an onset

nearly at 54.0 K in NCBCO. v of FFH theory has been extracted to be 5.76 at 54.0 K. The scaling function within the framework of FFH has been used to collapse resistive states above and below 54.0 K observed in the BKT transition in NCBCO. T_g in FFH theory can be replaced by T_{BKT} of the BKT theory to use the scaling relation near the BKT theory for NCBCO superconductor. Within the superconducting transition T_c and BKT transition temperature, T_{BKT} the resistive states can be well understood by FFH scaling function. Below T_{BKT} the scaling is not very prominent in NCBCO superconductors. The deviation of the scaling theory at $T \ll T_{BKT}$ is associated with the finite superfluid density below T_{BKT}.

4.5 References

[1] J.M. Kosterlitz, D.J. Thouless, J. Phys. C 6 (1973) 1181.

[2] V.L. Berezinskii, Zh. Eksp. Teor. Fiz. 61 (1971) 1141.

[3] B.I. Halperin, D.R. Nelson, J. Low Temp. Phys. 36 (1979) 599.

[4] V. Ambegaokar, B.I. Halperin, D.R. Nelson, E.D. Siggia, Phys. Rev. Lett. 40 (1978) 783.

[5] V. Ambegaokar, B.I. Halperin, D.R. Nelson, E.D. Siggia, Phys. Rev. B 21 (1980) 1806.

[6] I. Hetel, T.R. Lemberger, M. Randeria, Nat. Phys. 3 (2007) 700.

[7] J. Yong, M.J. Hinton, A. McCray, M. Randeria, M. Naamneh, A. Kanige, T. R. Lemberger, Phys. Rev. B 85 (2012) 180507 (R).

[8] I. Bozovic, X. He, J. Wu, A.T. Bollinger, Nature 536 (2016) 309.

[9] L. Benfatto, C. Castellani, T. Giamarchi, Phys. Rev. Lett. 98 (2007) 117008.

[10] P. Minnhagen, O. Westman, A. Jonsson, P. Olsson, Phys. Rev. Lett. 74 (1995) 3872.

[11] L. Benfatto, C. Castellani, T. Giamarchi, Phys. Rev. B 80 (2009) 214506.

[12] D.S. Fisher, M.P.A. Fisher, D.A. Huse, Phys. Rev. B 43 (1991) 130.

[13] D.A. Huse, M.P.A. Fisher, D.S. Fisher, Nature 358 (1992) 553.

[14] R.H. Koch, V. Foglietti, W.J. Gallagher, G. Koren, A. Gupta, M.P.A. Fisher, Phys. Rev. Lett. 63 (1989) 1511.

[15] M.C. Sullivan, R.A. Isaacs, M.F. Salvaggio, J. Sousa, C.G. Stathis, J.B.

Olson, Phys. Rev. B 81 (2010) 134502.

[16] P. Das, A.K. Ghosh, Physica C 548 (2018) 27.

[17] T. Sk, A.K. Ghosh, J. Low Temp. Phys. 198 (2020) 224.

[18] Y. Matsuda, S. Komiyama, Phys. Rev. B 48 (1993) 10498.

[19] S. Martin, A.T. Fiory, R.M. Fleming, G.P. Espinosa, A.S. Cooper, Phys. Rev. Lett. 62 (1989) 677.

[20] D.H. Kim, A.M. Goldman, J.H. Kang, R.T. Kampwirth, Phys. Rev. B 40 (1989) 8834.

[21] H.H. Wen, P. Ziemann, H.A. Radovan, S.L. Yan, Europhys. Lett. 42 (1998) 319.

[22] J. L. Tallon, C. Bernhard, H. Shaked, R. L. Hitterman, J. D. Jorgensen, Phys. Rev. B 51 (1995) 12911.

[23]Y. Ando, A. N. Lavrov, S. Komiya, K. Segawa, X. F. Sun, Phys. Rev. Lett. 87 (2001) 017001-1.

[24] A. Stangl, A. Palau, G. Deutscher, X. Obradors, T. Puig, Sci. Rep. 11 (2021) 8176.

[25] I. Bozovic, X. He, J. Wu, A. T. Bollinger, Nature 536 (2016) 309.

[26] L. Benfatto, C. Castellani, T. Giamarchi, Phys. Rev. B 77 (2008) 100506 (R).

[27] D.M. Broun, W.A. Huttema, P.J. Turner, S. Ozcan, B. Morgan, R. Liang, W. N. Hardy, D.A. Bonn, Phys. Rev. Lett. 99 (2007) 237003.

[28] N.R. Lee-Hone, J.S. Dodge, D.M. Broun, Phys. Rev. B 96 (2017) 024501.

[29] S. Steers, T.R. Lemberger, J. Draskovic, Phys. Rev. B 94 (2016) 094525.

[30] Y. Zuev, M.S. Kim, T.R. Lemberger, Phys. Rev. Lett. 95 (2005) 137002.

[31] D.R. Strachen, M.C. Sullivan, P. Fournier, S.P. Pai, T. Venkatesan, C.J. Lobb, Phys. Rev. Lett. 87 (2001) 067007.

[32] D.R. Strachen, M.C. Sullivan, C.J. Lobb, Phys. Rev. B 73 (2006) 012512.

[33] P.J.M. Woltgens, C. Dekker, J. Swuste, H.W. de Wijn, Phys. Rev. B 48 (1993) 16826.

[34] Z. Sefrioui, D. Arias, M. Varela, J.E. Villegas, M.A.L. de la Torre, C. Leon, G.D. Loos, J. Santamara, Phys. Rev. B 60 (1999) 15423.

[35] T. Horide, K. Matsumoto, P. Mele, A. Ichinose, R. Kita, M. Mukaida, Y. Yoshida, S. Horii, Appl. Phys. Lett. 92 (2008) 182511.

[36] H. Xu, S. Li, S.M. Anlage, C.J. Lobb, M.C. Sullivan, K. Segawa, Y. Ando, Phys. Rev. B 80 (2009) 104518.

[37] S.W. Pierson, M. Friesen, S.M. Ammirata, J.C. Hunnicutt, L.A. Gorham, Phys. Rev. B 60 (1999) 1309.

[38] C. Wengel, A.P. Young, Phys. Rev. B 54 (1996) R6869.

Chapter 5

Dynamic and static exponents in FFH scaling using superfluid phase stiffness in co-doped superconducting systems

5.1 Introduction

In Berezinskii - Kosterlitz - Thouless (BKT) phase transition, T_{BKT} is a transition temperature from a state with the bound vortex - antivortex pairs at low temperatures to another state of unpaired vortices and antivortices at higher temperatures **[1, 2]**. Current-voltage (*IV*) characteristics of cuprate superconductors reveals that T_{BKT} is obtained below the superconducting critical temperature, T_c. Nonlinearity in *IV* is explained with the help of an exponent, η. The nonlinearity in *IV* at zero external magnetic field below T_c can also be used to understand the underlying vortex states. Superfluid phase stiffness (SPS) is extracted following the Ambegaokar - Halperin - Nelson - Siggia (AHNS) theory **[3, 4]**.

Fisher, Fisher and Huse (FFH) introduced a scaling relation to explain the transition from the vortex glass (VG) state to the vortex fluid (VF) state **[5, 6]**.

The characteristic temperature at which the (VG to VF) transition occurs in a magnetic field is defined as the glass transition temperature, T_g. *IV* characteristics at finite magnetic fields are generally used to detect T_g. By using a scaling relation the resistive states are found to be collapsed for $T > T_g$ in the FFH formulation **[6]**. For any continuous phase transition the scaling relation is expressed by using a scaling function. In addition, the existence of glass transition can be proved by the scaling of *IV* characteristics. An important question remains whether the same FFH scaling relation can be used to identify the vortex unbinding state above T_{BKT} observed in the BKT phase transition. Understanding the variations of SPS (J_s), static exponent (v) and dynamic exponent (z) around T_{BKT} with T is a major step to investigate the applicability of the FFH scaling for BKT vortex system.

We have analysed *IV* characteristics of superconducting $Eu_{0.7-x}Ca_{0.3}Ce_xBa_2Cu_3O_{7-\delta}$ (ECCBCO) below T_c. The exponent η as a function of T has been extracted by using nonlinear *IV* curves. SPS has been extracted using the AHNS theory. T_{BKT} obtained from the η (T) is used to find out v and z. Dependences of both exponents with T have been studied. The FFH scaling theory has been applied to analyse the possible scenario of collapsing of the *IV* curves of several co-doped superconductors. Impact of the SPS on the data collapsing has also been studied.

5.2 Experimental

We have synthesized highly pure superconducting $Eu_{1-x-y}Ca_xCe_yBa_2Cu_3O_{7-\delta}$ (ECCBCO) by using the standard solid state reaction method [7]. The pure sample labeled as S6 (EBCO) is with x = 0.0, y = 0.0 and Ca doped sample, S7 (ECBCO) corresponds to x = 0.3, y = 0.0. Four other samples (ECCBCO) S8, S9, S10 and S11 are with a constant x = 0.3 but having a different Ce concentration, y. S8, S9, S10 and S11 correspond to y = 0.05, 0.1, 0.15 and 0.2 respectively. We have measured resistivity (ρ) as a function of T by using a closed cycle cryogenerator (JANIS) [8]. Resistivity measurements have been done by using a constant current 1.0 mA. All transport measurements of the bar shaped ECCBCO have been performed in the usual four probe method. We have shown a picture of a typical bar-shaped sample having the separation between two voltage leads of 1.05 mm in the inset of the **Figure 5.1**. *IV* measurements have been carried out at several constant T around T_c over a wide range of current of 100 nA through 5 mA.

5.3 Results and discussions

In **Figure 5.1** we have plotted the resistivity as a function of T for all ECCBCO samples (S6 to S11). In **Figure 5.2** we have shown the variation of $d\rho/dT$ as a function of T. Onset T_cs of respective samples have been obtained by taking the

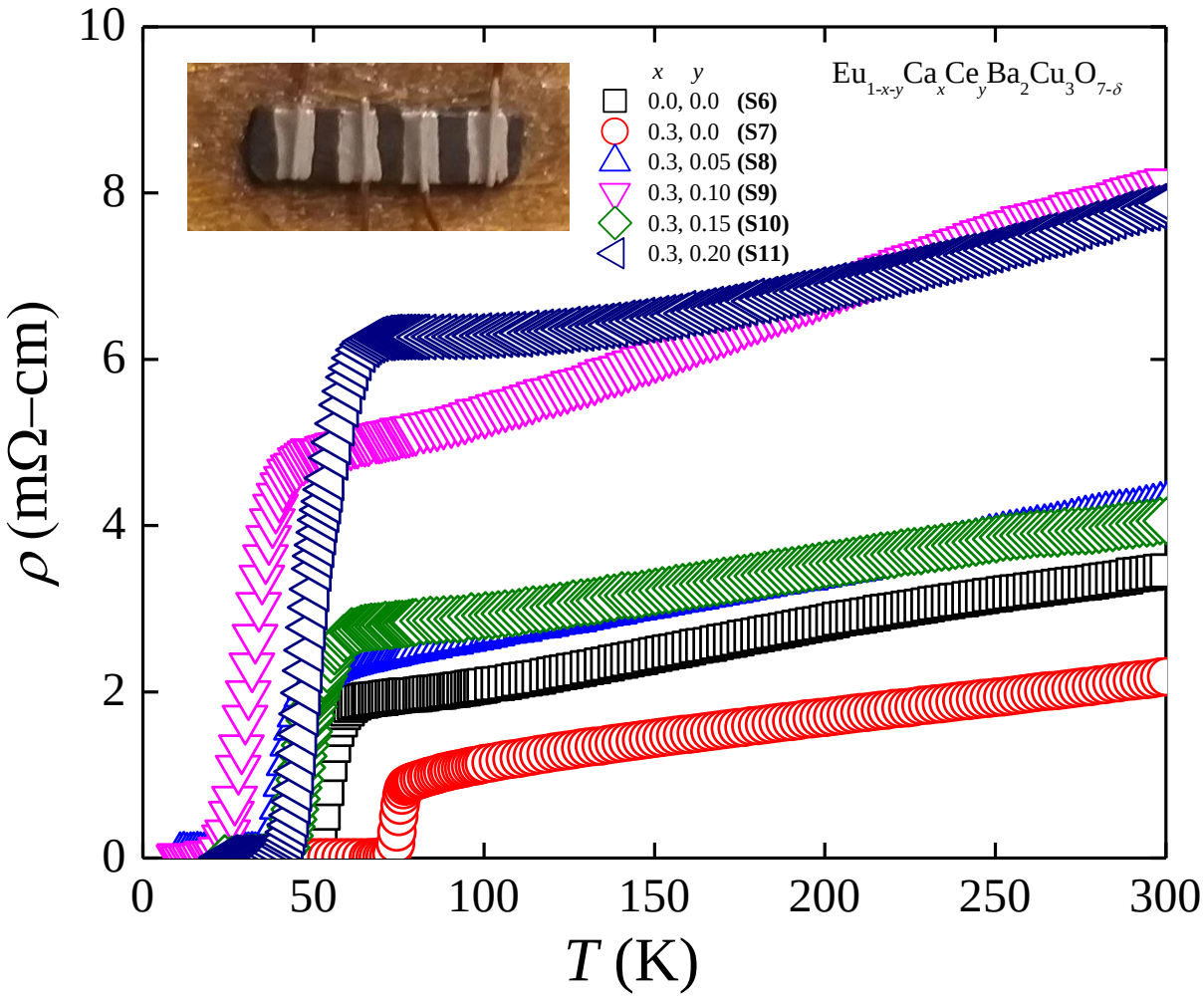

Figure 5.1 Resistivity as function of T in ECCBCO samples (S6 to S11).

T at which the abrupt change in $d\rho/dT$ occurs from the normal state. Clearly our T_c and T_c(R=0) are different in $d\rho/dT$ vs. T. Below the peak of $d\rho/dT$ vs. T we generally define as T_c(R=0). However, we have T_c which is actually known to be the onset of superconducting transition. Moreover, for $T < T_c$(R=0), *IV* measurements are not carried out (rather not possible because of negligible small

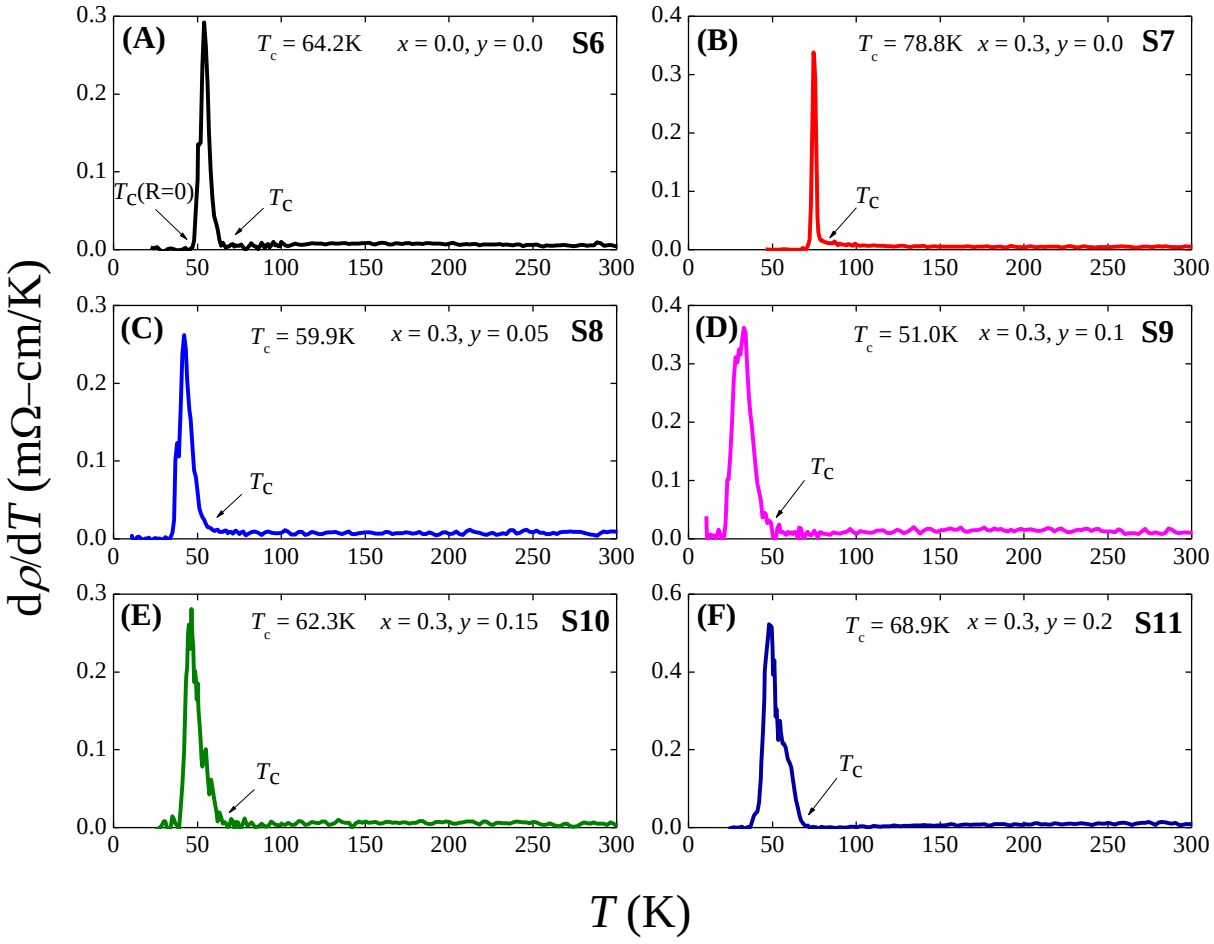

Figure 5.2 Variations of $d\rho/dT$ versus T in ECCBCO (S6-S11) samples. Panels correspond to individual samples. T_c is shown for each samples. Typical choice of T_c (R = 0) is shown for S6.

voltage drop) at zero (magnetic field) field. We do not applied any magnetic field for *IV* measurements. We have chosen T_c as the onset of superconducting transition. For the study of the BKT phase, one needs to consider the phase of pair and its distribution forms the vortex states (at zero field). However, at T =

T_c unbinding state is there. As we decrease T, at $T = T_{BKT}$ bound pairs formation starts (onset of BKT transition). In polycrystalline cuprate systems like EBCO, ECBCO, ECCBCO exhibit the BKT transition if one can tune it **[9-11]**. Several other cuprate crystals and bulk polycrystalline superconductors are also reported to be potential to exhibit the BKT phase transition **[12, 13]**. The onset T_cs are found to be 64.2K, 78.8K, 59.9K, 51.0K, 62.3K and 68.9K corresponding to S6, S7, S8, S9, S10 and S11 respectively. Normal states and variations of the hole doped and co-doped ECCBCO reveal analogous features as is observed in other electron doped superconductors **[14-16]**.

In **Figure 5.3 (A-F)** we have shown *IV* characteristics at several constant *T* for all the six (S6-S11) samples. We have also shown corresponding *EJ* in each *IV* plot as well. *E* is the electric field in mV/cm for corresponding voltage drop *V* in mV. The current density is *J* in mA/cm^2 for corresponding current *I* in mA. Nonlinear *IV* features are observed in the range of 50.0 K and 59.0 K in S6. Above 58.0 K to T_c = 64.2 K, *IV* becomes linear. In the inset of **Figure 5.3 (A)**, we have shown a representative nonlinear *IV* at 50.0 K. In the S7 sample, the nonlinear behaviour in *IV* is observed in the range of 74.0K and 77.0 K. In co-doped S8, S9, S10 and S11 samples, the nonlinearity in *IV* is observed in the range of (i) 33.0 K to 47.0 K, (ii) 16.0 K to 26.0 K, (iii) 39.0 K to 49.0 K and (iv) 43.5 K to 55.0 K respectively. In the inset of each panel in **Figure 5.3 (C-F)**, we have

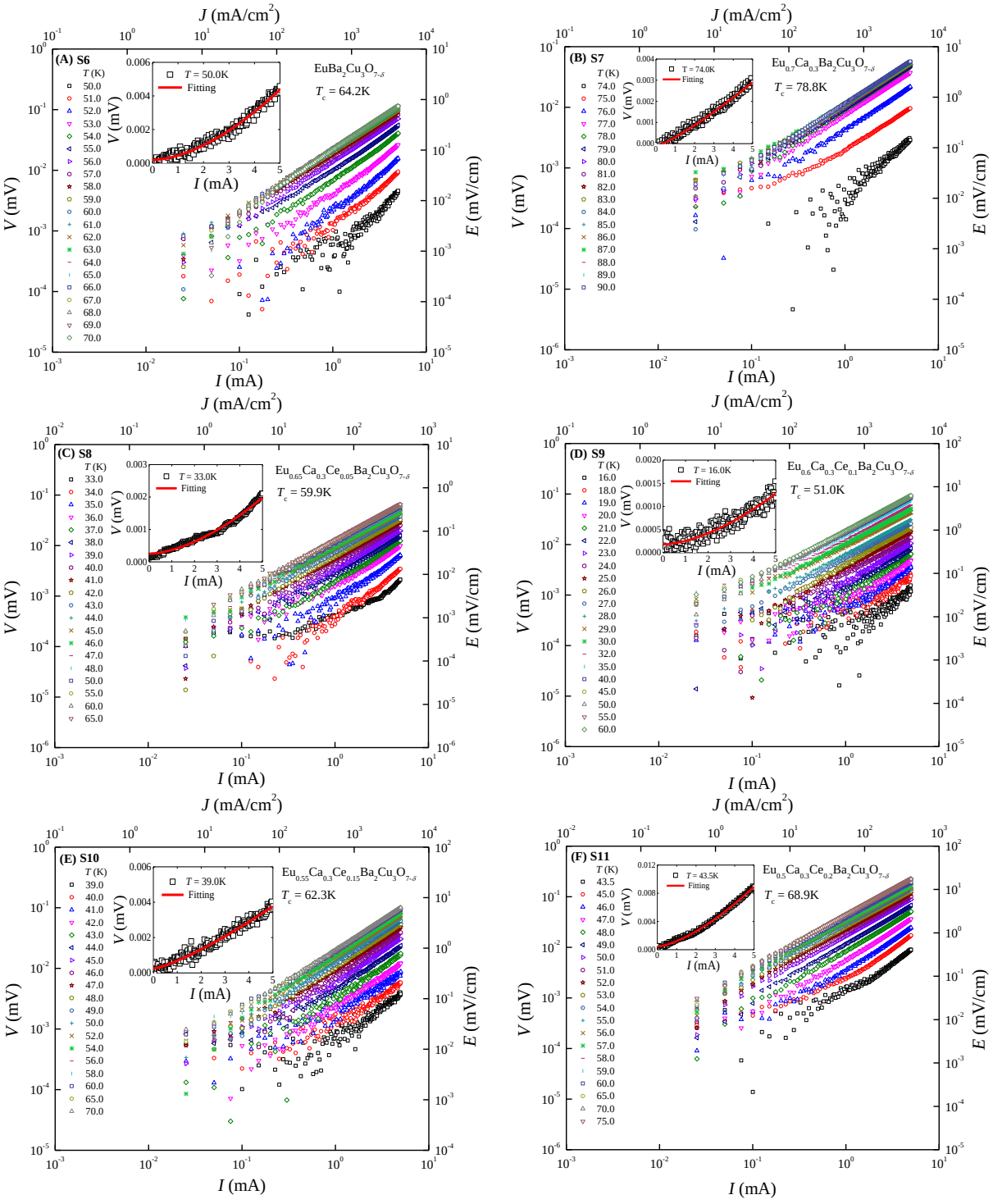

Figure 5.3 *IV* curves in log-log scale below T_c at several T of ECCBCO (S6-S11) superconductors. Inset of each plot shows the *IV* characteristic of the respective samples in linear scale. η is obtained by the fitting shown as the solid line in the inset using an equation $V = aI^{\eta}$.

shown representative nonlinear *IV*s of co-doped ECCBCO. Clearly in all samples below T_c, there are both linear and nonlinear groups of *IV* **[9, 10, 12]**.

Nonlinearity observed in *IV* over a wide range of *T* for each sample has been studied within the framework of the BKT transition at zero field **[11, 17]**. The nonlinear voltage can be expressed by an exponent η using the equation (1.1) following the idea of the BKT transition **[1, 2]**. The *IV* curves have been fitted by using the equation (1.1). In **Figure 5.3** we have shown *IV* plots in log-log scale at several *T* for all samples (S6-S11). In the insets of **Figure 5.3 (A-F)** we have shown the fitted nonlinear *IV* plots of respective samples. η has been extracted at several *T*. The nonlinear nature of *IV* vanishes at T_{BKT} at which η becomes 1.0 corresponding to the linear behaviour. Actually linear *IV* (for which $\eta = 1$) are also shown in the log (*I*)-log (*V*) scale. In **Figure 5.4** we have shown a combined plot of η versus *T*. Nonlinear behaviour of η (*T*) is observed in the pure (S6), hole doped (S7) and co-doped (S8-S11) samples. T_{BKT} are observed to be 58.0 K, 76.0 K, 46.0 K, 25.0 K, 49.0 K, 55.0 K corresponding to S6, S7, S8, S9, S10 and S11 respectively.

Here we have performed *IV* measurements in the zero (magnetic) field condition. There are several existing literature in which the BKT transition is detected in anisotropic quasi 2D polycrystalline superconducting system solely by the transformation of nonlinear to linear *IV*. It is well known that in presence of weak

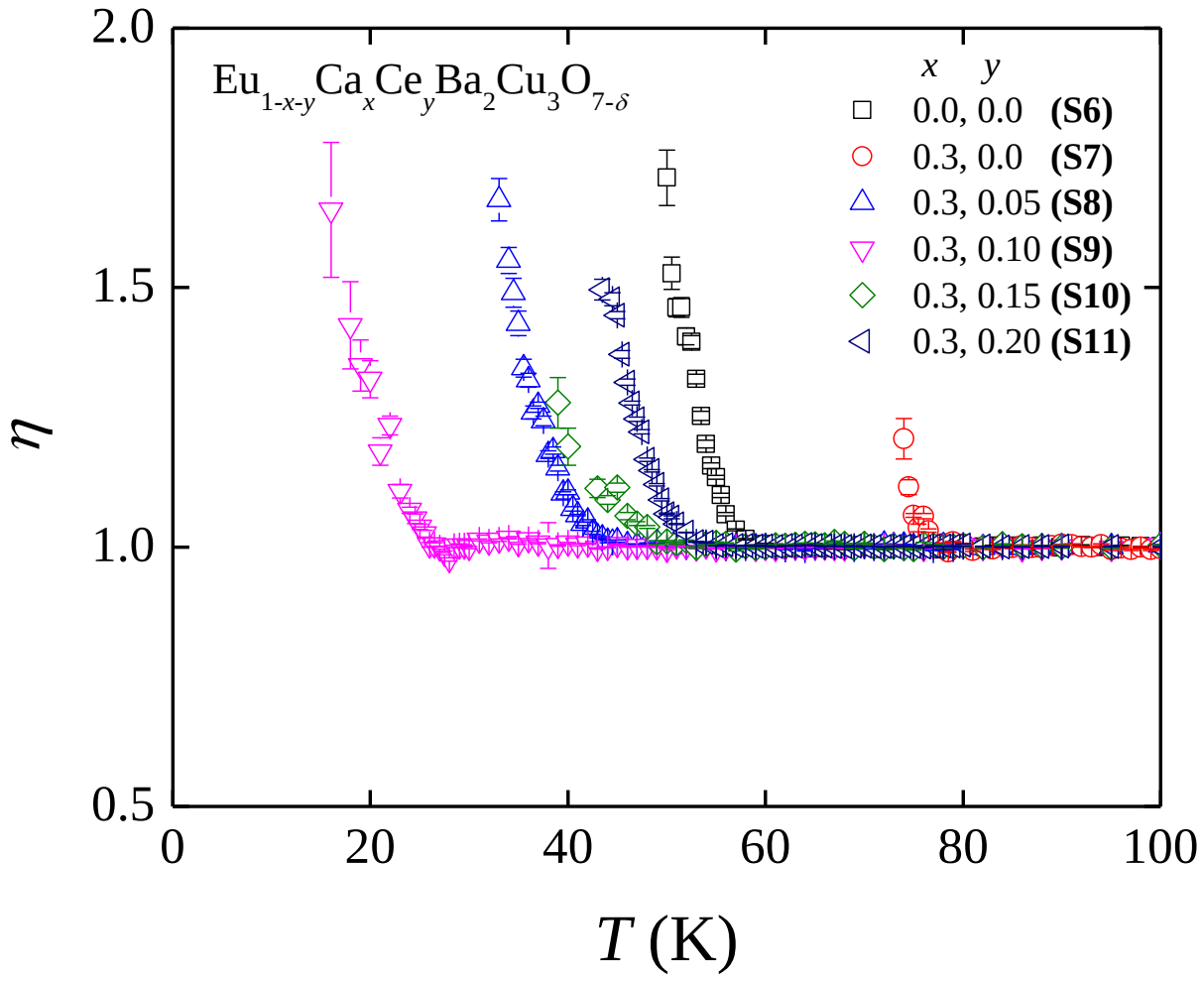

Figure 5.4 Variations of η as a function T of ECCBCO (S6-S11).

coupling in 2D superconducting system the BKT transition is observed **[18]**. In bulk EBCO system the broadening of the phase transition may depends on the elements we have used as doping purpose. We are dealing with a class of vortices different from type II superconductors. Formed vortices in such scenario are generally known to be bound pairs below T_{BKT}. Bound pairs are in the ordered

states. However, as we increase T, unbinding of paired states takes place and it is a disordered state above T_{BKT}. Nonlinearity in IV defines the size of bound vortex pairs [19]. To characterize such bound pairs by nonlinear IV the power law equation (1.1) is used. Above T_{BKT} free vortices results in linear IV. As BKT phase transition is basically related to the unbinding of vortices (a disordered state), it will be reasonable to comment that nonlinear to linear transformation in IV is one of the signature of the onset of the BKT phase transition. However we have not found a sharp jump of η from 3.0 to 1.0 at T_{BKT}. Rather a broadened transition in η (T) is observed. Below T_c (R=0) IV curves at zero field is not measured and therefore growth of η (T) with further lowering is restricted (below 3.0). Moreover, there are several other studies with an alternative analysis in which nonlinear IV has also been observed without a clear signature of a sharp jump [20, 21].

We have extracted the SPS, J_s (T) following the equation (1.2) within the framework of the AHNS theory [3, 4]. In **Figure 5.5** we have shown J_s as a function of T/T_c for all six samples. J_s is zero for $T > T_{BKT}$. Below T_{BKT}, J_s shows nonlinear increase with the decrease in T [22]. The estimated values of charge carrier density, n per m^3 and superfluid density, n_s per m^3 at experimentally lowest possible measured temperature are 1.14×10^{27} and 1.75×10^{6} for S6, 1.36×10^{27} and 7.62×10^{5} for S7, 1.09×10^{27} and 1.09×10^{6} for S8, 9.97×10^{26}

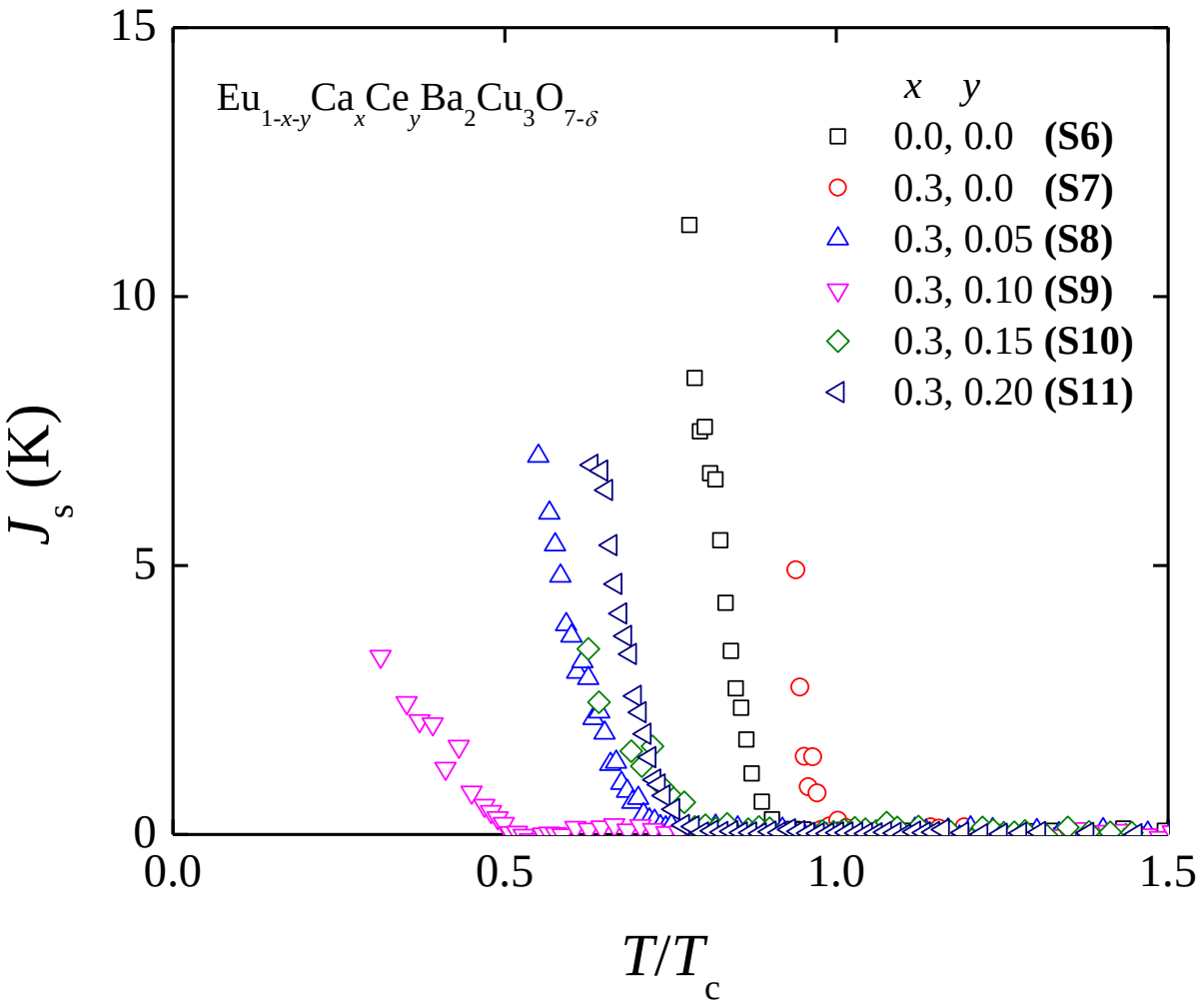

Figure 5.5 Variation of J_s as a function of T/T_c following AHNS theory in all ECCBCO (S6-S11) superconductors.

and 5.13×10^5 for S9, 1.12×10^{27} and 5.35×10^5 for S10,$1.2 \times 10^{27}$and 1.06×10^6 for S11 respectively **[17, 23-26]**. The linear variation of J_s (T) in several cuprate superconductors is reported **[27, 28]**. However, nonlinear increase in J_s (T) below T_{BKT} is observed in the superconducting systems over a wide range of T **[29]**. Nonlinear J_s (T) can be attributed to the presence of competitive nature

between the low T excitations of quasiparticles and the thermal phase fluctuations near T_{BKT} [30]. Even though the hole and electron doping in cuprate superconductors create a different pairing mediator the variations of SPS with T remain almost similar [31].

A scaling function, G_+ associated in the FFH scaling theory has a characteristic transition temperature, T_g which is generally determined by using the change in the curvature of the *IV* curves [5, 6]. We propose that the idea of FFH scaling can be used in the understanding of the *IV* curves at zero field BKT transitions [32]. T_{BKT} has been used as an equivalent temperature of the T_g. It is important to mention that the FFH theory applicable for Abrikosov vortex states has been used for a different vortex system related to BKT transition. We have performed scaling of *IV* data in two different cases (i) $T > T_{BKT}$ and (ii) $T < T_{BKT}$ by proposing T_{BKT} as analogous to T_g for all ECCBCO samples.

Firstly we express the FFH scaling relation as the equation (4.1). Within the framework of the FFH theory, G_+ is known as the scaling function, D is the dimensionality and v is the static critical exponent [33]. For using the scaling relation the linear resistivity $\rho_L(T)$ has been chosen at a current of 100 nA [34]. z of the FFH theory is determined by using the equation (4.2) for D = 3. By comparing it with the nonlinear equation (1.1), we have equation (4.3). We have

determined v related to the FFH theory. We have extracted v, by using the equation (4.4) [34].

We have shown v (T_g) in **Figure 5.6 (A)** for the sample S6. In the inset of **Figure 5.6 (A)**, we have shown the variation of ln (ρ_L) as a function of $ln\left(\left|1-\frac{T}{T_g}\right|\right)$ for $T_g = T_{BKT}$. v has been extracted from the slope of the fitting line. v related to FFH theory shows a clear jump at T_{BKT} in pure Eu-123 (S6) and co-doped Eu-123(S8-S11). From this observation we have tried to estimate FFH exponents. The jump observed in v is related to the unbinding of usual BKT vortices at higher T. *IV* characteristics exhibits nonlinear to linear transformation at a temperature, T_{BKT} which is below the onset superconducting transition temperature T_c. Considering T_{BKT} (used in BKT transition) as an order-disorder transition, we have used it in the FFH model in which we need T_g for scaling. In **Figure 5.6 (B)**, we have shown the variation of v (T_g) for S7. The curvature of the v (T_g) is changed in the hole doped sample. In **Figure 5.6 (C-F)**, we have shown v (T_g) for co-doped (S8-S11) samples following the same method as carried out for S6 and S7. An upward curvature in v (T_g) is visible in all co-doped (S8-S11) samples which is the same as is observed in the pure S6. However, v is found to be very sensitive to the co-doping and the growth in SPS is inversely related to v. As v decreases J_s increases as well. In addition, we have shown z (T) on the same plots in **Figure 5.6 (A-F)**. Converging nature of both v (T_g) and z (T) may have an origin in the unbinding

of vortex - antivortex pairs in a medium with the vanishing SPS [35, 36]. In the previously reported data $z > \nu$ [34], in our data we have estimated $\nu > z$. Larger ν are estimated in our data though in previous cases the maximum reported ν value is within 2. For S6 to S11 we have proposed T_{BKT} as T_g to perform FFH scaling and observed z is lowered with increasing temperature T which is in agreement with previously reported z-T variations [37, 38]. The extracted z is found to be within a range of 1.0 to 2.45 which is comparatively lower than reported in [34, 39] for the given samples (S6-S11).

In **Figure 5.7** we have shown the variations of $(\rho/\rho_L) - 1$ versus $(J/T)[|1 - (T/T_g)|]^{-2\nu}$ in log-log scale for both regions $T > T_{BKT}$ and $T < T_{BKT}$ for all (S6-S11) samples [33, 34]. Data collapsing is observed in the region $T > T_{BKT}$ associated with the zero SPS of all samples. $(\rho/\rho_L) - 1 \simeq 10^3$ is found to be the collapsed number for all samples. It indicates that scaling is successful by applying FFH scaling function for the unbinding BKT vortices. The data collapsing scenario remains the same even for the different medium consisting of different charge doping in S7-S11. It is important to mention that for each sample at $T > T_{BKT}$, we have observed data collapsing within different ranges of the independent variable because T_{BKT} varies from S6 to S11. For $T < T_{BKT}$ deviation of scaling has been found to be associated with finite superfluid density.

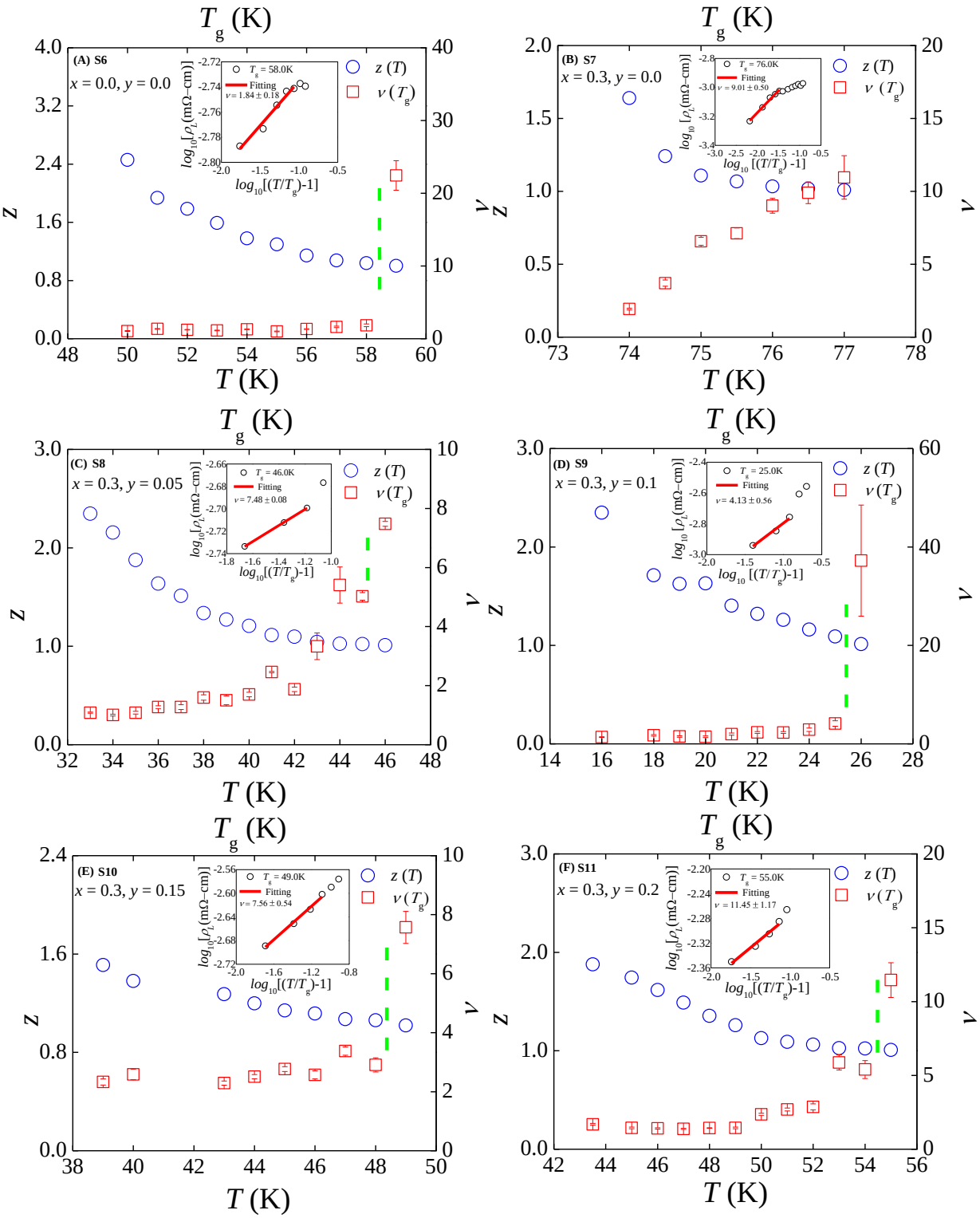

Figure 5.6 Variation of (i) static critical exponent v as a function of T_g, and (ii) dynamic critical exponent z, as a function of T in ECCBCO (S6-S11).

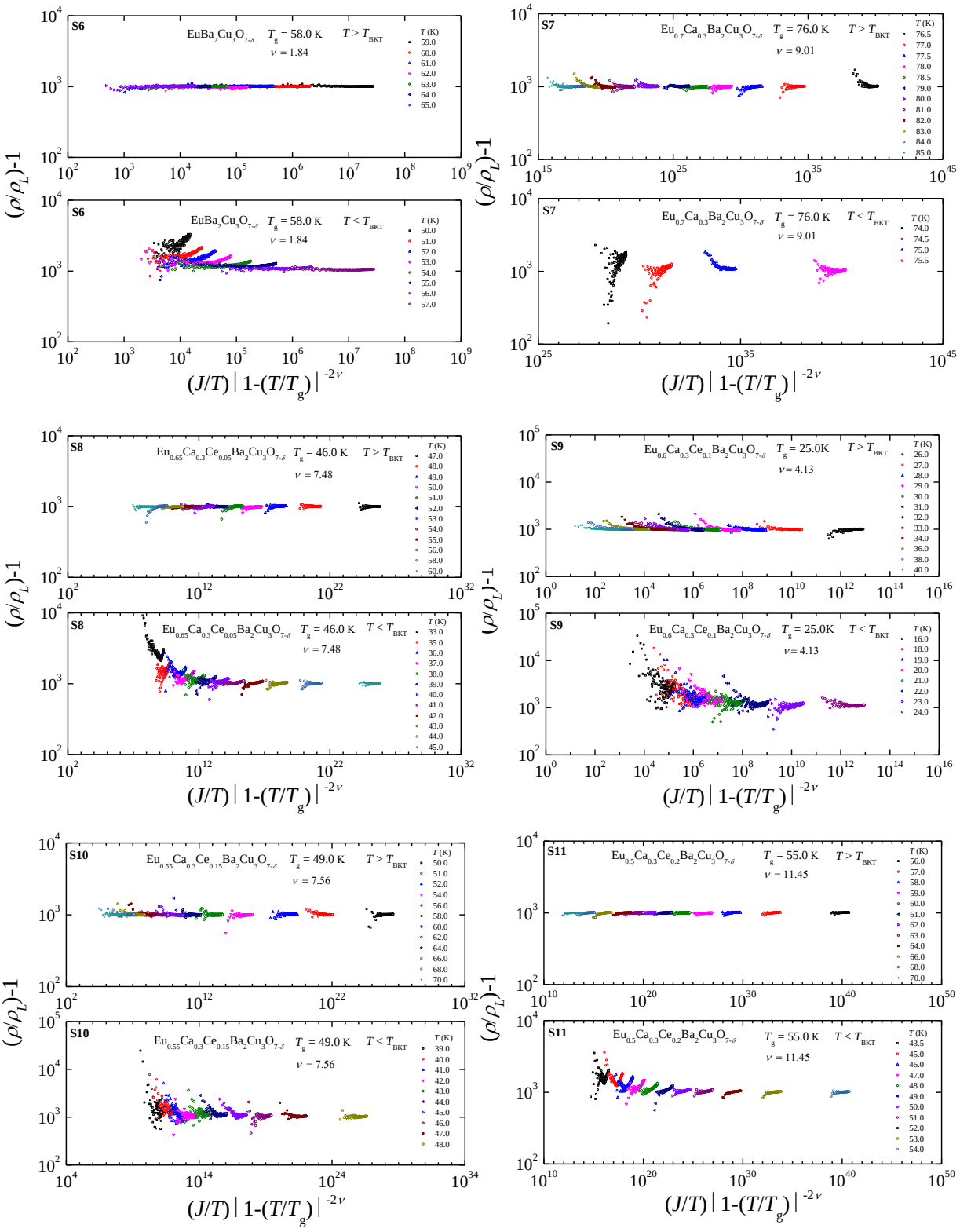

Figure 5.7 Variation of (ρ/ρ_L)-1 versus $(J/T)[|1-(T/T_g)|]^{-2\nu}$ in log-log scale for $T > T_{BKT}$ and $T < T_{BKT}$ in ECCBCO (S6-S11).

However, the deviation is observed to be independent of the nature of doping. In co-doped S9-S11 superconductors, deviation is not controlled one by the level of doping.

5.4 Summary

SPS of ECCBCO has been extracted following the AHNS theory and using nonlinear *IV* characteristics below T_c. Growth of SPS is found to be nonlinear and is independent of the nature of doping. The characteristic temperatures T_{BKT} of ECCBCO obtained from the *IV* characteristics have been used to extract v and z associated with the FFH scaling function. Converging nature of v and z is associated with the vanishing SPS. Below T_c, scaling has been achieved for above and below T_{BKT}. The observed overall scaling remains unaltered in unbinding in different mediums of charge density. The FFH scaling function is found to be very successful in explaining scaling of *IV* related to the BKT transition in several superconducting systems.

5.5 References

[1] V. L. Berezinskii, Zh. Eksp. Teor. Fiz 61 (1971) 1144.

[2] J. M. Kosterlitz, D. J. Thouless, J. Phys. C 6 (1973) 1181.

[3] V**.** Ambegaokar, B. I. Halperin, D. R. Nelson, E. D. Siggia, Phys. Rev. Lett. 40 (1978) 783.

[4] V. Ambegaokar, B. I. Halperin, D. R. Nelson, E. D. Siggia, Phys. Rev. B 21 (1980) 1806.

[5] D. S. Fisher, M. P. A. Fisher, D. A. Huse, Phys. Rev. B 43 (1991) 130.

[6] D. A. Huse, M. P. A. Fisher, D. S. Fisher Nature 358 (1992) 553.

[7] P. Das, A. K. Ghosh, Physica C 548 (2018) 27.

[8] T. Sk, A. K. Ghosh, J. Low Temp. Phys. 198 (2020) 224.

[9] D. H. Kim, A. M. Goldman, J. H. Kang, R. T. Kampwirth, Phys. Rev. B 40 (1989) 8834.

[10] H. H. Wen, P. Ziemann, H. A. Radovan, S. L. Yan, Europhys. Lett. 42 (1998) 319.

[11] Y. Matsuda, S. Komiyama, T. Onogi, T. Terashima, K. Shimura, Y. Bando, Phys. Rev. B 48 (1993) 10498.

[12] S. Martin, A. T. Fiory, R. M. Fleming, G. P. Espinosa, A. S. Cooper, Phys. Rev. Lett. 62 (1989) 677.

[13] T. V. Sukhareva and V. A. Finkel, Low Temperature Physics 46, 550 (2020).

[14] P. Fournier, P. Mohanty, E. Maiser, S. Darzens, T. Venkatesan, C. J. Lobb, G. Czjzek, R. A. Webb, R. L. Greene, Phys. Rev. Lett. 81 (1998) 4720.

[15] N. P. Armitage, P. Fournier, R. L. Greene, Rev. Mod. Phys. 82 (2010) 2421.

[16] N. R. Poniatowski, T. Sarkar, S. D. Sarma, R. L. Greene, Phys. Rev. B 103 (2021) L020501-1.

[17] I. Bozovic, X. He, J. Wu, A. T. Bollinger, Nature 536 (2016) 309.

[18] P. G. Baity, X. Shi, Z. Shi, L. Benfatto, and D. Popovic B 93, 024519 (2016).

[19] S. W. Pierson, M. Frieson, S. M. Ammirata, J. C. Hunnicutt, L. A. Gorham, Phys. Rev. B 60 (1999) 1309.

[20] I. V. Kuzmin, Technical Physics Letters 36, 400 (2010).

[21] K. Yu. Terent'ev, Physics of the Solid State 53, 2409 (2011).

[22] I. Hetel, T. R. Lemberger, M. Randeria, Nature Phys. 3 (2007) 700.

[23] J. L. Tallon, C. Bernhard, H. Shaked, R. L. Hitterman, J. D. Jorgensen, Phys. Rev. B 51 (1995) 12911.

[24] Y. Ando, A. N. Lavrov, S. Komiya, K. Segawa, X. F. Sun, Phys. Rev. Lett. 87 (2001) 017001-1.

[25] A. Stangl, A. Palau, G. Deutscher, X. Obradors, T. Puig, Sci. Rep. 11 (2021) 8176.

[26] L. Benfatto, C. Castellani, T. Giamarchi, Phys. Rev. B 77 (2008) 100506 (R).

[27] W. N. Hardy, D. A. Bonn, D. C. Morgan, R. Liang, K. Zhang, Phys. Rev. Lett. 70 (1993) 3999.

[28] C. Panagopoulos, T. Xiang, Phys. Rev. Lett. 81 (1998) 2336.

[29] L. Benfatto, S. Caprara, C. Castellani, A. Paramekanti, M. Randeria, Phys. Rev. B 63 (2001) 174513-1.

[30] E. W. Carlson, S. A. Kivelson, V. J. Emery, E. Manousakis, Phys. Rev. Lett. 83 (1999) 612.

[31] C. Weber, K. Haule, G. Kotliar, Nature Phys. 6 (2010) 574.

[32] P. Das, A. K. Ghosh, Physica C 593 (2022) 1354005.

[33] D. R. Strachen, M. C. Sullivan, C. J. Lobb, Phys. Rev. B 73 (2006) 012512-1.

[34] D. R. Strachen, M. C. Sullivan, P. Fournier, S. P. Pai, T. Venkatesan, C. J. Lobb, Phys. Rev. Lett. 87 (2001) 067007-1.

[35] I. Bozovic, X. He, J. Wu, A. T. Bollinger, J. Supercond. Nov. Mag. 31 (2018) 2683.

[36] V. J. Emery, S. A. Kivelson, Nature 374 (1995) 434.

[37] H. Xu, S. Li, S. M. Anlage, C. J. Lobb, Phys. Rev. B 80 (2009) 104518-1.

[38] K. Medvedyeva, B. J. Kim, P. Minnhagen, Phys. Rev. B 62 (2000) 14531.

[39] R. H. Koch, V. Foglietti, W. J. Gallagher, G. Koren, A. Gupta, M. P. A. Fisher, Phys. Rev. Lett. 63 (1989) 1511.

Chapter 6

An evidence of the second order BKT phase transition in three dimensional underdoped RE-123 superconductors

6.1 Introduction

Berezinskii - Kosterlitz - Thouless (BKT) phase transition is generally observed in the 2D XY spin and many other systems **[1-3]**. The theory of the BKT phase transition can be applied and tested in many other systems including both in two dimensional (2D) and three dimensional (3D) superconductors. In 2D superconducting layers the BKT phase transition has been observed in several cuprate superconductors. In cuprates the possible occurrence of the BKT phase transition may be related to the interplay between different length scales and energy scales **[4, 5]**. Energy scales which are associated in the BKT phase transition may not be universal **[4]**. Vortex core energy also plays an important role to identify the BKT phase transition temperature (T_{BKT}) from the variation of the superfluid phase stiffness (SPS) **[4, 6-8]**.

Several experimental observations are there assuring the occurrence of the BKT

phase transition in superconducting materials. The BKT phase transition in a quasi-2D bulk polycrystalline superconducting system is observed experimentally **[9]**. Anisotropic optimally doped Bi-2212 system exhibits sharp BKT downturns controlled by the stiffness of each isolated bilayer **[10]**. In a superconducting system T_{BKT} can be detected from the transformation of the nonlinear behaviour in current-voltage (*IV*) to linear nature below the superconducting transition T_c **[11]**. The SPS can be extracted from η, the nonlinear exponent of *IV* characteristics **[11, 12]**. A sharp jump of SPS at the transition is known to be a signature of the BKT phase transition **[13, 14]**.

According to the BKT theory vortices are in a bound pair state below T_{BKT} whereas above T_{BKT} vortex-antivortex pairs unbinds. Possibility of the BKT transition is investigated by superfluid density, n_s measurement in 2D disordered superconducting film **[4]**. n_s shows linear dependence with T_c in underdoped layered cuprates (quasi-2D) **[15]**. A quasilinear T dependence of n_s is also observed in some underdoped cuprates **[16, 17]**. There are several studies in which the sharp BKT transition is found to be suppressed by different causes. Thermal excitations is one of such causes for the disappearance of sharp BKT jump in cuprates **[4]**. Intrinsic inhomogeneities are also known to be responsible for smearing out the discontinuous jump in underdoped cuprates **[4]**.

Even though the BKT phase transition is generally observed in several 2D superconducting systems, there is enough evidence that interlayer coupling plays an important role **[18]**. In several quasi-2D and 3D systems the signature of the BKT is also detected in experiments **[19]**. The BKT behaviour can be observed even in bulk sample since the phase variation is identical in nature (only different in magnitude) as it is observed in 2D system. Even in single crystals unit cell with more than one layer is coupled. In bulk this scenario is randomly oriented in different grains. For two neighbouring grains (for example) BKT states are separated by grain boundary in real space in polycrystals and the phases of Cooper pairs will be different. However, there is no reason to suppress the BKT transition. The origin of the BKT states is independent of the crystal type i.e. polycrystalline or single crystal because the vortex associated here is originated as a result of the BKT transition is an intrinsic effect.

However, it is an open question whether the BKT transition is really a sharp transition or not because the gradual change in η with T is very common in superconductors. We have investigated the broadening of the BKT phase transition in three different 3D superconducting systems. We have shown experimental transport results below the critical temperature of three high quality bulk underdoped cuprate superconductors (i) $Nd_{0.6}Ca_{0.3}Ce_{0.1}Ba_2Cu_3O_{7-\delta}$ (S12), (ii) $Nd_{0.55}Ca_{0.3}Ce_{0.15}Ba_2Cu_3O_{7-\delta}$ (S13) and (iii) $Nd_{0.5}Ca_{0.3}Ce_{0.2}Ba_2Cu_3O_{7-\delta}$ (S14).

We have extracted η, SPS and discussed nature of the observed BKT phase transition in 3D cuprate systems.

6.2 Experimental

We have prepared superconducting NCCBCO (S12, S13 and S14) by using solid state synthesis method. Transport measurements of bar shaped samples have been performed by using four probe techniques using a closed cycle cryogenerator (JANIS CCR) **[20, 21]**. Resistivity of respective samples has been measured as a function of temperature at a fixed current of 1 mA in the range of temperature 10K to 300K. We have measured *IV* characteristics in zero magnetic field condition at fixed temperature around the onset superconducting transition temperature (T_c) using a range of current of 100 nA to 5 mA.

6.3 Results and discussions

In **Figure 6.1** we have shown resistivity as a function of T in superconducting $Nd_{0.6}Ca_{0.3}Ce_{0.1}Ba_2Cu_3O_{7-\delta}$ (S12), $Nd_{0.55}Ca_{0.3}Ce_{0.15}Ba_2Cu_3O_{7-\delta}$ (S13) and $Nd_{0.5}Ca_{0.3}Ce_{0.2}Ba_2Cu_3O_{7-\delta}$ (S14). The T_cs are 69.4K, 67.9K and 72.8K corresponding to S12, S13 and S14 respectively. All three superconductors

exhibit different normal states and superconducting phase transitions. Because of the random orientation of the grains it is reasonable to say that these superconducting samples are more isotropic and hence the systems are more 3D in nature even though superconducting planes are 2D **[22-24]**. Moreover, the typical separation between two 2D superconducting planes (~ 5.8 Å) is comparable to the typical coherence length (~ 10.0 Å in RE-123) which makes these systems 3D in nature below T_c **[25]**.

In **Figure 6.2 (A-C)** we have shown the *IV* characteristics below T_c in log - log scale for NCCBCO (S12, S13 and S14) respectively. Because of the higher level of noise at very low current we have shown that range of current up to 0.01 mA in **Figure 6.2 (A-C)**. Nonlinearity in *IV* has been observed over a wide range of temperatures below T_c in all three samples. Nonlinearity in *IV* can be explained within the BKT framework. Each *IV* is fitted by using the equation (1.1) related to BKT phase transition. Nonlinearity (*IV*) is absent above T_c which justifies that is solely originated in the superconducting state. The nonlinear *IV* has its origin in the behaviour of SPS with *T*. It may so happen that one minor of the factors for that is the distribution of T_c. If one believes that the nonlinearity is an effect of grain boundary, the nonlinearity (in *IV*) would be observed above T_c. But that is not observed. Nonlinearity in *IV* is observed at $T < T_{BKT}$ and it vanishes above T_{BKT}. However, it is true that granularity affects resistivity in the normal state (as

observed in S14). We believe that these effects (increasing resistivity) remain effective in the backdrop of the pair formation and BKT phenomena. Moreover, superconductivity is a phenomenon considered in the *k*-space (not in real space) and the BKT as mentioned earlier depends on phase distribution (in space) of Cooper pairs. There are number of studies in which the BKT has been explored in bulk polycrystals including moderately anisotropic superconductors **[26-29]**.

We have used very long annealing duration which is generally used to have uniform excess oxygen content and hence helps getting homogeneous T_c. Even if there is a weak T_c inhomogeneity from grain to grain, the formation of BKT states is not much affected in 2D superconducting plane. Rather it may affect the interlayer coupling. However quasi-2D nature of superconductor remains almost unaltered. Moreover, concentration of Ce at the rare earth (Nd) sites (doping carrier concentration) may cause of higher normal state resistivity. Of course, it effects BKT states as well as the BKT transitions. HTS has short coherence length which is responsible for broadening in superconducting transition (ρ-T for a fixed I). Moreover longer annealing makes sample homogeneous as reveal from other characterizations. It is true that carrier concentration is not solely responsible for controlling nonlinearity. In addition, we have focused on the nature of nonlinearity, not on the exact cause.

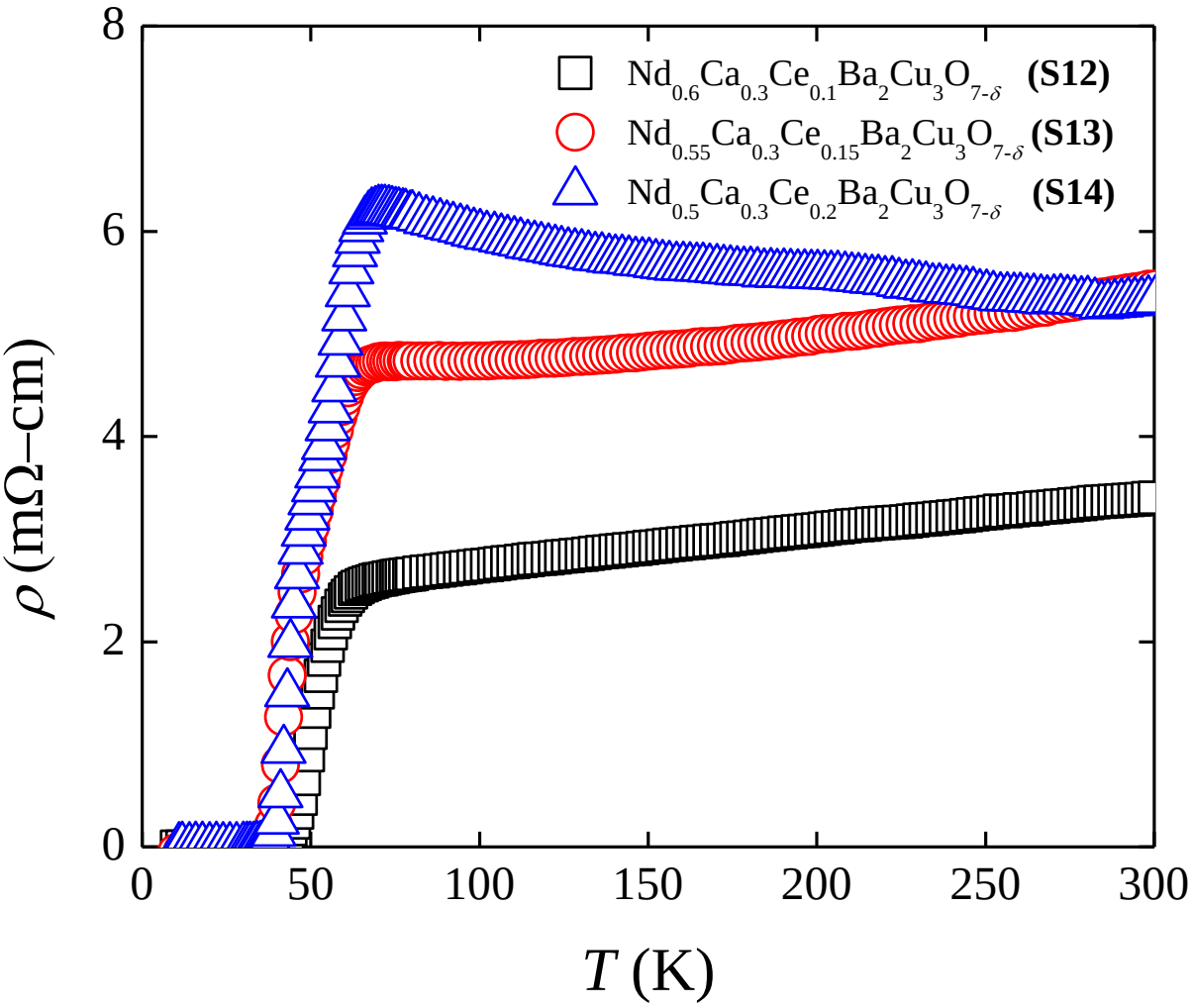

Figure 6.1 Resistivity as a function of temperature in $Nd_{0.6}Ca_{0.3}Ce_{0.1}Ba_2Cu_3O_{7-\delta}$ (S12), $Nd_{0.55}Ca_{0.3}Ce_{0.15}Ba_2Cu_3O_{7-\delta}$ (S13) and $Nd_{0.5}Ca_{0.3}Ce_{0.2}Ba_2Cu_3O_{7-\delta}$ (S14).

In the inset of **Figure 6.2 (A-C)**, we have shown a representative fitting line which is used to extract the exponent representing the nonlinear nature of the *IV* curve. η has been extracted from fitted *IV* at a constant temperature. η is known to be related with the SPS, J_s as following the equation (1.2) **[30-32]**.

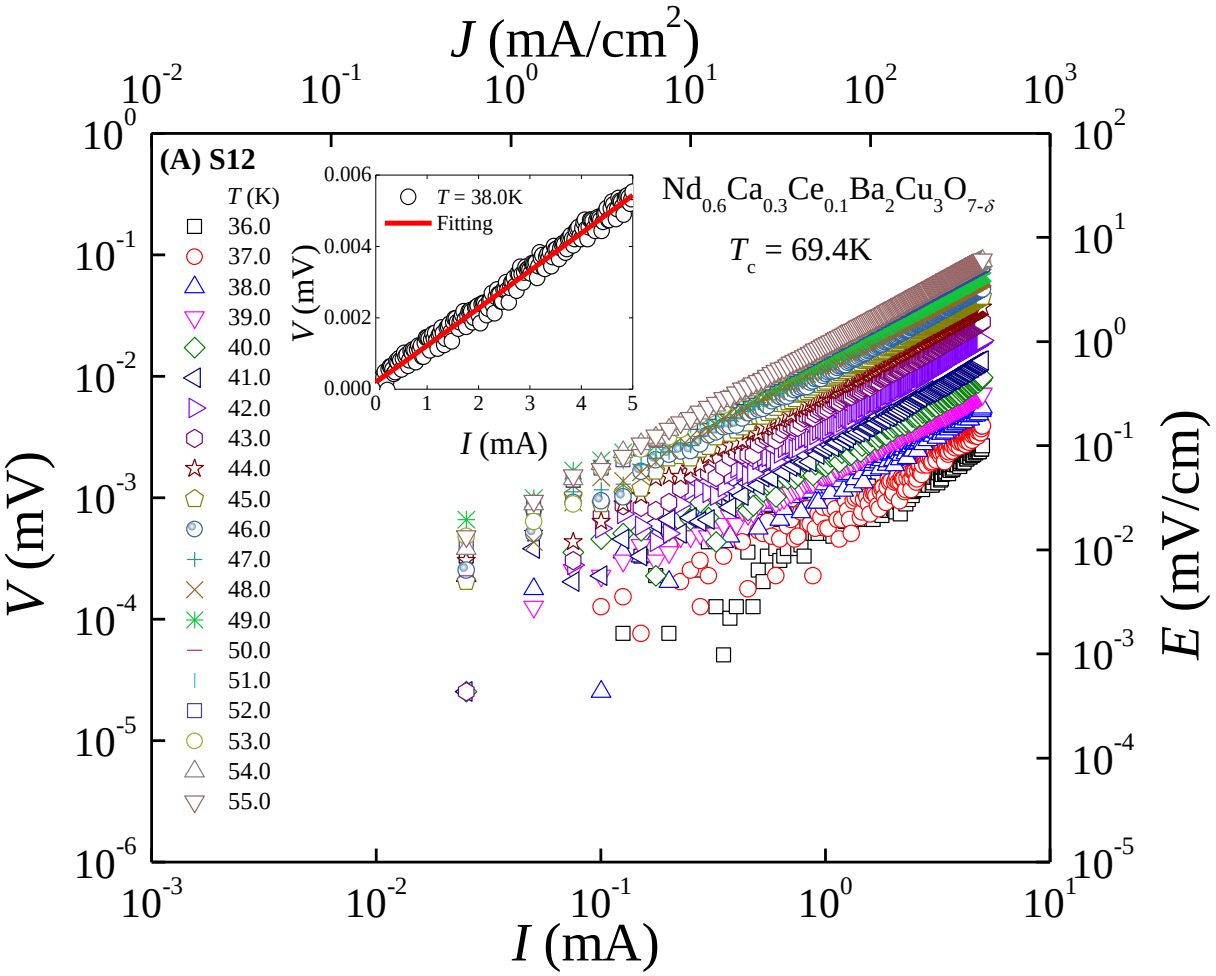

Figure 6.2 (A) Current-voltage (*IV*) characteristics at several T below T_c is shown in log - log scale for $Nd_{0.6}Ca_{0.3}Ce_{0.1}Ba_2Cu_3O_{7-\delta}$ (S12). In the inset the representative nonlinear *IV* curve is given at T = 38.0K for S12 in linear scale. In the inset the fitting is shown following the equation $V = aI^{\eta}$ to extract the exponent η related to BKT transition.

A remarkable signature of the BKT phase transition is the sharp jump of η at the transition T_{BKT} from η (T_{BKT}^{-}) = 3 to η (T_{BKT}^{+}) = 1.0. Therefore, the onset of the

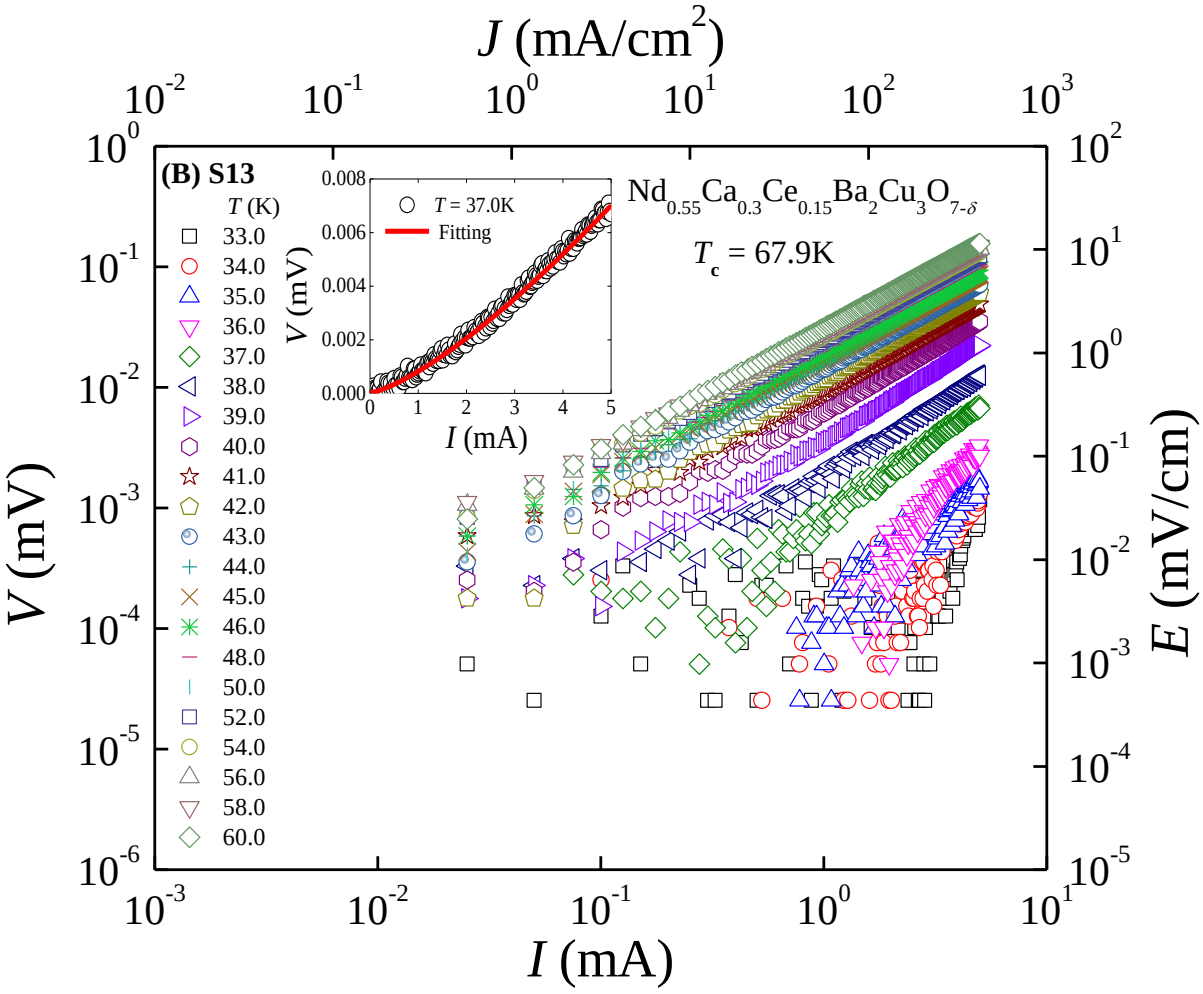

Figure 6.2 (B) Current-voltage (*IV*) characteristics at several T below T_c is shown in log - log scale for $Nd_{0.55}Ca_{0.3}Ce_{0.15}Ba_2Cu_3O_{7-\delta}$ (S13). In the inset the representative nonlinear *IV* curve is given at T = 37.0K for S13 in linear scale. In the inset the fitting is shown following the equation $V = aI^{\eta}$ to extract the exponent η related to BKT transition.

BKT phase transition is the lowest temperature at which η becomes 1.0. Variations of η as a function of T for S12, S13 and S14 are shown in **Figure 6.3**.

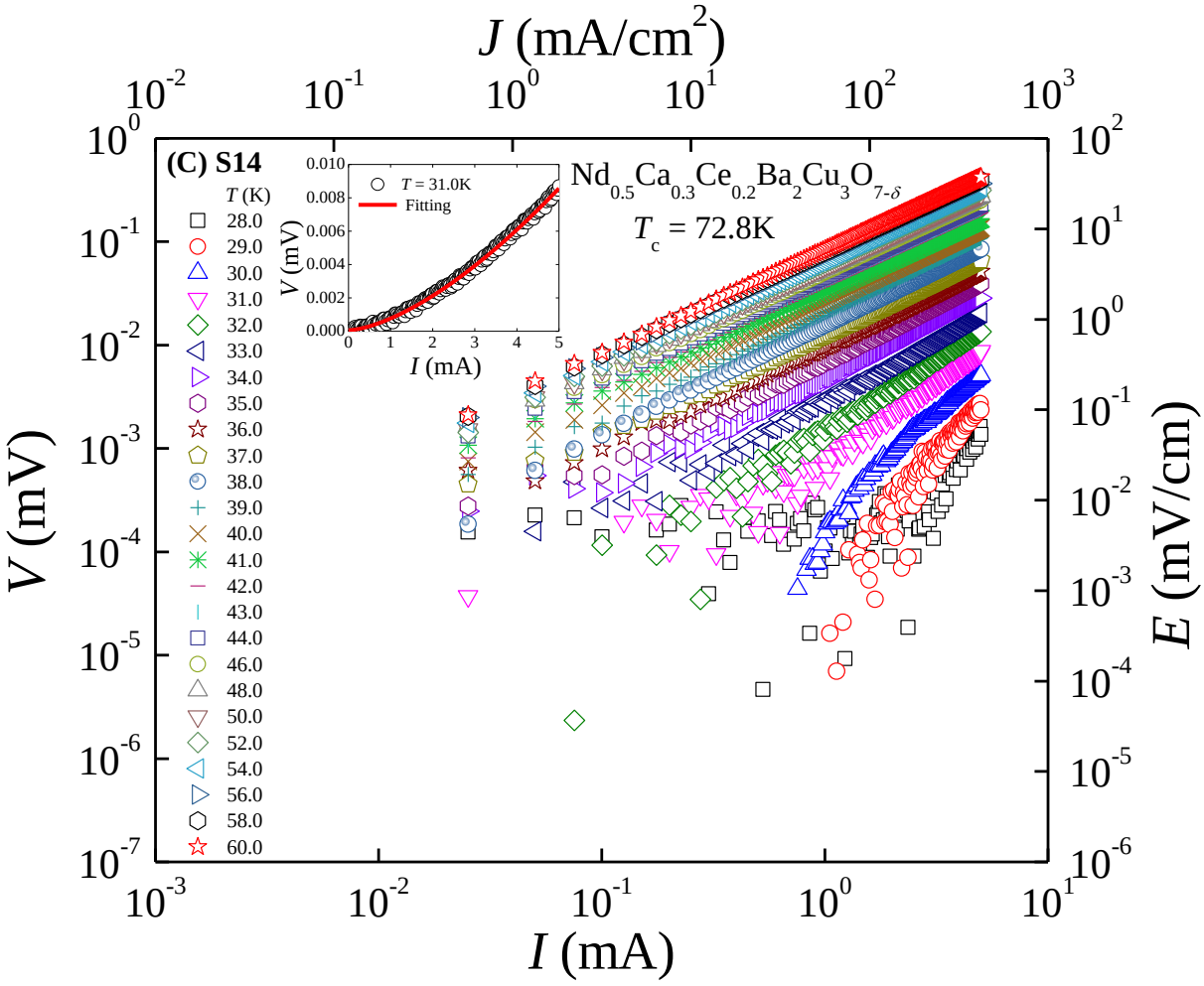

Figure 6.2 (C) Current-voltage (*IV*) characteristics at several T below T_c is shown in log - log scale for $Nd_{0.5}Ca_{0.3}Ce_{0.2}Ba_2Cu_3O_{7-\delta}$ (S14). In the inset the representative nonlinear *IV* curve is given at T = 31.0K for S14 in linear scale. In the inset the fitting is shown following the equation $V = aI^{\eta}$ to extract the exponent η related to BKT transition.

T_{BKT} corresponding to η = 1.0 of NCCBCO (S12, S13 and S14) are found to be 44.0K, 45.0K and 42.0K respectively. However, the transition to η = 3.0 is not observed even at much lower $T \sim T_c$ ($\rho \simeq 0$). Moreover, *IV* measurements done

in zero magnetic field condition have not been carried out below T_c ($\rho \simeq 0$) as the voltage drop is negligibly small. We have observed the maximum values of η are 1.15 at 36.0 K for S12, 3.38 at 33.0 K for S13 and 2.64 at 28.0 K for S14. Nature of the variation of η (T) is therefore clearly broad in nature in all three samples. NCCBCO123 is a 3D system as Y123, which is evidenced by T dependence of the superfluid density near T_c [33, 34]. In NCBCO, there are two 2D superconducting planes. BKT states are formed in individual layers but in two layers (per unit cell). This effectively makes the system 3D or quasi-2D. Broadening of BKT has been observed even in 2D systems and it is found to be disorder sensitive **[3]**. Broadening of $\frac{1}{\lambda^2}$, also a measure of superfluid density, versus T in the 2D system of Bi-2212 has been observed as a result of quantum fluctuations **[10]**. Therefore both indicated that broadening of the BKT is there even in 2D systems. We have observed that the BKT phase transition is possible in 3D system such as NCCBCO which is nothing but a coupled 2D system.

Low-T_c superconductors generally exhibit first order superconducting transition whereas generally HTSs exhibit 2nd order (superconducting) phase transition. This is detected from sharp or continuous variation of $\rho - T$. BKT transitions and superconducting transitions are highly inter-linked via phase of the Cooper pairs. Moreover, as a result of moderate anisotropy NCBCO is not a 2D system. The exponent, η, we never reached to η = 3. It indicates that the BKT transition is broad enough (in T) down to 10.0 K though it shows onset (T_{BKT}). Smearing out

of the sharp transition at T_{BKT} is in cuprate superconductors is very sensitive to several factors **[3, 10]**. A continuous variation of η (T) reveals that the observed BKT phase transition is a second order phase transition in 3D superconductors.

An approach is generally needed to extract the BKT transition temperature, T_{BKT}. According to an approach a BKT line, $J_s = 2T/\pi$ and experimental J_s (T) are plotted together. If J_s shows a discontinuous jump at the intersection with the BKT line **[11]**:

$$J_s(T_{BKT}^{-}) = \frac{2}{\pi}T_{BKT}, J_s(T_{BKT}^{+}) = 0 \qquad \ldots\ldots\ldots\ldots\ldots\ldots (6.1)$$

The intersection point of J_s (T) with $2T/\pi$ is related with the occurrence of the BKT phase transition at T_{BKT} in the 2D XY model **[11]**. However, the absence of a sharp jump and intersection is very common. The SPS, J_s (T) has been extracted from the nonlinear IV curves of several superconductors **[35-37]**. We have extracted SPS, J_s as a function of T following a relation between η and J_s as given in equation (6.1). In **Figure 6.4 (A - C)** we have shown extracted J_s (T) corresponding to samples S12, S13 and S14 respectively. The SPS, J_s (T) vanishes at $T = T_{BKT}$ and exhibits a nonlinear behaviour below T_{BKT}. The estimated values of charge carrier density, n per m^3 and superfluid density, n_s per

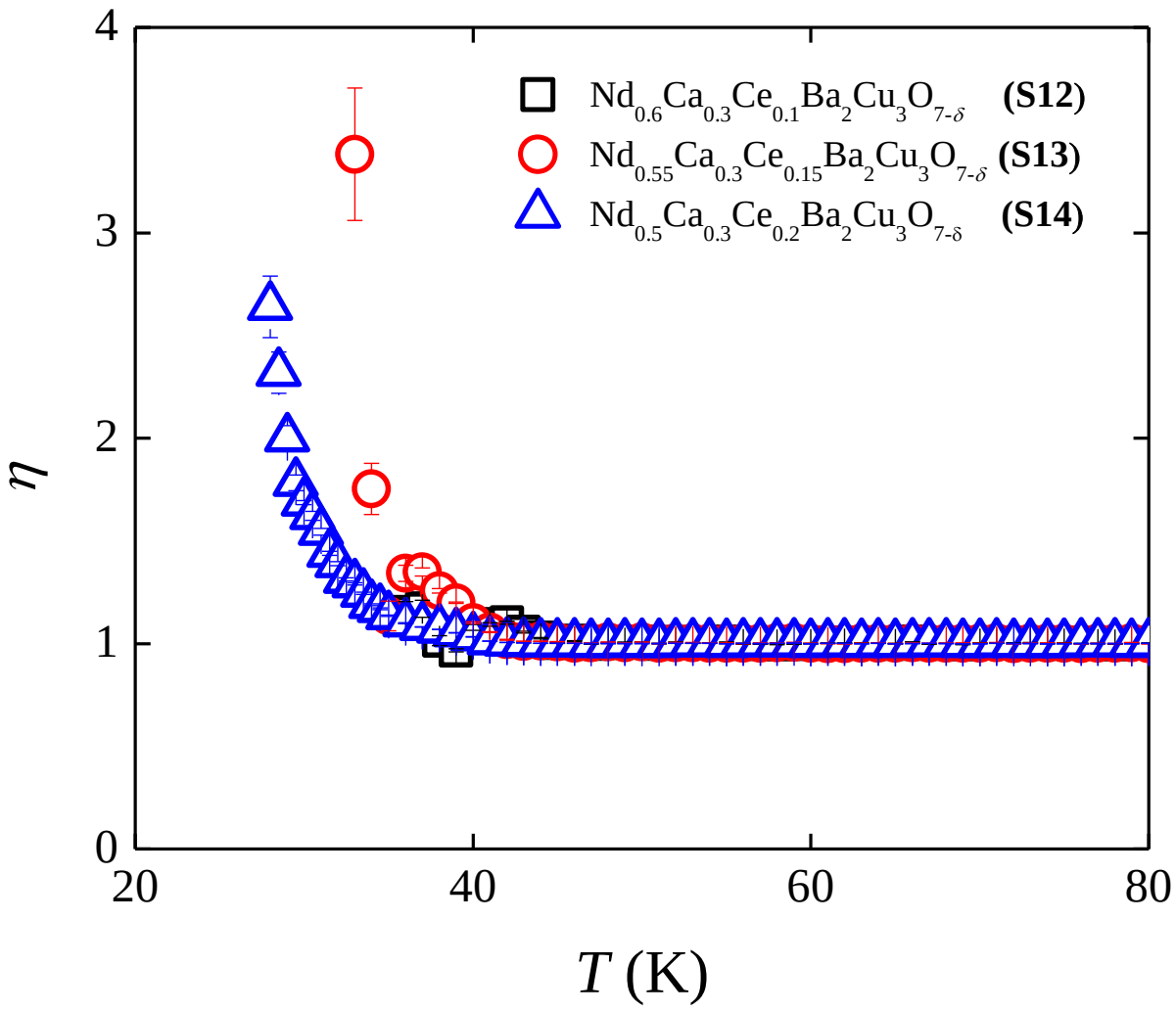

Figure 6.3 Variation of η as a function of T in (A) $Nd_{0.6}Ca_{0.3}Ce_{0.1}Ba_2Cu_3O_{7-\delta}$ (S12), (B) $Nd_{0.55}Ca_{0.3}Ce_{0.15}Ba_2Cu_3O_{7-\delta}$ (S13) and (C) $Nd_{0.5}Ca_{0.3}Ce_{0.2}Ba_2Cu_3O_{7-\delta}$ (S14) respectively.

m^3 at experimentally lowest possible measured temperature are 1.21×10^{27} and 2.67×10^5 for S12, 1.19×10^{27} and 3.87×10^6 for S13, 1.26×10^{27} and

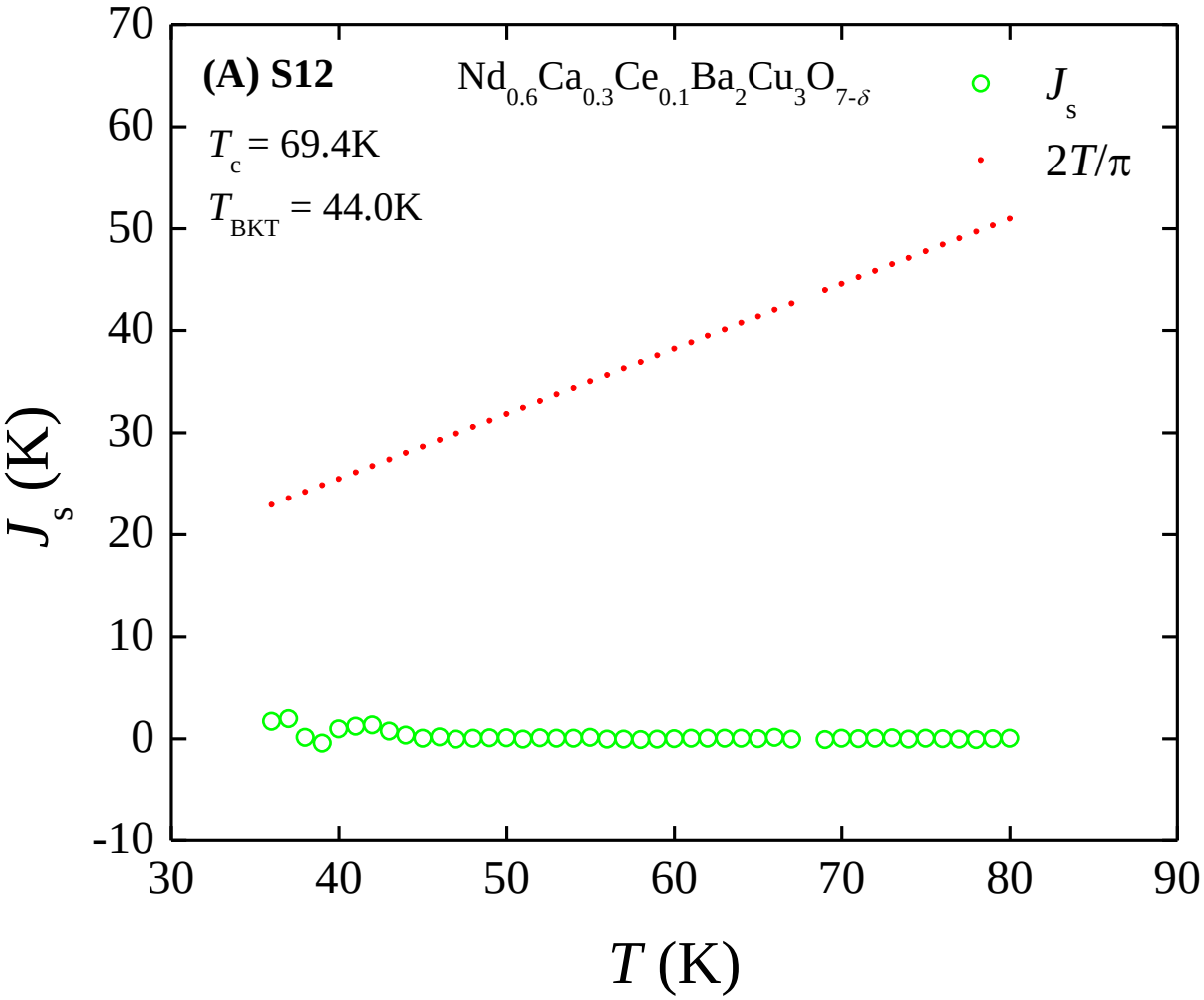

Figure 6.4 (A) Temperature dependence of the superfluid phase stiffness of $Nd_{0.6}Ca_{0.3}Ce_{0.1}Ba_2Cu_3O_{7-\delta}$ (S12).

2.26×10^6 for S14 respectively **[7, 38 - 41]**. Within the range of T_{BKT} to T_c ($\rho \simeq 0$) a finite J_s together with a nonzero resistivity coexist. Below T_{BKT}, J_s increases upto T_c ($\rho \simeq 0$). Clearly there is no sharp jump in $J_s(T)$.

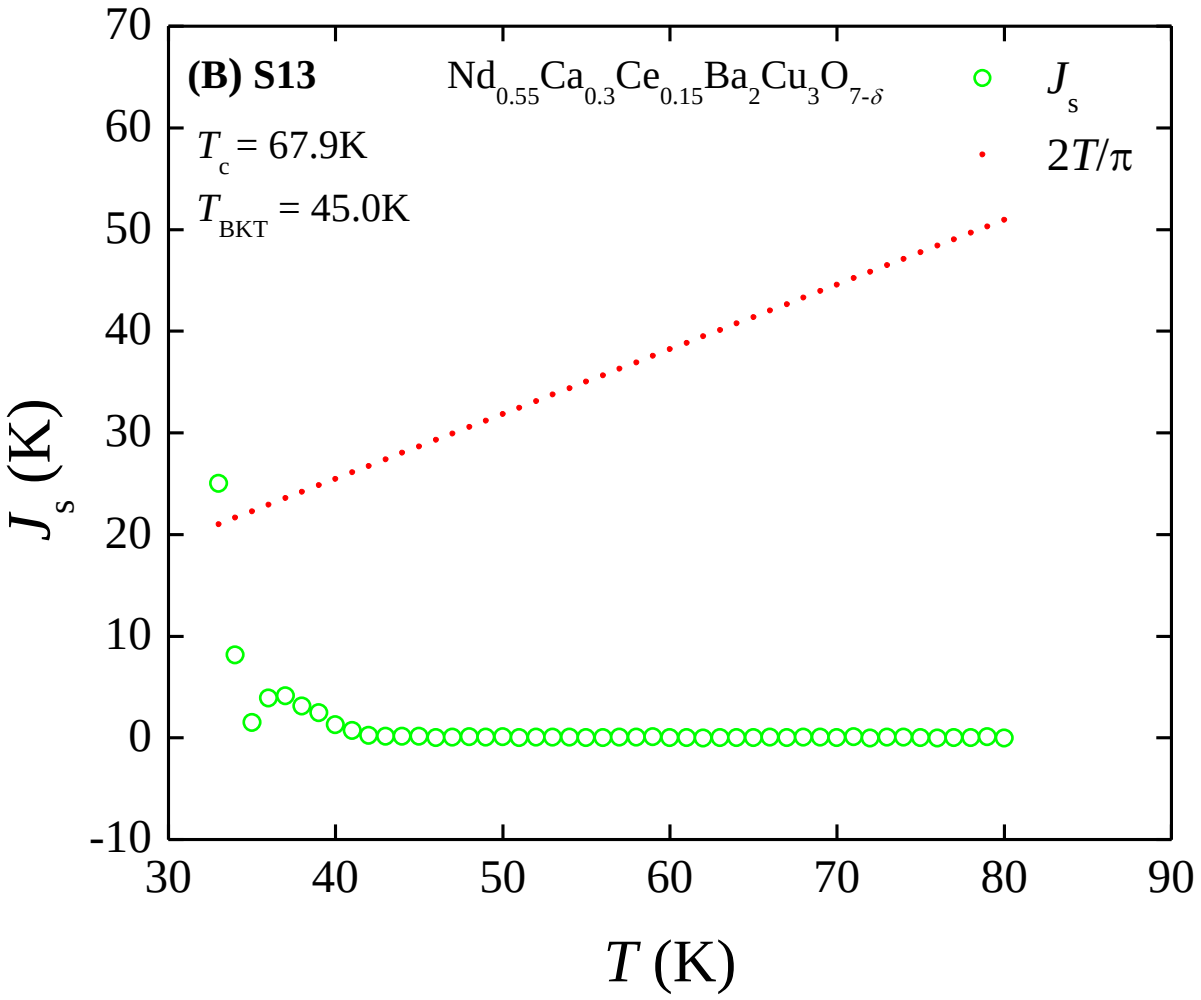

Figure 6.4 (B) Temperature dependence of the superfluid phase stiffness of $Nd_{0.55}Ca_{0.3}Ce_{0.15}Ba_2Cu_3O_{7-\delta}$ (S13).

We have observed a broad $J_s(T)$ in the presence of vortex-antivortex pair state which is only observed below the BKT transition and we attribute this observation to the second order nature of the BKT phase transition. Depending on several factors such as interlayer coupling the nature of the BKT transition

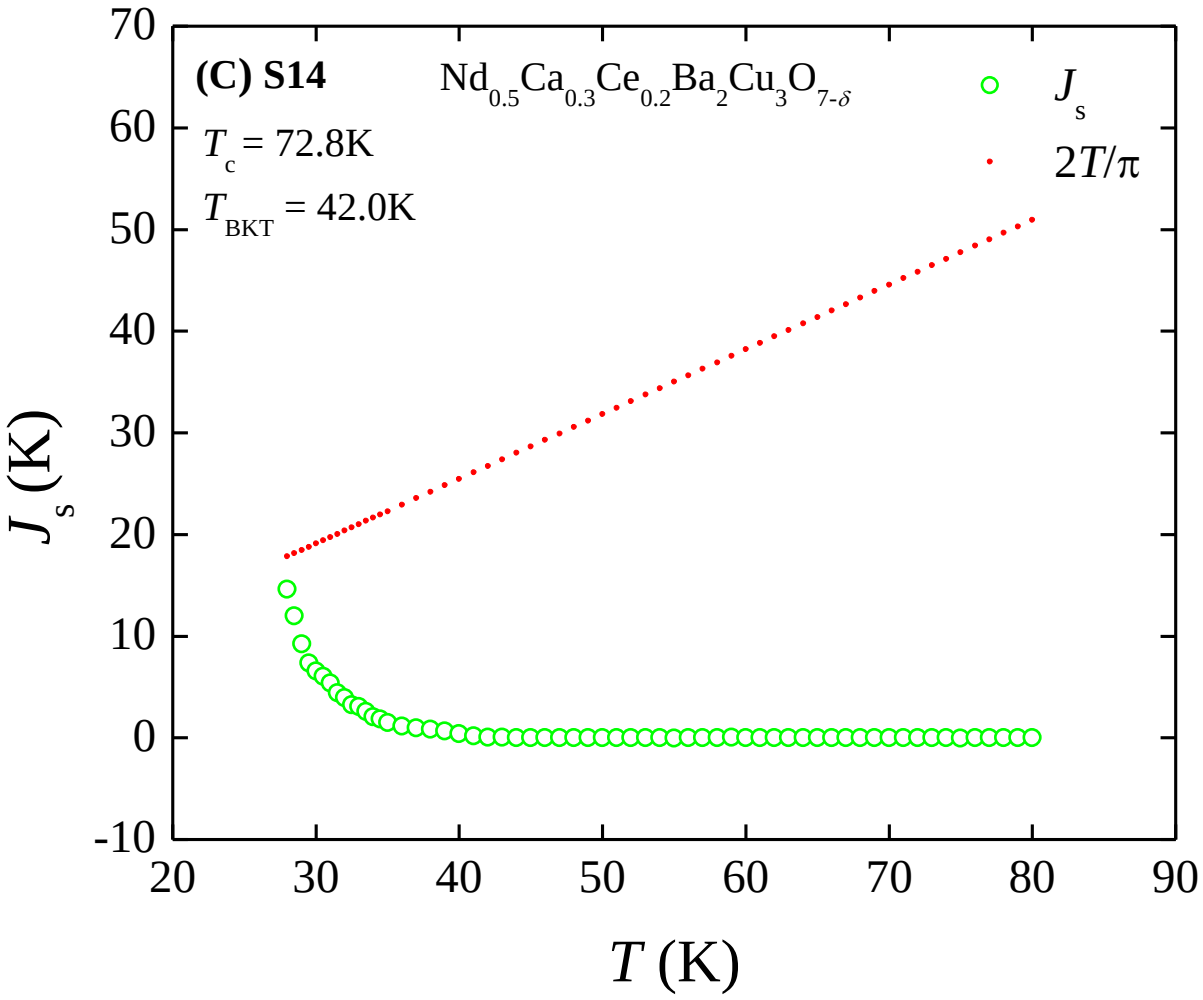

Figure 6.4 (C) Temperature dependence of the superfluid phase stiffness of $Nd_{0.5}Ca_{0.3}Ce_{0.2}Ba_2Cu_3O_{7-\delta}$ (S14).

may be a second order transition in several HTS.

In **Figure 6.4 (A-C)** we have also shown $J_s = 2T/\pi$ in addition to the experimental J_s (T). However, no intersection point is observed in **Figure 6.4 (A-**

C). The absence of the intersection reveals that a complete BKT transition is absent even though J_s increases from 0 below $T = T_{BKT}$.

We explain how it is possible to observe a second order BKT phase transition in a 3D cuprate system. Actually it is known that in a superconductor, the unbinding of vortex - antivortex pairs takes place at T_{BKT} in a 2D system. However, in a 3D system more than one layer is there and each layer is having such unbinding phenomenon **[42, 43]**. On cooling the vortex phase at T_{BKT}, vortex - antivortex pairs are formed in individual superconducting layers. However, the vortex - antivortex pair formation process is affected by interlayer coupling which is generally proportional to the square of the correlation length of the 3D system. Therefore, the BKT phase transition becomes a continuous process and further lowering temperature is necessary to have a critical number of vortex-antivortex pairs. The binding process is completed (corresponding to η = 3.0) once the number of vortex - antivortex pairs attains a minimum critical number.

6.4 Summary and few important future directions

Nonlinear *IV* characteristics of three cuprate superconductors exhibits onset of the BKT phase transition. The variation of exponent with T does not show any abrupt change at T_{BKT}. A continuous change in η (T) reveals that the BKT

transition in 3D cuprate superconductors is a second order phase transition. Associated changes in the experimental SPS with *T* also supports the continuous nature of the BKT transition. There is no intersection point between experimental J_s (*T*) and $2T/\pi$ line revealing that in 3D the smearing out the sharp transition. Even though the phase correlations in the individual superconducting planes should show the sharp BKT phase transition, any coupling between layers broadens it. Therefore, in a 3D superconducting system the incomplete BKT phase transition is observed in *IV* measurements to be a second order transition.

A microscopic analysis of the BKT phase transition is possible by using the nonlinear to linear transformation of the *IV* characteristics. The SPS extracted and described in chapter 3, 4, 5 and 6 can be described in a more generalized way even though we have used superconductors of three different categories - (i) electron doped, (ii) hole doped and (iii) co-doped cuprates. In all three cases, the variation of the SPS with *T* is found to be nonlinear and broadened, reflecting the absence of the sharp and complete BKT transition. However, the onset has been clearly detected and a possibility of second order BKT phase transition can be tuned in cuprate superconductors. Even though the individual 2D superconducting planes may exhibit the BKT, random coupling of individual layers broadens the BKT transition. This observation is found to be almost independent of the nature (electron or hole) of doping. However, the maximum SPS observed from nonlinear *IV* is very sensitive to the doping level of samples.

Enhancing the SPS by changing the doping level and controlling the rearrangement of the distribution of the BKT vortices may lead to the enhancement of the depairing current density as well as the transport critical current density.

First time we have shown that the FFH scaling function can be successfully used to understand nonlinear to linear transformation of *IV* characteristics and the broadened BKT phase transition. The existence of the BKT vortices and its impact on the transport properties in 3D dimensional superconducting systems can be understood by using the FFH scaling function. Even though we have suggested using the FFH scaling function in collapsing the *IV* curves in cuprates on both sides of T_{BKT}, our methodology and procedure can be extended to even non-cuprate superconductors showing the BKT phase transition.

6.5 References

[1] J. M. Kosterlitz, D. J. Thouless, J. Phys. C 6 (1973) 1181.

[2] V. L. Berezinskii, Sov. Phys. JETP 34 (1972) 610.

[3] I. Maccari, L. Benfatto, C. Castellani, Phys. Rev. B 96 (2017) 060508(R).

[4] J. Yong, T. R. Lemberger, Phys. Rev. B 87 (2013) 184505.

[5] J. H. Koo, G. Cho, Mod. Phys. Lett. B 20 (2006) 539.

[6] L. Benfatto, C. Castellani, T. Giamarchi, Phys. Rev. Lett. 98 (2007) 117008.

[7] L. Benfatto, C. Castellani, T. Giamarchi, Phys. Rev. B 77 (2008) 100506(R).

[8] M. Mondal, S. Kumar, M. Chand, A. Kamlapure, G. Saraswat, G. Seibold, L. Benfatto, P. Raychaudhuri, Phys. Rev. Lett. 107 (2011) 217003.

[9] M. A. Dubson, S. T. Herbert, J. J. Calabrese, D. C. Harris, B.R. Patton, J. C. Garland, Phys. Rev. Lett. 60 (1988) 1061.

[10] J. Yong, M. J. Hinton, A. McCray, M. Randeria, M. Naamneh, A. Kanigel, T. R. Lemberger, Phys. Rev. B 85 (2012) 180507.

[11] G. Venditti, J. Biscaras, S. Hurand, N. Bergeal, J. Lesueur, A. Dogra, R. C. Budhani, M. Mondal, J. Jesudasan, P. Raychaudhuri, S. Caprara, L. Benfatto, Phys. Rev. B 100 (2019) 064506.

[12] P. G. Baity, X. Shi, Z. Shi, L. Benfatto, D. Popovic, Phys. Rev. B 93 (2016) 024519.

[13] D. R. Nelson, J. M. Kosterlitz, Phys. Rev. Lett. 39 (1977) 1201.

[14] D. McQueeney, G. Agnolet, J. D. Reppy, Phys. Rev. Lett. 52 (1984) 1325.

[15] Y. J. Uemura et al., Phys. Rev. Lett. 62 (1989) 2317.

[16] D. M. Broun, W. A. Huttema, P. J. Turner, S. Ozcan, B. Morgan, R. Liang, W. N. Hardy, D. A. Bonn, Phys. Rev. Lett. 99 (2007) 237003.

[17] Y. Zuev, M. S. Kim, T. R. Lemberger, Phys. Rev. Lett. 95 (2005) 137002.

[18] S. Hikami and T. Tsuneto, Prog. Theor. Phys. 63, (1980) 387.

[19] P. Das, A. K. Ghosh, Physica C 593 (2022) 1354005.

[20] P. Mandal, D. Rakshit, I. Mukherjee, T. Sk, A. K. Ghosh, Phys. Lett. A 436 (2022) 128072.

[21] S. Haldar, A. K. Ghosh, Solid State Commun. 347 (2022) 114716.

[22] N. E. Hussey, J. R. Cooper, R. A. Doyle, C. T. Lin, W. Y. Liang, D. C. Sinclair, G. Balakrishnan, D. McK. Paul, A. Revcolevschi, Phys. Rev. B 53 (1996) 6752.

[23] P. Pugnat, G. Fillion, H. Noel, M. Ingold, B. Barbara, Europhys. Lett. 29 5 (1995) 425.

[24] E. S. Sadki, Z. H. Barber, S. J. Lloyd, M. G. Blamire, A. M. Campbell, Phys. Rev. Lett. 85 (2000) 4168.

[25] K. Tomimoto, I. Terasaki, A. I. Rykov, T. Mimura, S. Tajima, Phys. Rev. B 60 (1999) 114.

[26] Y. Matsuda and S. Komiyama, Phys. Rev. B 48 (1993)10 498.

[27] S. Martin, A. T. Fiory, R. M. Fleming, G. P. Espinosa and A. S. Cooper, Phys. Rev. Lett. 62 (1989) 677.

[28] D. H. Kim, A. M. Goldman, J. H. Kang and R. T. Kampwirth, Phys. Rev.

B 40 (1989) 8834.

[29] H. H. Wen, P. Ziemann, H. A. Radovan and S. L. Yan, Europhys. Lett. 42 (1998) 319.

[30] P. Das, A. K. Ghosh, Physica C 548 (2018) 27.

[31] V. Ambegaokar, B. I. Halperin, D. R. Nelson, E. D. Siggia, Phys. Rev. Lett. 40 (1978) 783.

[32] V. Ambegaokar, B. I. Halperin, D. R. Nelson, E. D. Siggia, Phys. Rev. B 21 (1980) 1806.

[33] S. Kamal, D. A. Bonn, N. Goldenfeld, P. J. Hirschfeld, R. liang, W. N. Hardy, Phys. Rev. Lett. 73 (1994) 1845.

[34] Kathleen M. Paget, Brent R. Boyce, Thomas R. Lemberger, Phys. Rev. B 59 (1999) 6545.

[35] A. M. Kadin, K. Epstein, A. M. Goldman, Phys. Rev. B 27 (1983) 6691.

[36] A. T. Fiory, A. F. Hebard, W. I. Glaberson, Phys. Rev. B 28 (1983) 5075.

[37] K. Epstein, A. M. Goldman, A. M. Kadin, Phys. Rev. Lett. 47 (1981) 534.

[38] J. L. Tallon, C. Bernhard, H. Shaked, R. L. Hitterman, J. D. Jorgensen, Phys. Rev. B 51 (1995) 12911.

[39] Y. Ando, A. N. Lavrov, S. Komiya, K. Segawa, X. F. Sun, Phys. Rev. Lett. 87 (2001) 017001-1.

[40] A. Stangl, A. Palau, G. Deutscher, X. Obradors, T. Puig, Sci. Rep. 11 (2021) 8176.

[41] I. Bozovic, X. He, J. Wu, A. T. Bollinger, Nature 536 (2016) 309.

[42] S. W. Pierson, Phys. Rev. B 51(1995) 6663.

[43] M. Friessen, Phys. Rev. B 51(1995) 632.